ESCUELA TÉCNICA SUPERIOR DE INGENIERÍA
(ICAI)

PhD thesis

Highly Sensitive Microwave Sensors for Liquid Dielectric Characterization

Author
Mahdieh Gholami Mayani

Supervisors
Prof. Romano Giannetti
Prof. Javier Matanza Domingo

Madrid
Oct 2022

Abstract

This thesis focuses on two novel sensors that are designed, tested and characterized with liquid solvents. The first dielectric resonator sensor is based on a dielectric resonator (DR) fed by a slot-coupling mechanism in the ground plane of a microstrip transmission line. The second sensor fed by a parallel microstrip transmission line is shielded by a metallic housing box to prevent radiation loss. The obtained devices are fully passive sensors that a radio frequency signal can interrogate. The cavity perturbation technique is used to study the impact of the liquid under test on the resonant frequency and modal distribution; full-wave simulations corroborate the theoretical results. A prototype of the first proposed sensor tuned to work in the 2.45 GHz band has been designed, manufactured and measured in different ethanol concentrations. For the second sensor, the simulated results as well as the theoretical concept are studied. Furthermore, the sensor has been fabricated and tested without shield, showing high accuracy. Additionally, the thesis presents a review on the recent metamaterial-based electromagnetic sensors, particularly on the structures that integrate the metamaterials in antenna or transmission lines for their further integration in measurement instruments. The approach followed in the review is to highlight sensitivity and quality factor (Q-factor) as they are crucial parameters in any sensor. For more insight into the metamaterial-inspired sensors, an open complementary split ring resonator (OCSRR)-loaded monopole antenna is used as a liquid sensor for discrimination of ethanol solvents with different concentrations. The sensor part is integrated with the electronic parts including a voltage-controlled oscillator (VCO) and a zero-biased Schottky Diode Detector (SDD) allowing the sensor to be low cost and portable. Indeed there are some limitations on the sensitivity level of Metamaterial-inspired sensors and saturation level of sensing by increasing the liquid percentage in the solvent under test. Consequently, the approach toward DR sensors is much beneficial to higher sensitivity and less loss as followed in this thesis.

Resumen

Esta tesis se centra en dos sensores novedosos que se diseñan, prueban y caracterizan con disolventes líquidos. El primer sensor de resonador dieléctrico se basa en un resonador dieléctrico (DR) alimentado por un mecanismo de acoplamiento de ranura en el plano de tierra de una línea de transmisión de microcinta. El segundo sensor, alimentado por una línea de transmisión microstrip paralela está protegido por una caja de carcasa metálica para evitar la pérdida de radiación. Los dispositivos obtenidos son sensores completamente pasivos que una señal de radiofrecuencia puede interrogar. La técnica de perturbación de la cavidad se utiliza para estudiar el impacto del líquido bajo prueba en la frecuencia resonante y la distribución modal; las simulaciones de onda completa corroboran los resultados teóricos. Se ha diseñado, fabricado y medido en diferentes concentraciones de etanol un prototipo del primer sensor propuesto sintonizado para trabajar en la banda de 2,45 GHz. Para el segundo sensor, se estudian los resultados simulados así como el concepto teórico. Además, el sensor ha sido fabricado y probado sin escudo, mostrando una alta precisión. Adicionalmente, la tesis presenta una revisión sobre los sensores electromagnéticos basados en metamateriales recientes, particularmente sobre las estructuras que integran los metamateriales en antenas o líneas de transmisión para su posterior integración en instrumentos de medición. El enfoque seguido en la revisión es resaltar la sensibilidad y el factor de calidad (factor Q), ya que son parámetros cruciales en cualquier sensor. Para obtener más información sobre los sensores inspirados en metamateriales, se utiliza una antena monopolo cargada con un resonador de anillo abierto complementario (OCSRR) como sensor de líquido para la discriminación de disolventes de etanol con diferentes concentraciones. La parte del sensor está integrada con las partes electrónicas, incluido un oscilador controlado por voltaje (VCO) y un detector de diodo Schottky con polarización cero (SDD), lo que permite que el sensor sea portátil y de bajo coste. De hecho, existen algunas limitaciones en el nivel de sensibilidad de los sensores inspirados en metamateriales y el nivel de saturación de detección al aumentar el porcentaje de líquido en el solvente bajo prueba. En consecuencia, el enfoque hacia los sensores DR es muy beneficioso para una mayor sensibilidad y menos pérdidas como se sigue en esta tesis.

To Artin ...

"This sky Where we live Is no place to lose your wings So love, love Love."
HAFEZ (IRANIAN POET)

Agradecimientos (Acknowledgment)

Firstly, I am extremely thankful to my patient and supportive supervisors, Prof. Romano Giannetti and Prof. Javier Matanza Domingo. I have to mention that without their constant supports and assistance, this thesis was impossible and I'd like to express my great thanks to other professors, Prof. Francisco Javier Herraiz Martínez and Prof. Carlos Rodríguez-Morcillo García, who have supported me throughout this research project. I am extremely grateful for friendly environment in my PhD. I'd also like to thank my colleagues in the IIT and ICAI. This work has been funded by "IIT Strategic PhD Research Grants" and "Proyectos de Investigación Propia" programs from Universidad Pontificia Comillas.

Mahdieh Gholami Mayani
Madrid
Oct, 2022

Contents

List of Figures

List of Tables

Acronyms

EM	Electromagnetic
VNA	Vector Network Analyzer
MUT	Material Under Test
Q-factor	Quality factor
MTM	Metamaterials
LH	Left-Handed
ϵ	Permittivity
μ	Permeability
RH	right-Handed
TL	Transmission Line
SRR	Split Ring Resonator
CSRR	Complementary Split Ring Resonator
MMIC	Monolithic Microwave Integrated Circuit
RF	Radio Frequency
CPW	Co-planar waveguide
LUT	Liquid Under Test
SSRR	Symmetrical Split Ring Resonator
PET	Polyethylene terephtalate
IDC	Interdigital Capacitor
OCSRR	Open Complementary Split Ring Resonator
SCSRR	Single-ring Complementary Split Ring Resonator
CRLH	Composite Right-/Left-Handed
SRCR	Split Ring Cross Resonator
CS-SRR	Complementary Symmetric Split Ring Resonator
CAS-SRR	Complementary Asymmetric Split Ring Resonator
CBS-SRR	Complementary Bi Symmetric Split Ring Resonator
E field	Electric field
H field	Magnetic field
NRI	negative-refractive index
OCSRR	Open Complementary Split Ring Resonator
DR	Dielectric Resonator
DRS	Dielectric Resonator Sensor
UWB	Ultra Wide Band

Chapter 1

Introduction

1.1 Metamaterials and properties

Metamaterials (MTMs) were first introduced by Veselago in 1968 [1]. Veselago introduced the idea of a left-handed (LH) triad for magnetic and electric fields propagation, based on the electrodynamics properties of the materials. It was a speculation on the existence of substances with simultaneously negative values of permeability μ and permittivity ϵ; In contrast, conventional materials show a right-handed electromagnetic field orientation. Due to the lack of practical proof and experimental confirmation, the Left-Handed Materials (LHM)-based research area was not explicit. First revolutionary attempts were made for discovering negative permittivity by the periodic wire medium, followed by artificially creating negative permeability using an array of split ring resonators (SRR). Indeed, some kind of complex structures, like periodic wire medium combined with SRRs, could be modelled globally as they showed LH properties. Inspired by the experimental analysis, LHM are also called negative refractive index materials. Eventually, after 30 years, the first LH material as an artificial effective material was experimentally demonstrated by Smith *et al* [2]. This breakthrough lead to a vast variety types of resonators based on metamaterial concept. In recent years, electromagnetic metamaterials, defined as artificially effective structures, have attracted significant attention among the microwave community [3–10]. The second turning point in metamaterials (MTM) history was in 2005 when Smith discovered that the gradient refraction index medium can be employed in the optical frequency range in order to control wave propagation. The transformation from microwave to optical frequency lead to a wide range of terahertz (THz) MTM resonators [11, 12].

It is worth mentioning that the definition of MTMs, not requiring the negative permittivity and/or negative permeability, can be extended beyond the LHMs; i.e., the conscience of MTMs is controlling the electromagnetic (EM) waves ef-

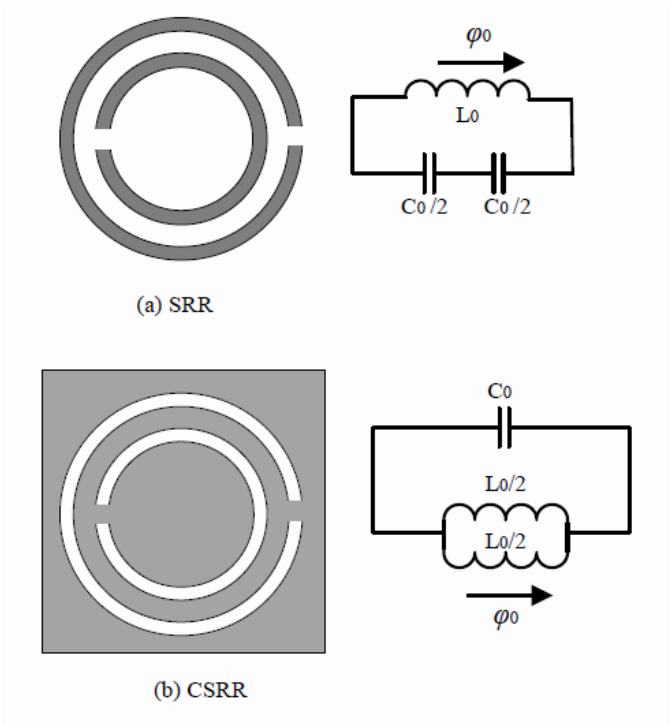

Figure 1.1: Topology of circuit models of (a) Split Ring Resonator (SRR) and (b) complementary SRR and equivalent [16]

ficiently with a high quality factor (Q-factor), revolutionizing the right-handed electromagnetic wave theory [13].

Indeed, MTMs can be defined as a periodic or non-periodic structure in a macroscopic scale such that its functionality is based on the unit-cell structural parameters and their constitutive materials. To satisfy the homogeneity theory, the unit-cell size should be smaller than the guided wavelength (λ_g), better if less than $\lambda_g/10$; thus MTMs are beneficial to decrease the size of structures efficiently. As the MTM unit-cell functionality depends on its architecture, there is a great controlling ability leading to the existence of a flexible functionally-viable structure which is not available in nature. These benefits can be considered as the major advantages of MTMs [14]. Some unusual MTM properties such as negative refractive index and backward wave propagation do not occur in the conventional resonant elements.

Generally, MTM resonators can be categorized into microwave-, terahertz- and plasmonic- metamaterials, depending on their operation frequencies [15]. Metamaterial resonators can be used in different configurations employed by TLs and antennas.

For more insight into the metamaterial resonator functionality, split ring resonator with high Q-factor has a quick response to the field variation, shown in Fig. 1.1. This resonator is excited by a magnetic field perpendicular to the resonator which acts as a magnetic dipole. The complementary SRR (CSRR) as the

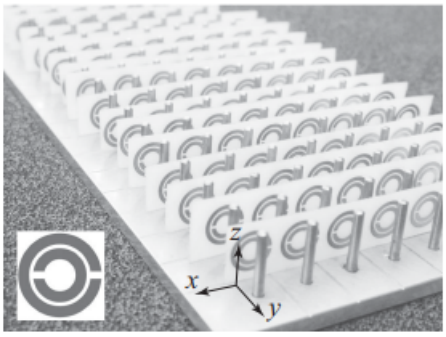

Figure 1.2: First experimental LH setup, structured by thin wires and SRR array to create a simultaneous negative permeability and negative permittivity [18].

dual counterpart of the SRR can be excited by an electric field parallel to its axis. This behavior is proved based on the Babinet principle [14]. According to the first experimental left-handed setup, thin wires and SRRs were combined to constitute a left-handed property. This structure is shown in Fig. 1.2. The resonance of the SRR can be described by $\omega_{0r}^2 = 3pc^2/\left(\pi \ln\left(2w/\delta\ a^3\right)\right)$ where p is the period, c is the speed of light, w is width of the rings and δ is defined as spacing between the rings of SRR [17]. It is expected that by decreasing the width of the resonator when the other parameters are constant, the resonant frequency increases. It is also important that as a result of larger overall currents and slightly different overlapping resonances, a second ring in the unit cell enhances the magnetic activity and effective permeability as well as the bandwidth in the unit cell.

In MTM-inspired resonators, by increasing the frequency, the component dimensions are proportionally reduced leading to a sufficiently-negligible time delay in wave propagation inside the element at resonant frequency. It is worth mentioning that the width of the resonator, size of substrate material, and the substrate material itself can affect the resonance frequency. For the metamaterial components, at microwave frequencies, the size of MTM components becomes less than at least $\lambda/10$ and thereby reducing parasitic effects. According to the fundamental and originality of LH MTMs, they can be extended to 2D and potentially 3D isotropic structures, due to having effective homogeneity [19]. In this thesis, we study the planar configurations, compatible with planar transmission lines. The MTM topology as homogeneous media can be described in the lumped-element modeling of TLs including capacitance and inductance for each unit cell. Negative refractive index (NRI) transmission-line MTMs are constituted by a transmission line (TL) loaded with series capacitors and shunt indicators, periodically. In the microwave frequencies, the MTMs are fabricated with printed circuit boards (PCB) on different commonly-used substrates such as FR4 and Rogers. In addi-

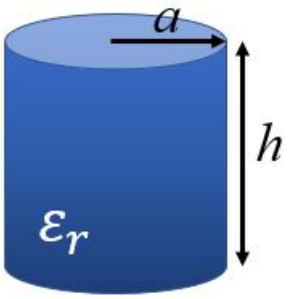

Figure 1.3: Schematic of the dielectric resonator made up of the ceramic material with permitivity ϵ_r.

tion, Metamaterials with a compact size much smaller than the λ_g benefit from a high Q-factor [20]. The resulting small footprint makes them highly compatible with MMIC-based components, with the net result that it is possible to design very small devices, even including the RF front end [21].

Due to their unusual properties not found in nature, there has been an ever-increasing use of metamaterials in many applications, for example sensors used for cost-efficient and label-free detection approach [22, 23]. Metamaterial resonators with high Q-factor and more compact size than that of ordinary resonators are successfully applied to sensor application, especially in real-time identifications.

1.2 Dielectric Resonators (DR)

Dielectric Resonators (DR) are made up of ceramic materials and some commercial polymers. The schematic of the DR cavity resonator is shown in Fig. 1.3. As they have been used as oscillators, filters, and antennas for decades, these resonant elements have a high dielectric permittivity, which allows them to store a great deal of energy within the DR and cause low dissipation (loss) [24–27]. Recently, DR with high efficiency, compact size and cost-effectiveness have attracted the researchers' consideration in sensing applications, however at very high frequency ranges (Called as Whispering-Gallery Modes at THz and optical frequency ranges) [26, 28–32]. At a given frequency, the size of the DR is inversely proportional to the relative permittivity of its constitutive material. The higher the relative permittivity of the constitutive material of DR, the lower the size of the DR. Contrariwise, the impedance matching and bandwidth are reduced by increasing the permittivity constant [33] resulting in having a quite narrow bandwidth. This narrow bandwidth is undesired in most applications, but this may be beneficial in some applications such as sensors. The dielectric cylindrical cavity resonator is

conceptually similar to a circular waveguide. The total energy corresponding to the electric and magnetic fields are stored inside the cavity, affected by the dielectric permittivity of the DR. Indeed, Frequency-domain-based sensors are favored to work with narrow bandwidths and high Q-factor values.

1.3 Motivation and objective of the thesis

Microwave techniques can be effectively applied as a rigorous solution to characterize and classify materials and solutions. These techniques are useful to indicate the imbalances in the concentration of certain electrolytes in blood or urine such as sodium chloride (NaCl) and glucose, and to discriminate blood alcohol, all in comparison with typical level existing in healthy samples. Sensors working in the radio frequency (RF) and the microwave regime are one of the best techniques for sensing, characterize and classify materials due to their versatility, low-power consumption, easy fabrication and cost effectiveness. Regarding the power consumption, most of them are fully passive, which means that no batteries are needed. To discriminate small variations of the material of interest, it is critically needed to have a high resolution sensors. In order to achieve this goal, high quality and low loss factors are prerequisites for sensor operation.

This thesis has been devoted to the design, implementation and measurement of highly-sensitive sensors for discrimination of small percentages of liquids and materials under test. These sensors are the first step towards a fully developed product for biomedical applications in hospitals and laboratories and also they are useful in the food industries to discriminate different materials with different compositions. As the metamaterial sensors are limited by their sensitivity level and their response will show saturation by increasing the value of the liquid/material solvents, DR sensors are suggested to tackle this issue. The DR sensors, with highly confined electromagnetic field inside of the dielectric and acting as a cavity, are beneficial for discrimination of diluted ethanol, sugar, and salt concentrations, even with very small concentrations. This property as well as their ability for integration with electronic devices such as transceivers prompted DR sensors to be studied for their application in biomedical research.

This work contributed to review on metamaterials-inspired sensors and their classification, design and analysis of dielectric resonator sensors including mode analysis for antenna-based DR sensor (DRA) and DR sensor housted by metalic box (DRS). Asides, the permittivity and material parameters were extracted using defined models and they were used in the simulation process. There is a good comparison between measurements and simulations for the fabricated and designed sensors. To achieve a handheld sensord device, electronic parts are suggested and a detector has been studied, designed and practically used in this thesis.

1.4 Organization of this thesis

This thesis is organized into six chapters; Chapter 1 introduces metamaterials and their properties as well as their applications in the sensor field. Chapter 2 deeply concentrates on the literature review of the metamaterial sensors and how different classes of MTM sensors work. Chapter 3 is based on the proposed sensors in the field of dielectric resonators and the principle operation and modal analysis are shown. Then the perturbation method has been applied and discussed to explain the sensor functionality. In chapter 4, the simulated and measured results corresponding to the proposed sensors are shown and discussed. Chapter 5 is mainly focused on the portable application of the sensor using electronic parts such as receiver and transmitter for reading the sensor response and a metamaterial sensor has been applied to make a proof of this concept. Finally Chapter 6 is specified to the conclusion, discussion and suggested future works.

Chapter 2

Performance Analysis of Metamaterial Sensors: Literature Review

In this section, different types of metamaterial (MTM) sensors are explained in detail and their functionalities are discussed. Different configurations as well as advantages and disadvantages are shown and they have been summarized into two tables for comparison. Metamaterial-based sensors, requiring neither pre- nor post- processing phases in material characterization, can be used in real-time sensing systems and they benefit from higher sensitivity and quality factor (Q-factor) compared to the conventional resonators.

Material characterization can be carried out using several variational parameters such as transmission or reflection coefficient, phase variation and changing in coupling coefficient between resonators. Additionally, impedance variation measurement is one of the conventional methods in this field [34].

As the MTM-based sensors represent a wide variety of highly-sensitive sensors, the lack of proper classification may hinder access to clear comparison and assessments. According to the reviewed papers in this thesis, the sensor's readout can be based on the notch-depth/peak-magnitude comparison between extracted transmission frequency responses, or on discrimination of the frequency shift in reference to the original frequency response in a real-time approach. In addition, the perturbation of the symmetry plane can lead to a linear/angular asymmetric response or change in the coupling coefficient between loaded resonators. To clarify these differences, in this review chapter, MTM-based sensors are classified into three main categories which correspond to the main sections of the chapter, and then further subdivided based on the physical structures in subsections. The proposed classification is the first comprehensive one of metamaterial-based sensors; It is shown in Fig. 2.1. The diagram shows three main sets as follows:

1. Frequency-variation sensors:
   In the frequency-variation sensors, the material characterization is based on the notch-depth or peak-magnitude comparison of the extracted transmission response. This kind of sensors is mainly used for solid or liquid material sensing.

2. Coupling-based sensors:
   In the coupling-based sensors, the functionality is based on the perturbation of the symmetry plane when the transmission line (TL) is coupled to the resonator due to either a linear/ angular displacements or asymmetric dielectric loading. The (material under test) MUT can be characterized when the coupling coefficient between cross-coupled resonators changes while the sample is placed over the resonators or positioned between them.

3. Frequency-splitting sensors (as so called differential sensors):
   In differential sensors, the sensor response demonstrates a single notch when two paths of the sensor (reference path and MUT path) are loaded with same materials and two notches when the MUT path is loaded by different material from that of the reference material.

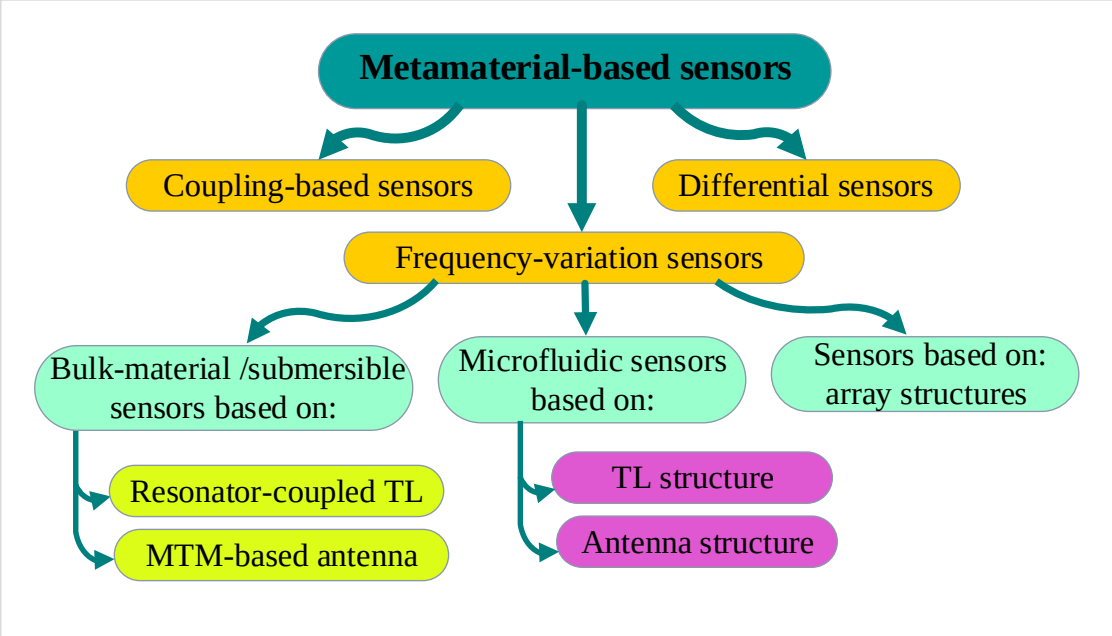

Figure 2.1: Classification chart of metamaterial sensors

2.1 Frequency-variation sensors

In the frequency variation sensors, when coupled with a microstrip TL or coplanar waveguide (CPW), the MTM resonator displays a particular pattern that identifies a specific MUT. For example, in liquid samples, by increasing the impurities percentage in water, the reflection coefficient decreases. This behavior is due to a decrease in free water molecules and hence higher loss factor. The sample is verified and characterized based on the notch-depth or peak-magnitude comparison in the measured transmission response; additionally, there is a shift in resonance frequency due to a change in capacitance of the original structure. The change in resonant frequency strongly depends on the thickness and permittivity of single-/multi-layer dielectric samples placed over the resonator surface.

In addition, it is also possible to design submersible sensors. They can be used for discrimination of different concentrations of liquids while the sensing part is inserted into the liquid under test (LUT).

The geometry and orientation of the resonators play a crucial role in sensitivity factor. Inserting the MUT/LUT over the sensitive areas of the resonators leads to higher Q-factor and, consequently, higher sensitivity; i.e., in sensitive areas of resonators, the electromagnetic fields are intensively confined and better electromagnetic interaction will be achieved, leading to sharper response and higher sensitivity. Here, the sensitivity (%) has been defined as [35]:

$$Sensitivity = \frac{\partial\ (freq)}{\partial\ (\epsilon_r)} \simeq \frac{\Delta f}{\Delta \epsilon_r} \tag{2.1}$$

where $\Delta\epsilon_r$ is the differential input of the sensor which is the difference between relative permitivity of the MUT/LUT and the reference material (mostly air) and Δf is the frequency shift corresponding to the change in the ϵ_r of the sample. It is worth noting that in some studies, the frequency shift per percentage is considered as sensitivity.

Frequency-variation sensors can be classified into three sub categories: bulk-material detection and submersible sensors, microfluidic sensors and sensors based on the array structures. The submersible sensors, dropped into the liquid or solid content, can be used in the food industries and farms and also for multi-layer dielectric samples with thick height. Microfluidic sensors identify small variations of the MUT and benefit from a compact size and accurate responses. The principle of operation is based on exciting the resonant frequency of the resonant element when liquid samples, flowing through the microfluidic channel, are loaded over the high electric field confinement areas of the resonators. Another strategy used for increasing the sensitivity and Q-factor of sensors is designing the sensor using a periodic (array) structure. In array structures, each constitutive element of the

array can create a special phase shift [36], thereby the current waves have a phase shifting behaviour from point to point along the array unit-cells leading to an optimum phase response and therefore, a desired sensor response is obtained [37]. It is demanding that a reflection coefficient shows a deep notch at the resonant frequency and higher quality factor which can be fruitful for the sensor application. For the wave travelling on the array structure, the maximum quality factor may depend on the propagation constant. As mentioned, a real-time change in the propagation constant is using periodic structures which creates an appropriate phase shifting whereby this concept can be interpreted as a change in equivalent TL parameters and subsequent a change in variation of propagation constant [38].

Several studies have been conducted based on shift in the resonant frequency, as reviewed in following subsections. Sensors reviewed in this section are summarized in Table 2.1.

2.1.1 Bulk material detection and submersible sensors

In this section, the sensor structures are applied to bulk materials, i.e., the sensor is either immersed into the liquid to be tested or a relatively big amount of solid MUT is placed over the resonant element of the sensor. In this category, the sensor is immersed into the solvent for the liquid characterization. Generally, this class of sensors includes two different configurations: sensors based on resonator-coupled TLs and sensors comprising metamaterial-inspired antennas.

Sensors based on resonator-coupled TLs

A submersible sensor based on two split ring resonator (SRR) resonators coupled to a microstrip TL is used for detection of solid and liquid materials with permittivity ranging from 2.45 for paraffin oil to 22.52 for acetone. It shows a good frequency variation between 2.98% to 21.9% respectively [39]. In [40], a rectangular complementary split ring resonator (CSRR) etched on the ground plane of a microstrip transmission line which resonates around 1.164 GHz is used to sense different dielectric materials such as Teflon, RO3003, FR4 with thickness of 2 mm to 3 mm as shown in Fig. 2.3. Similarly, the permittivity and thickness of a multi-layer dielectric substance are investigated in a non-invasive manner in [41, 42]. Similar to SRR resonators, complementary split ring resonators creates a bandstop (notch) in transmission coefficient and can characterize the MUT based on the shift in its resonant frequency. It should be considered that the narrower the stop band, the greater Q-factor. In [41], a CSRR coupled to the microstrip transmission line is used for the characterization of multi-layer dielectric samples.

It is worth mentioning that modifying conventional SRR resonators effectively enhance the electric field confinement and the sensor efficiency. Some factors are

straightforwardly contributing to the Q-factor of the SRR such as radiation loss so that the fewer value is identified as the main aspect for achieving higher quality [43]. The distributed capacitances exist in the conventional SRR configuration, inducing more radiating power from the element. By optimizing the SRR structures to a spiral SRRs, the electric field within the split gap is highly lessened due to a zero-potential difference at the conjunction, resulting in less radiation loss and higher quality factor. In addition, broad-side coupled resonators benefit from having parallel E and H fields establishing and no power radiation. Moreover, the smaller resonator size in the planar arrays have smaller material loss and radiation dissipation and consequence higher Q-factor [44].

Another important step in improving the sensor efficiency is establishing the relationship between the value of coupling coefficient and physical structure of coupled resonators which requires finding the physical dimensions and characteristic frequencies. The coupling between two general resonators are shown in Fig. 2.2.

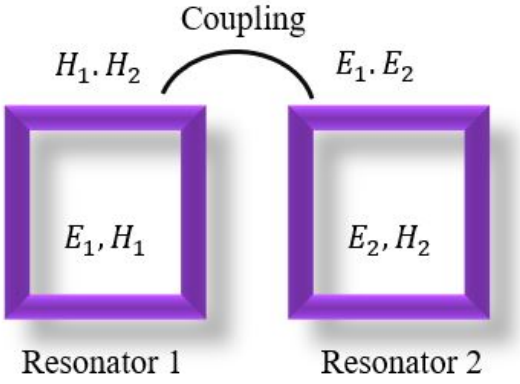

Figure 2.2: Electromagnetic coupling between two general resonators

According to the general theory of coupling [45, 46], the coupling coefficient of coupled radio frequency (RF)/microwave self-resonant elements may be defined as the ratio of coupled energy to the stored energy between them which is mathematically described as follows:

$$M = \frac{\iiint_v \epsilon E_1.E_2 dv}{\sqrt{\iiint_v \epsilon \left|E_1\right|^2 dv \times \iiint_v \epsilon \left|E_2\right|^2 dv}} + \frac{\iiint_v \mu H_1.H_2 dv}{\sqrt{\iiint_v \mu \left|H_1\right|^2 dv \times \iiint_v \mu \left|H_2\right|^2 dv}} \tag{2.2}$$

Where E and H represents the electric and magnetic field components respectively and M is defined as coupling coefficient. The indices 1 and 2 correspond to the first

and second resonator. Accordingly, for a resonator coupled to a TL,the coupling coefficient and quality factor are straightforwardly dependent on the spaced gap between resonator and coupled line and also on the external quality factor of the resonant element. This coupling is basically through fringe fields which exponentially decay outside the region. This mutual coupling can be simulated by a mutual capacitor or inductor (depending upon which E or H field is stronger respectively). In addition, by modifying the resonator structure and hence improving the coupling capacitor/inductor, the stored energy between resonator and coupled line increases, leading to a stronger coupling ratio and consequently more sensitivity in the sensor applications. Based on this concept, numerous modifications in SRRs have been made and used in sensing applications. A Hexagonal Complementary SRR is a different type of resonator with a principle of operation similar to the CSRR. It is employed for measuring the complex permittivity of solid and liquid materials [42]. However, it uses a liquid container for liquid samples which makes it bulky. Another modified resonator is the S-shaped resonator which is coupled to the microstrip TL. It has been tested for solid materials and creates resonant frequency shift around 150 MHz for FR4 and 100 MHz for RO4003C when the samples are placed over the resonator surface [47].

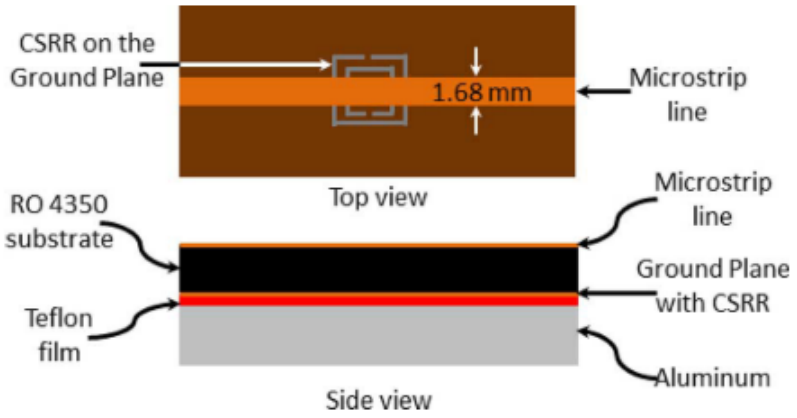

Figure 2.3: CSRR resonator etched on the ground plane of a microstrip TL [40]

In [48], a symmetrical split ring resonator is coupled to spur-line feed lines with a coupling gap in both sides. The spur line acts as a filter rejecting undesired harmonic frequencies, therefore the improved sensitivity and Q-factor makes this sensor qualified for detecting and characterizing smaller variation of permittivity. This sensor is applied to Rogers 5880, Rogers 4350 and FR4 films. Its structure is shown in Fig. 2.4.

As a different resonator, [49] suggests a labyrinth resonator, in a broadside coupling to the microstrip TL for testing the chemical liquids like ethanol- and

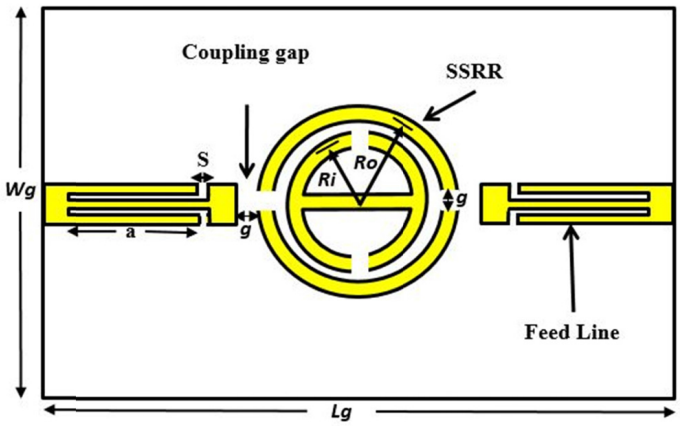

Figure 2.4: Symmetrical Split Ring Resonator (SSRR) is applied to spur-line feed lines [48]

methanol-water mixture with the frequency shifts of about 25 MHz and 15 MHz, respectively. This structure is presented in Fig. 2.5.

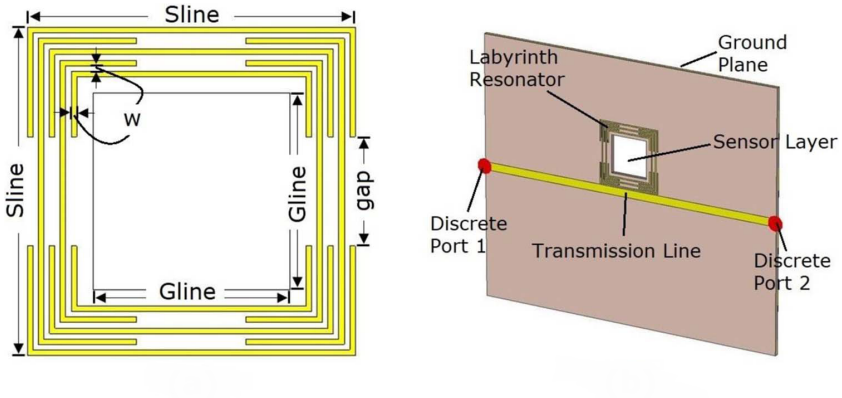

Figure 2.5: Labyrinth resonator in a broadside coupling to the microstrip TL [49]

A flexible microwave sensor is designed and fabricated in [50]. It is composed by a two-turn CSRR resonator etched on the conducting strip of a CPW TL. This has been developed on PET substrate. This sensor is suggested to be used in a robotic hand skin for material detection as it is flexible. This sensor is validated experimentally for Rogers RO4003C, Nelco N4350-13, FR4, and Rogers RO3010, attached to the CSRR.

Some attempts have been made to increase the coupling between the resonator and the host line [51]. A microstrip split ring as a conventional half-wavelength resonator resonating at 2 GHz is investigated in different orientations to determine

the sensitive spot in the gap, shown in Fig. 2.6. The coupling between the line and resonator increases when the gaps corresponding to the TL and resonator meet each other. In this case, higher sensitivity is achieved by extending the inner part of the gap. This sensor has been tested by measuring glucose concentration within the range of $1\,\mathrm{g\,L^{-1}}$ to $15\,\mathrm{g\,L^{-1}}$ with steps of $1\,\mathrm{g\,L^{-1}}$ [51].

Figure 2.6: Half-wavelength resonator coupled to a microstrip TL in different orientations [51]

A double-sided spiral-ring resonator (comprising four resonators) is proposed in [52] for characterizing thin films and deionized water-ethanol/methanol mixtures. The proposed sensor structure is shown in Fig. 2.7. This sensor suffers from complexity in fabrication as these four resonant elements on both sides are connected using vias from top to bottom. The sensitivity of sensor is estimated around 0.547 % at 300 MHz.

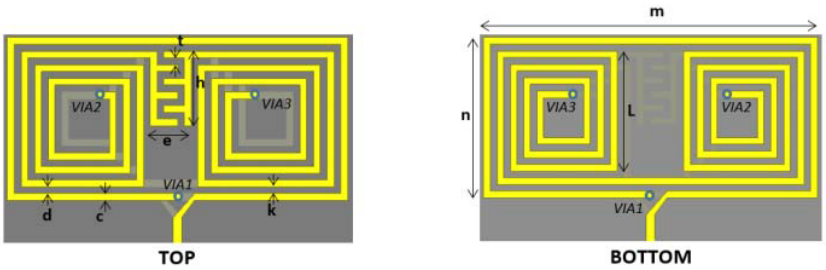

Figure 2.7: Attempts made to increase the sensitivity, double-sided spiral-ring resonator [52].

Another approach for improving the coupling coefficient and hence, the sensitivity, is aligned-gap and centered-gap multi SRRs [53]. Generally speaking, the field confinement of conventional SRRs can be enhanced by modifying the resonator structures to detect any dielectric perturbation [54]. Increasing the split gap number, i.e., more capacitors in the SRR circuit model, is an efficient solution made by aligned gap and centered gap. This structures are shown in Fig. 2.8. Increasing the high-field region at the split of the proposed aligned-gap multi-ring SRR results in an increment in the capacitance value; also, combining multiple SRRs in the centered-gap SRR contributes to decreasing the whole size of structure. The

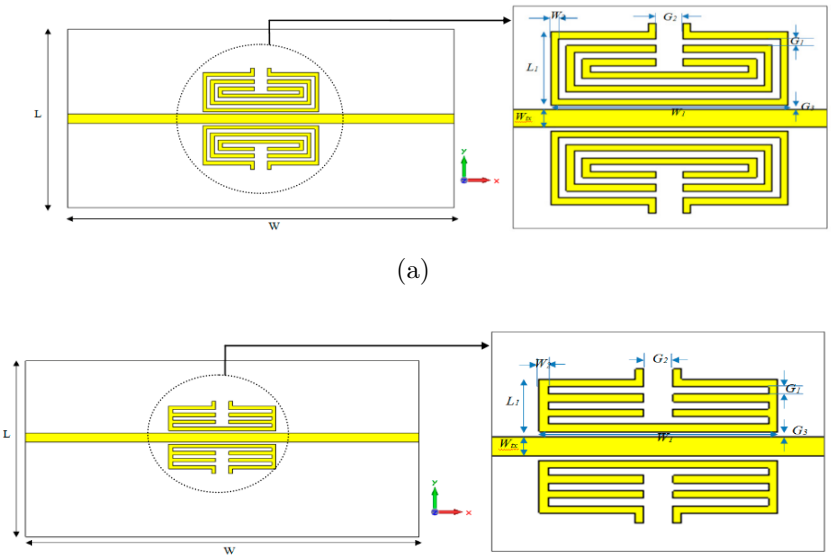

Figure 2.8: Schematic view of the (a) aligned gap and (b) centered gap [53]

measurements of the paper show a considerable improvement in sensitivity and Q-factor compared to the conventional SRR structures. In another approach [55], a compact SRR-based sensor is surrounded by a square TL to make the sensor very compact. This sensor is applied to the measurement of distilled water, alcohol and acetone. The SRR sensitive part should be submerged in the MUT for testing the chemical solvent.

An interdigital capacitor (IDC) connected to a spiral resonator as the constitutive resonant elements is suggested in [56]. There is no change in the resonant frequency after a specific thickness level and this is called saturation.

Another microwave sensor based on CPW uses a meander open complementary SRR (OCSRR) for liquid complex permittivity detection in a container implemented on the sensing area [57]. Up to 58.7 MHz shift in resonant frequency is achieved while ethanol concentration was varied from 0 % to 100 %.

Sensors based on metamaterial-based antennas

Aside from TL-coupled resonators, in many practical cases, planar metamaterial-based antennas have been analyzed and envisaged as sensors. An ultra wide band monopole antenna loaded by three metamaterial unit-cells is proposed in [58], for sensing the pH in solutions of NaOH and HCL, shown in Fig. 2.9. The pH factor decreases when solution is concentrated by acidic substance leading to an increase in dielectric constant. This behavior can be interpreted by noticing that

the dielectric properties and the loss factor are affected by the change in the ionic bonds between water molecules and dissolved ions. Two antennas placed on both sides of the solution container measure the reflection and transmission coefficients.

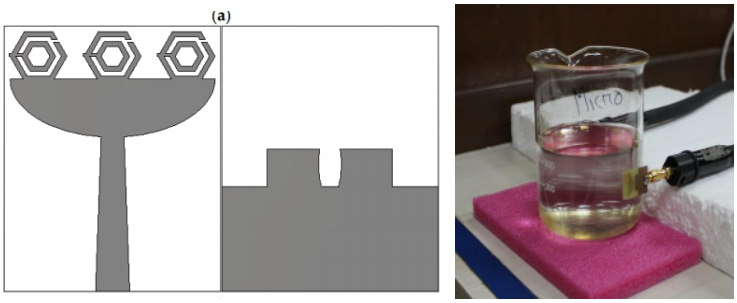

(a) (b)

Figure 2.9: UWB monopole antenna loaded by three metamaterial unit-cells [58]

Instead of using two antennas separately, authors in [59] proposed a sensor consisting of two monopole antennas which are coupled to the square- and circular-split ring resonator, placed on the same substrate. It is used to characterize the glucose concentration in blood plasma. The resonant frequency of the squared and circular resonators are 8.3 GHz and 1.9 GHz respectively. A modified version of this sensor is suggested in [60] in which the SRR, excited by two monopole antennas, is used as a submersible sensor while the MUT permittivity ranges from 20 to 40 for four liquid samples such as acetone, propyl alcohol, methanol and ethylene glycol. 23.52 % relative frequency shift and wide dynamic range are achieved. This structure shows improved results compared to the previous study [58]. The sensors configurations are illustrated in Figs. 2.10a and 2.10b.

Another sensor using coplanar waveguide configuration, proposed in [61], consists of an IDC which is implemented at the back surface of a patch- antenna. The antenna resonating at 2.4 GHz is suitable for the analysis of permittivity from 1 to 80 (air to water). This is useful for bulk liquid materials as a submersible sensor. It is illustrated in Fig. 2.11. The application of IDC in sensors is also presented in [62] where the IDC resonator and vias are employed in conventional printed dipole antenna in order to decrease the size of antenna with a radiation pattern similar to dipole antenna. In addition, [63] presents an IDC-based antenna in microstrip configuration for glucose monitoring. The measurement dynamic range is narrow, between 1 to $4\,\mathrm{g\,L^{-1}}$. This IDC-based sensor is depicted in Fig. 2.11.

In [64], a circular SRR as a radiating element fed by a microstrip TL is used for detection of breast cancer. In the simulations, samples such as MCF7, MDA-MB-231, HS578T and T47D are investigated. The dielectric permittivity ranging from 1 to 35.07 creates the maximum frequency shift of 30 MHz per sample. This

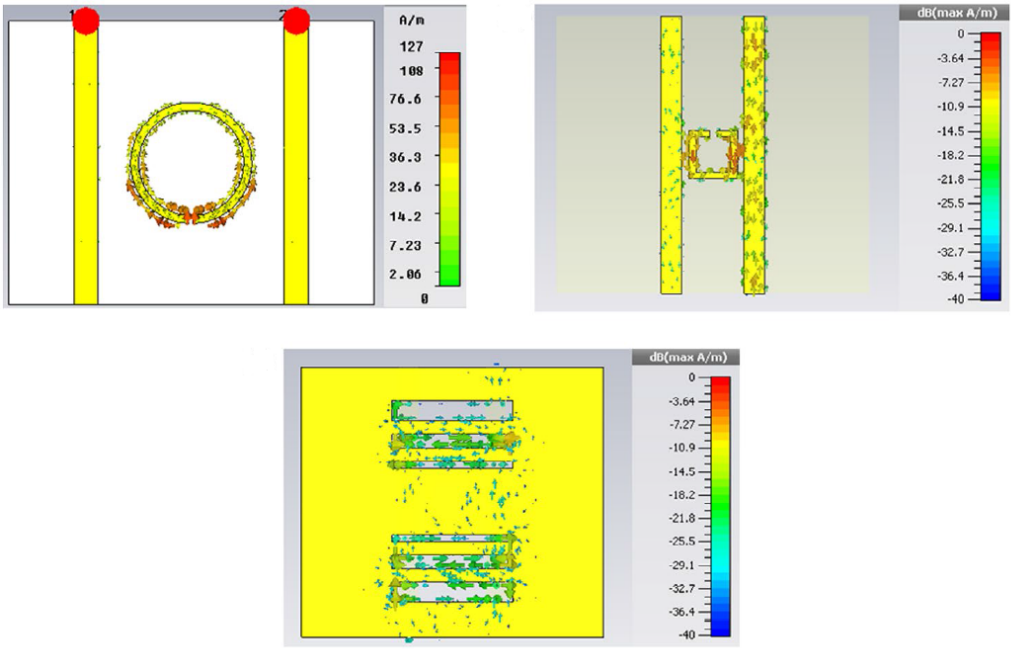

(a)

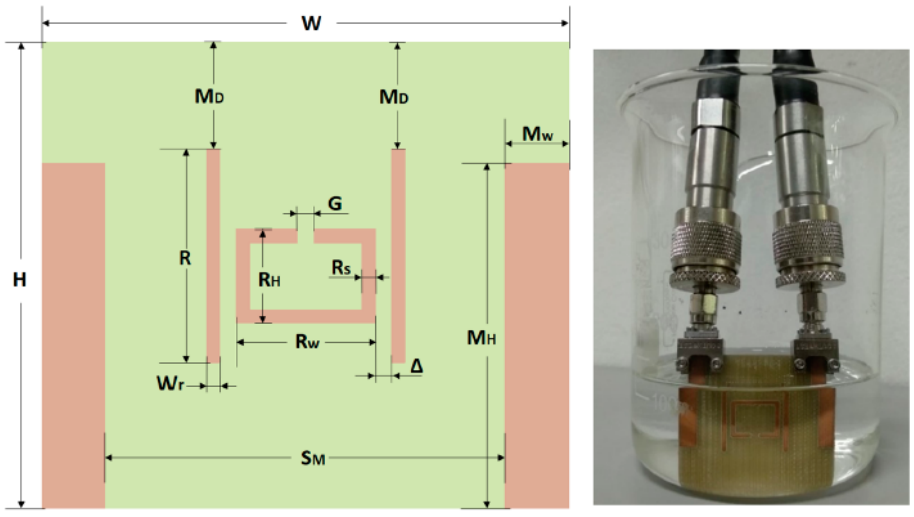

(b)

Figure 2.10: (a) Two monopole antennas coupled to the circular and square resonators; the yellow large surface shows defected ground plane [59], (b) The modified resonator is employed to improve the sensitivity [60]

(a)

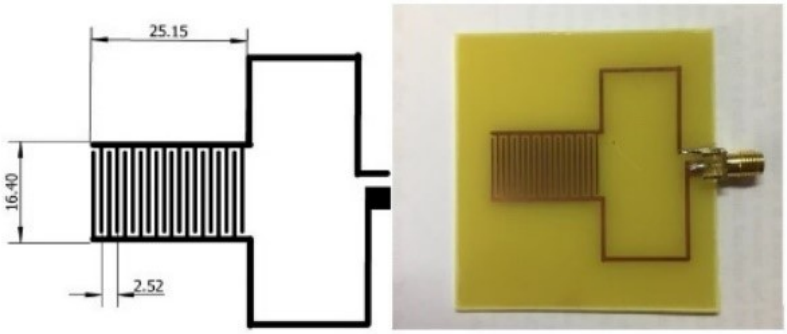

(b)

Figure 2.11: The IDC-based sensors suggested in [61] (a) and [63] (b) .

sensor has not been experimentally validated yet.

The possibility of multi-band planar microwave sensors is shown in [65] and [66]; the first one is based on different-sized CSRR etched resonators and the second one comprises two pairs of concentric single ring complementary split ring resonators. The different sizes of resonators create multiple resonant frequencies. The proposed sensor in [66] as a quad-band sensor operates in the ISM and WiMAX frequency bands (1.87 GHz, 2.46 GHz, 3.49 GHz and 4.34 GHz) and has been experimentally tested with petroleum and edible oil samples.

In addition to multi-resonant responses, a novel approach is employed in [67] for simultaneously identifying the permittivity and permeability. In this paper, the highest intensity of electric and magnetic fields are localized in different areas of CSRR resonator coupled to the TL. In this approach, these parameters can be estimated by measuring the frequency response and Q-factor in two separated areas of the MTM resonator.

Although many sensors show adequate shift in resonant frequency and high sensitivity, the major drawback of this class of sensors is the quantity of sample which is needed to cover the metamaterial resonant element. As the sample quan-

tity is reduced, the corresponding capacitance will decrease leading to a negligible shift and decreasing the response of the sensor. Therefore, these kinds of sensors are mainly used in food-quality monitoring, soil properties and moisture identification and every application in which the amount of MUT is not a problem. In addition, in many structure designs, the sensitivity level is limited and even may be saturated after passing a specific level as the sensitivity is straightforwardly limited by the resonant constitutive part.

In some specific applications such as biological tests, sensors able to detect a small amount of samples are needed. In the next subsection, the microfluidic sensors tackling this problem, are reviewed.

2.1.2 Microfluidic sensors

This section is devoted to review microfluidic metamaterial-inspired sensors. The microfluidic channel containing a liquid sample in micro/nano litres is placed on the high electric field confinement areas of the resonant element, leading to a shift in the resonant frequency of the sensing structure. This type of sensors with little volumes benefits from a compact size and accurate response.

Several architectures are proposed in this class of sensors to measure the dielectric properties of the liquids under test. This class of sensors is also beneficial for hazardous chemicals [68]. This section is divided into two categories including the microfluidic sensors based on the TL and the sensors based on the antenna configuration.

TL-based microfluidic sensors

In order to increase the sensitivity, the ordinary TL has been replaced by a metamaterial TL [69]. For conventional coupled TLs, there is a challenging task to achieve a broad bandwidth and tight coupling. The composite right-/left-handed (CRLH) TLs are used as a promising alternative to ordinary TLs. The dispersion diagram of the CRLH is shown in Fig. 2.12. In the balanced condition, metamaterials can behave in a broad bandwidth such that there is no gap between the backward and forward transitions, resulting in a wideband impedance matching [19].

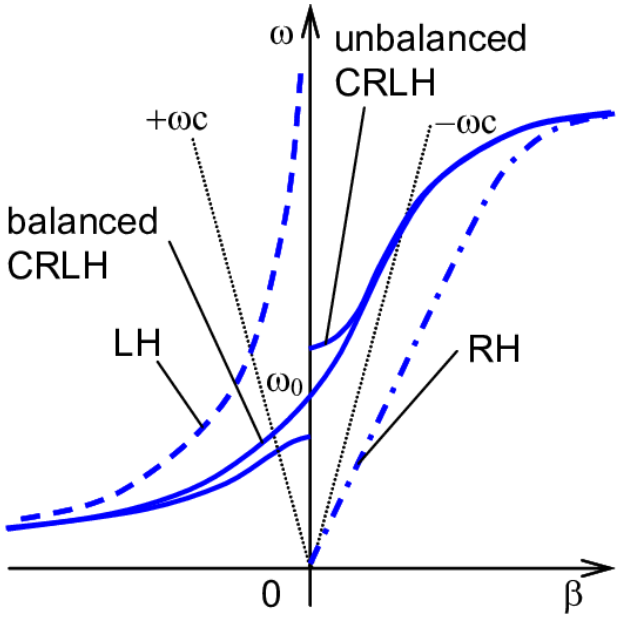

Figure 2.12: Dispersion diagram for left-and right-handed transmission lines. Dashed-dotted: conventional (right-handed) transmission line; dashed: idealized left-handed TLM; solid: composite right/lefthanded TLM for the balanced case (continuous line) and unbalanced (discontinuity at β=0) [70].

Regarding these facts, a metamaterial CRLH coupled-line sensor is proposed in [69] which enables a significant sensitivity enhancement. Another trend toward improving the coupling coefficient is using an IDC in the gap region of the SRR to concentrate the fields in a larger area [71]. As one of the challenges in some applications is the resolution of the sensor, the integration of IDC and SRR can successfully increase the overall sensitivity. This sensor has been tested with a glucose solution when the liquid is placed over the IDC gap of the SRR by a microfluidic channel. Here, the transmission coefficient (S_{21}) is normalized with the unloaded sensor response to eliminate the impact of glucose losses. The estimated sensitivity of the sensor is $2.60 \times 10^{-2}\,\mathrm{MHz/mgdL^{-1}}$ which has been improved compared to the reported work in [69]. The structures proposed in [69] and [71] are illustrated in Fig. 2.13a and b respectively.

With regard to the advantages of the CSRR resonator and its strong coupling ratio to the microstrip TL, a microfluidic sensor is studied in [72]. It consists of a tube with mixtures of water and methanol, attached along the edge of a CSRR resonator as the most sensitive area. This sensor is shown in Fig. 2.14.

In some structures like in [73], the microfluidic channel is inserted into the resonator by drilling. Another multiple SRR resonators coupled to the feeding microstrip TLs are demonstrated in [74]. The micro capillary filled by the solvent

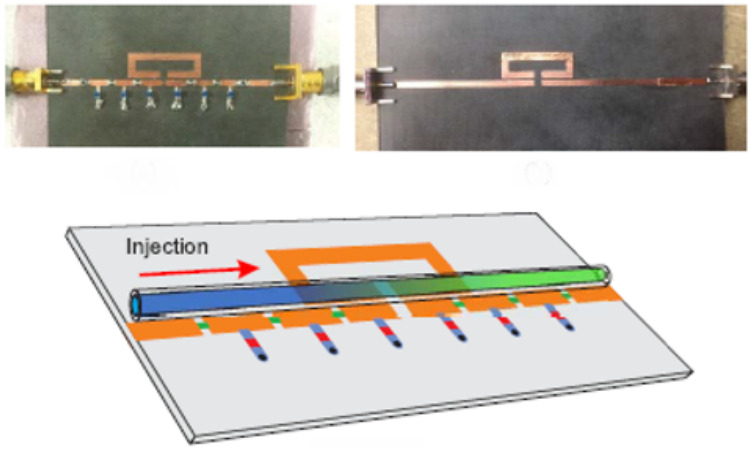

(a)

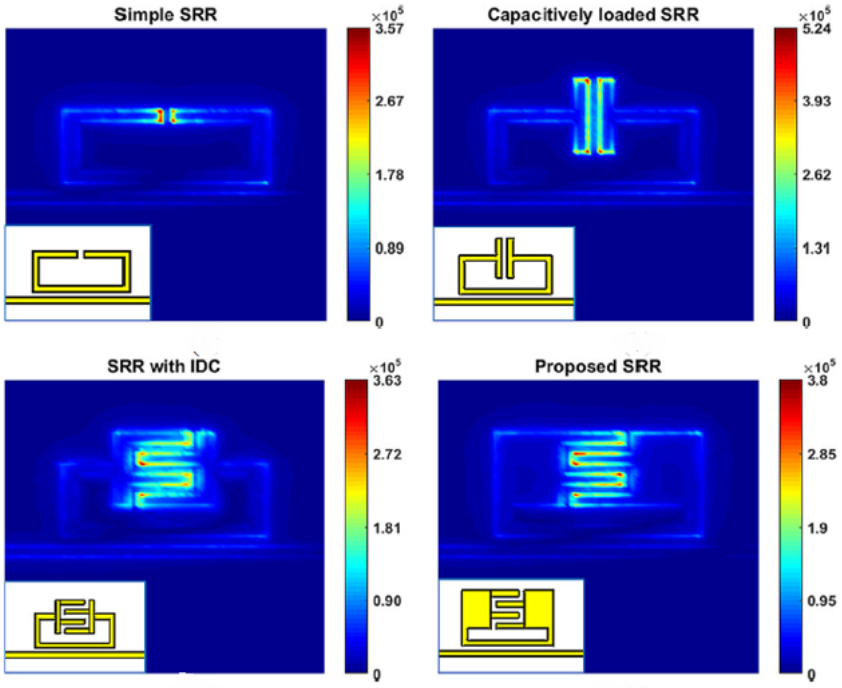

(b)

Figure 2.13: Attempts made to increase the sensitivity (a) CRLH-TL coupled to the resonator [69], (b) extended-gap resonator [71]

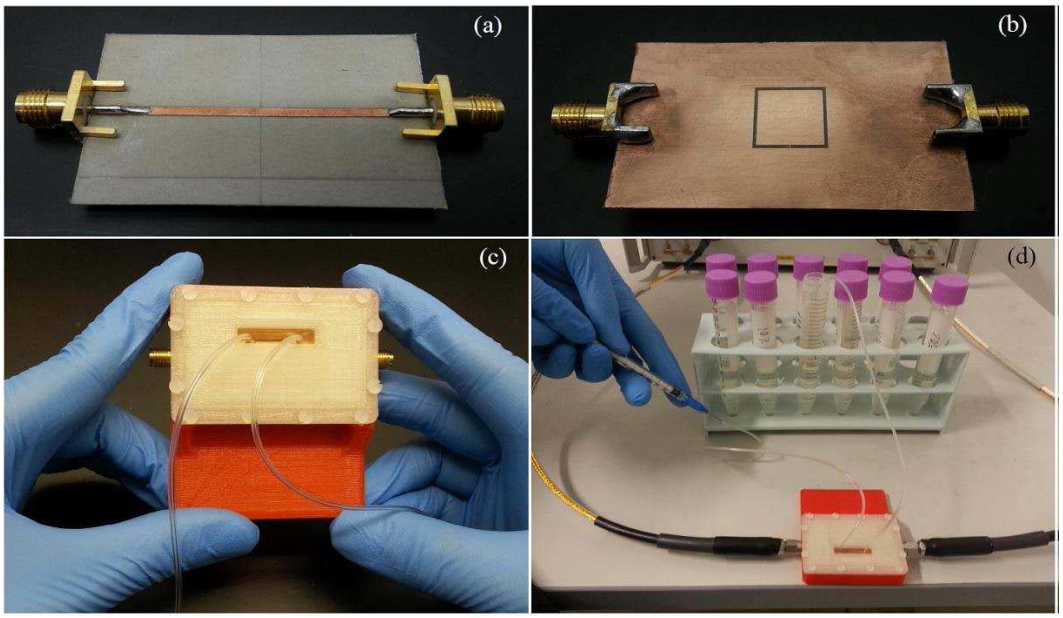

Figure 2.14: CSRR coupled to TL implemented by the microfluidic channel [72]

is placed over the sensitive gap of the resonator. It suffers from a long length in addition to a difficult implementation as the microfluid vertically passes the resonator by drilling.

In the CPW configuration, an IDC is proposed resulting in integrating the microwave micro technology and microfluidic [75]. The microfluidic channel is placed on top of the IDC. The de-ionized water and ethanol mixtures with the permittivity ranging from 20 to 40, obtain a frequency shift between 16 GHz to 21 GHz.

The multiband sensing makes the sensor structure more flexible in many applications as they can codify multi-chemical material properties [76]. To this end, different sizes of MTM resonators are used. To improve the sensor efficiency, the coupling between individual MTM unit-cells must be eliminated. In addition, in order to have a smooth liquid flow, a larger fill area and so higher Q-factor, a meandering microfluidic line is implemented beneath the resonator as shown in Fig. 2.15.

Antenna-based microfluidic sensors

In addition to the sensors constituted by resonator coupled to a TL, the sensing properties can be extracted using variation in frequency response of an antenna. In [77], the channel is implemented on the most sensitive area of metamaterial CSRR resonator etched on a monopole antenna. The antenna reflection coefficient

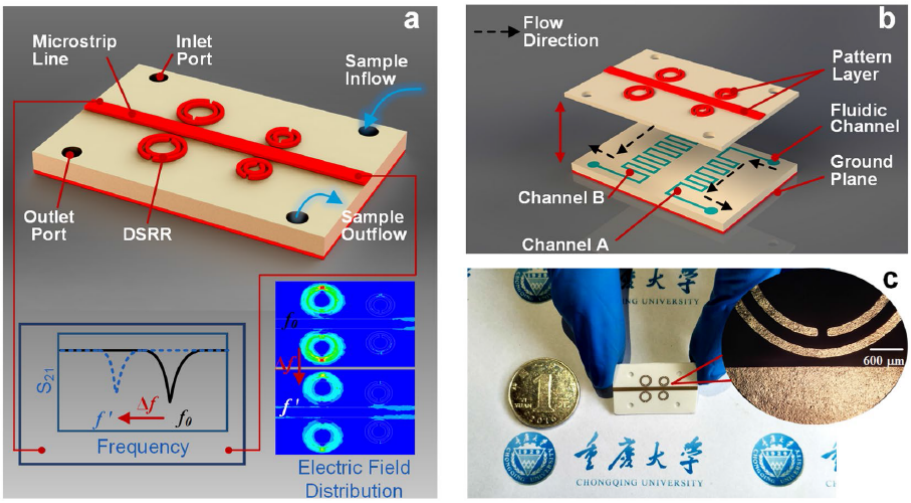

Figure 2.15: Multiband sensor including a meander microfluidic channel implemented beneath the resonators in order to increase the sensitivity [76].

is changed for 10% ethanol concentration variation and is compared with the deionized water and air as references. Antenna-based sensors can be a promising alternative to TL-based sensors in some applications, due to using one port in measurement and also enabling an antenna-like structure remote sensing approach [78,79]. The representation of this antenna-based sensor is shown in Fig. 2.16.

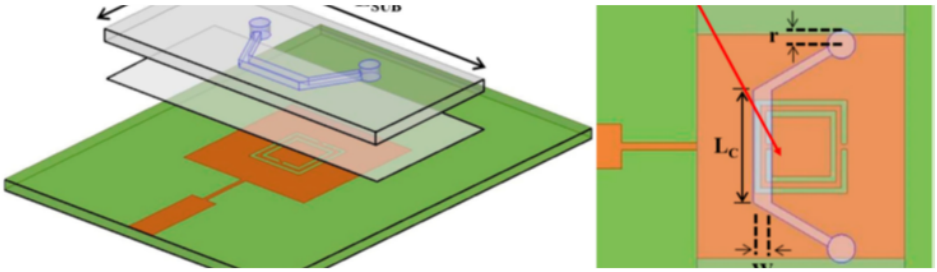

Figure 2.16: Monopole antenna applied as a microfluidic MTM sensor [77]

2.1.3 Sensors based on array structures

Periodic structures represent a potential candidate for sensor applications as they benefit from high resolution and accuracy [80]. As stronger left-handedness is achieved by improving the loading shunt inductances and also series capacitances, therefore, increasing the order of resonant elements and the number of MTM stages

may enhance the transmission/reflection peaks/notches [81]. Researchers in [82] proposed a structure creating a deep notch at the resonant frequency. Following this strategy, a meta-surface made up of 44 rectangular spiral SRR with high Q-factor is studied in [83] for characterizing different dielectric layers such as FR4 and polyimide. In [84], fractal SRRs are employed, leading to more compact sizes compared to conventional SRR resonators. It operates as a dual band sensor at 0.1 THz and 0.22 THz and is used for thickness measurement.

An array structure comprising 10×10 unit-cells provides a sensitivity of 150 MHz per unit relative permittivity. It has been applied for solid samples of teflon, plexiglass, and Rogers with frequency shifts up to 1233 MHz and also to liquid samples of Iso-propyl alcohol, ethanol, methanol, and deionized water with frequency shifts up to 130 MHz [85]. Its functionality is based on creating a strong peak when a lossy substrate or resistive liquid material is added to the resonant surface. For more flexibility in the sensor function, a tunable metamaterial array structure is proposed in [86] wherein a varactor diode is placed at the right side of split corresponding to split ring resonator. The resonant frequency can be changed by the inverse voltage applied to the varactor diode. This sensor is used in the food industry and has also been suggested for temperature and pressure sensing.

Although this class of sensors has a precise response and it benefits from good accuracy, generally speaking, the major drawback of these structures is the amount of MUT needed on the sensor surface. This is because the large area of array structures. For instance, one antenna in array configuration is introduced in [87] with trenches between resonators where the liquid should be inserted to change the resonant frequency. As a consequence, a large-scale amount of liquid for sensing approach is needed.

2.2 Coupling-based sensors

As mentioned before, this class of sensors operate on the basis of the variation of the coupling coefficient between cross-coupled resonators when the sample is placed on the sensitive resonant elements or between them. As depicted in Fig. 2.17a, a sensor including two coupled resonators is proposed in [97] and the sample under test is positioned between them. The electric coupling coefficient between resonators changes when the dielectric permittivity of MUT is altered. An analytical scheme is presented in this study [97] for the estimation of the coupling coefficient. This sensor has been experimentally tested with Diclad 880, Rogers 5870, Rogers 4003, TMM10i and Rogers 6010.

Based upon the coupling perturbation approach, another sensor is proposed in [98] for glucose tracking in the range of 1.25 % to 10 %. The container, placed on the gap region between resonators, needs 6 µL for the measurement process.

This sensor is shown in Fig. 2.17b. By increasing the impurities in the solvent such as glucose as a non-metalic material, there is a decrease in the effective dielectric constant and consequently a decrement in load impedance. This trend affects the reflection coefficient of the sensor straightforwardly; the reflection coefficient follows a downward tendency.

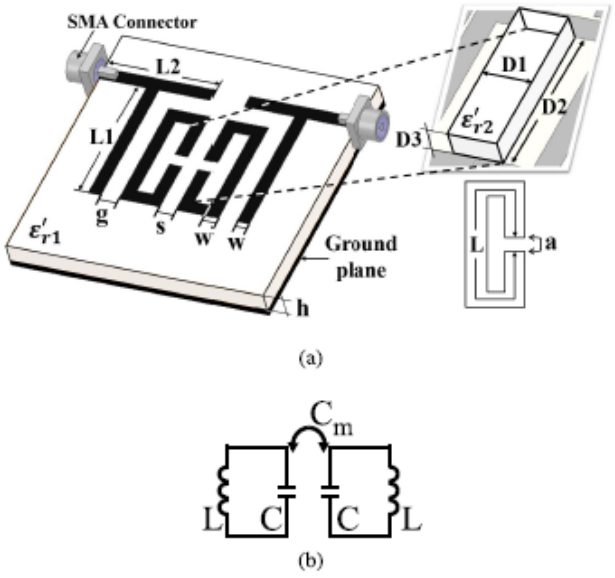

(a)

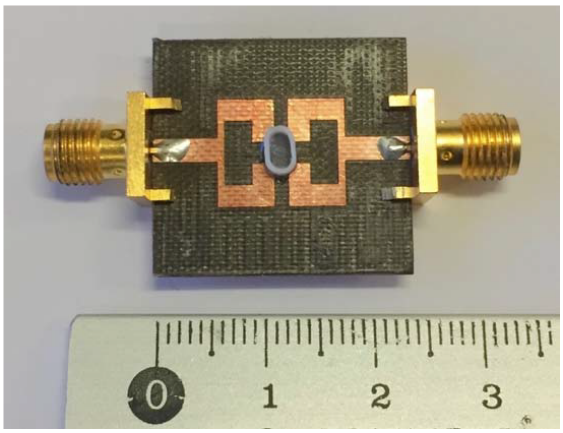

(b)

Figure 2.17: Characterizing the MUT specifications using estimation of the coupling coefficient between coupled resonators (a) for solid characterization [97] and (b) for liquid characterization using a container [99].

2.3 Differential sensors

To improve the microwave sensor functionality against environmental interferential aspects, one solution is using frequency-splitting sensors, commonly known as differential sensors [89]. In differential sensors, the principle of operation is based on the measurement of the cross-mode insertion loss created by the difference between the dielectric constants corresponding to the MUT and the reference material. This class of sensors may be highly sensitive to any perturbation in symmetry behavior. This symmetry is achieved when the host TL is coupled to two equal resonators. The resonator loaded with the sample under test creates a notch different from that of the unloaded resonator. Consequently, the MUT is identified using the information extracted by comparing the two notches; two non-identical samples will create two different split notches in the frequency response.

Smith et al., in [88] demonstrate a differential sensor based on a microstrip TL coupled to two identical SRR resonators. In this study, one resonant element is loaded with a sample different from the reference one. This sensor is shown in Fig. 2.18 and has been checked with solid materials.

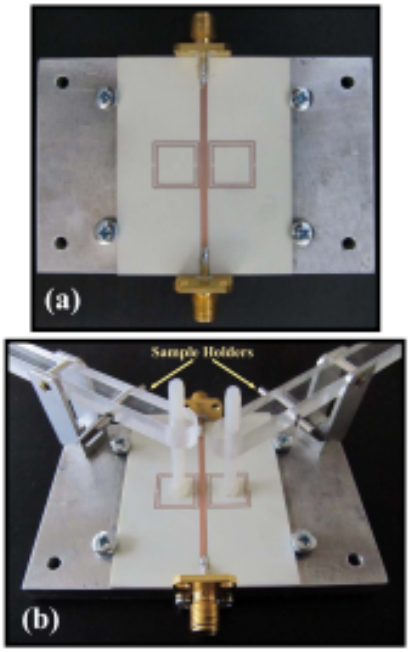

Figure 2.18: Microstrip TL coupled to identical SRRs with two non-identical samples creating two split notches as a differential sensor [88]

It should be considered that in this approach, the negative effects of the cou-

pling between resonators can be efficiently avoided by separating the resonators through splitter/combiner divisions. Based on this concept, a sensor in differential mode is studied in [89], wherein SRR resonant elements are coupled to a splitter/combiner with ethanol channels placed on top of the gap region of SRRs as illustrated in Fig. 2.19. Two transmission zeroes arise from disturbing the symmetrical axis and the notch depth and frequency between these transmission zeroes indicate the complex dielectric constant. In this reference, the structure has been fabricated on Rogers 3010 with ϵ_r= 10.2 and tanδ = 0.0023.

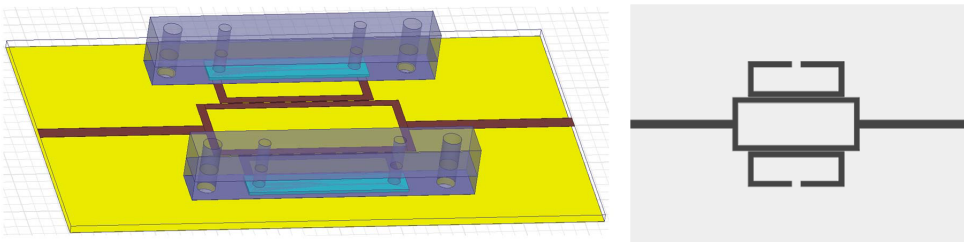

Figure 2.19: Differential sensor using splitter/combiner and microfluidic channels placed on top of the gap region of the SRRs [89]

In [100], an open complementary split ring resonator (OCSRR), resonating at 1.5 GHz is employed in a differential sensor, and [91] uses a squared-OCSRR for sodium monitoring with a sensitivity of 4.3 dB/g/L and dynamic range around 80. The usage of vias in OCSRRs resonator makes the fabrication more complicated than that of [89]. Similar to [89], in [93] a splitter section is used to weaken the disturbing coupling effects. This sensor, proposed by Su et al., consists of a splitter coupled to two CSRRs resonating at 1.9 GHz for solid samples with 300 MHz shift in the resonant frequency [93]. Both designs studied in [89] and [93] need an optimization process for a precise design.

Since composite right-/left-handed (CRLH) TLs improve the sensitivity, two CRLH TLs are employed in [94], in direct down conversion architecture. This CRLH constituted by an IDC is loaded with the MUT directly, as shown in Fig. 2.20. Compared to the sensors based on conventional TLs, this sensor demonstrates improved sensitivity in a wideband operation (4.2–8 GHz). Using the nonlinear dispersion characteristic of metamaterial TLs, this sensor can characterize the complex dielectric specifications. It is expected that when the number of metamaterial unit-cells increases, the higher sensitivity is achieved, at the cost of larger size. Moreover, by increasing the sample volume, the insertion loss will rise. However, this creates a saturation behavior after a large enough volume leading to an independency in the insertion losses. The sensor suggested in [94] has been tested with solid materials and liquids such as ethanol and methanol.

As two different phase responses are emerged when the lines are loaded by

different materials, there may be a relation between the phase variation and sensitivity. Due to the specific features of metamaterial TLs, MTM-inspired sensors provide higher phase difference compared to the conventional ones. According to this, an interferometry sensor improved by two CRLH TLs is proposed in [95]. Its efficiency has been only tested with solid materials.

Following the differential concept, in [96], the sensitivity is analyzed using two coupled resonators as Complementary Symmetric Split Ring Resonator (CS-SRR), Complementary Asymmetric Split Ring Resonator (CAS-SRR) and Complementary Bi Split Ring Resonator (CBS-SRR). These sensors, providing dual notch bands, has 34 to 45 percent sensitivity for solid materials. The relative permittivity ranges from 1.006 to 16.5. In more details, the sensitivity of CS-SRR sensor is between 15 to 34 % and 24 to 56 % corresponding to the first and second resonances respectively. The sensitivity of CAS-SRR sensor is between 11 to 25 % and 25 to 60 % for the first and second resonances respectively. The sensitivity of CBS-SRR sensor is between 12 to 33 % and 18 to 40% for the first and second resonances respectively. The proposed sensor configurations are shown in Fig. 2.21.

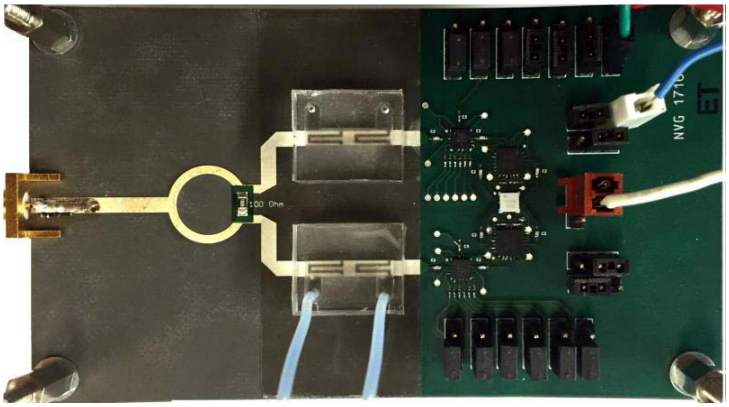

Figure 2.20: Improved sensitivity in a wideband operation(4.2 –8 GHz) using the nonlinear dispersion characteristic of metamaterial TL [94]

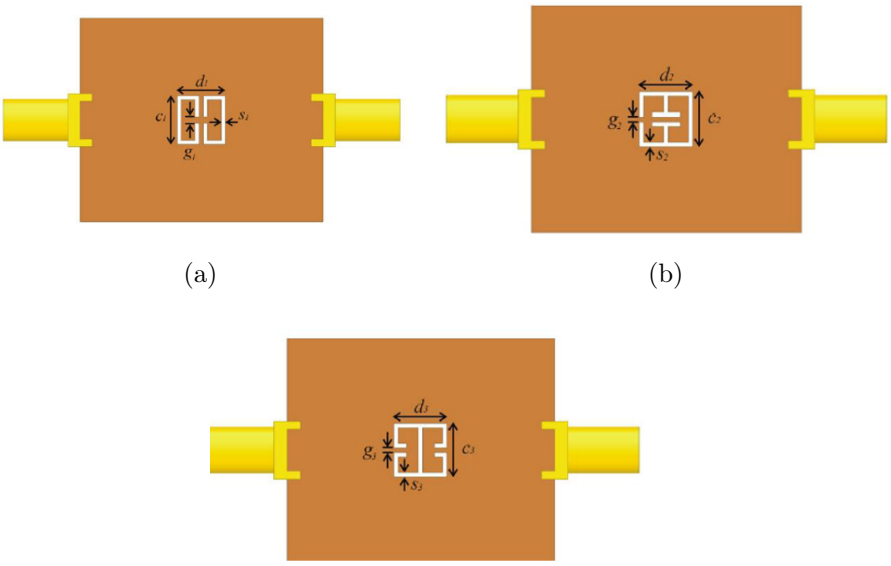

Figure 2.21: Differential sensors based on (a) CS-SRR, (b) CAS-SRR, (c) CBS-SRR etched on the ground plane of microstrip TL [96]

A summary of the differential sensor class is presented in Table 2.2.

Table 2.1: FREQUENCY-SHIFT SENSORS (Data are provided based on the original source papers)

Ref	Type of TL and resonator (Structure)	Material Under Test (MUT)	Sensitivity (Freq. shift (MHz)/%)/	Operation frequencies	Size (mm×mm)
[39]	SRR	thin films, paraffin, aceton, chloroform, oils	2.98% to 21.9%	1.8 GHz	12×6
[40]	CSRR	teflon, RO3003, FR4	0.33%	1.164 GHz	6×6
[41]	CSRR	multi-layer	348 MHz	S-band	6×6
[42]	hexagonal CSRR	banzene, hexane, teflon, PVC	900 MHz	5.3-8.2 GHz	4×4
[47]	S-shaped	RO4003, FR4	150 MHz	1.6-1.9 GHz	35×35
[48]	SSRR	Rogers 5880, Rogers 4350, FR4	90 MHz	2.22 GHz	2 π × 15.85
[49]	labyrinth resonator	methanol/ethanol-water	15-25 MHz	4 -5 GHz	2π × 15.87
[50]	CSR	Rogers RO4003C, RO3010, nelco N4350-13, FR4	24.6% upto 44.82%	0.8-2 GHz	12.8×12
[51]	Split Ring	glucose in low concentration	20%	2 GHz	20×15
[52]	Double-Sided SRR	ethanol/methanol-water	0.547%	300 MHz	20×9.6
[53]	multi SRR	Duroid, rexolite, FR-4, pexiglass	300 MHz	5 GHz	2.1 × 9.9
[55]	SRR	Alcohol and Acetone	1.4 GHz	4.19 GHz	6.7×6.7
[56]	IDC+SRR	rubber, plastic, magnetite, ferrite core	45 MHz	2.2-2.8 GHz	44×24
[57]	OCSRR	ethanol, methanol, butanol	126 MHz	330 MHz	4.1 × 4.6
[58]	hexagonal SRR	NaOH, HCL	2 dB/(1 unit PH)	3-20 GHz	19×23.35
[59]	SRR, defected ground plane	glucose	100 MHz	8.3 GHz	2π ×6.5
[60]	SRR	acetone, propyl alcohol, methanol, ethylene glycol	23.52%	5.198 GHz	16×10.5
[61]	IDC	air to water	300 MHz	2.4 GHz	15×33.7
[63]	IDC	glucose	9 MHz/gdL^{-1}	4.1 GHz	25.15×16.4
[65]	CSRR	plexiglas, PVC, teflon	570 MHz	1.5,2.4,3.8,5.8 GHz	2π ×6.3
[66]	SCSRR	petrolium, kerosene, edible oil	100 MHz	1.87,2.64,3.49,4.34 GHz	2π ×7.5
[67]	CSRR	Rogers 6006, FR4, carbonyl-Iron rubber	380 MHz	2.47 GHz	7×7
[68]	CSRR	BNP, AG, AM	20-100 MHz	4.48 GHz	5.24×5.24
[69]	Open-loop Resonator	Toluene, IPA, ethanol, methanol	900 MHz	2.6 GHz	20×7
[71]	IDC+SRR	glucose	70 MHz	3.96 GHz	5×3
[72]	CSRR	ethanol	400 MHz	1.8 GHz	11×11
[73]	CSRR	ethanol	50 MHz	2.35 GHz	6.2×6.2
[75]	IDC	ethanol	63 MHz	20 GHz	1.3×0.18
[74]	SRR	ethanol, methanol	125 MHz	2.1 GHz	-
[77]	CSRR	ethanol	300 MHz	4.16 GHz	5×5
[83]	SRR	FR4, polyimide, Rogers	15%	0.2 THz -1.6 THz	0.036 × 0.036
[84]	fractal SRR	photo-resist, quartz glass	37.8 GHz	0.22 THz	0.3×0.3
[85]	SRCR	ethanol	600 MHz	8.9-10.4 GHz	6×6

Table 2.2: DIFFERENTIAL SENSORS(Data are provided based on the original source papers)

Ref	Type of TL and resonator (structure)	Material Under Test (MUT)	Sensitivity (freq shift (MHz)/%)	Operation Freq	Size (mm× mm)
[88]	SRRs	Rogers 3006, 3010, FR4	350 MHz	2.1 GHz	11×11
[89]	SRR	ethanol	60 MHz	0.87 GHz	25 × 9
[90]	SRRs	NaCl, KCl, CaCl_2, urin samples	12.27 dB/g/L	0.95 GHz	24× 8.17
[91]	OCSRR	ethanol, methanol, sodium	4.3 dB/g/L	1.2 GHz	14× 4.35
[92]	SRR	Rogers RO5880, RO4003, RO3006	200 MHz	1.75 GHz	0.125λ_g × 0.125λ_g
[93]	CSRR	Rogers RO3010, 4003, arloncuclad 250	300 MHz	1.9 GHz	7.86×4.8
[94]	IDC + CRLH TLs	ethanol, methanol, xylene, DMSO	1.3 GHz	4.2-8 GHz	2π × 3.5
[95]	IDC	rohacell foam	60 dB/ ($\Delta\varepsilon = 10\%$)	2.3 GHz	-
[96]	CS-SRR, CAS-SRR, CBS-SRR	solid MUTs	10-50 %	4-8 GHz	6×6

Chapter 3

Proposed DR Sensors: Theoretical Analysis

In frequency-domain category, many structures have been applied to characterize liquid materials and solutions. In many cases, this type of sensors such as submersible ones, require a big amount of fluid material as they should be merged in the solution [39, 101]. In some applications such as biological testing, the necessity to afford this volume of material is squandering. To tackle this problem, microfluidic sensors are proposed. Microfluidic sensors with low volumes and high accuracy are promising as they can be developed in chip-based compact configurations [92], [102]. Compared to the submersible sensors, microfluidic sensors suffer from more complexity and cost as a microfluidic channel is located on the most sensitive area of the resonators. A comprehensive review was given in previous section. Although the aforementioned sensors demonstrate an acceptable sensitivity and dynamic range, the detection of small variations in permittivity of samples is limited by the resonant elements; especially in some structures, the saturation behavior emerges after a specific level. Indeed, there is a limitation in the range of capacitors in the planar resonators which can be incorporated as sensing elements. As a result, the sensitivity is limited in the planar resonator-based sensors. In addition, by decreasing the operation frequency, the size of structures gets larger, considered as a serious concern. In order to increase the sensitivity, several attempts have been made. For instance, substrate-integrated waveguide (SIW) technology maintaining the functionality of conventional waveguides benefits from high Q-factor and high power handling capability [103]. However, they suffer from complexity in fabrication. The array configuration is another strategy for increasing the sensitivity and Q-factor. This type of sensors with high performance suffer from large surface area and hence, the need for a big amount of sample [104].

Dielectric Resonators (DR) are made up of ceramic materials and some commercial polymers. Their high dielectric permittivity, leading to high stored energy

within the DR cavity and low dissipation (loss) factor, makes these resonators a promising alternative. These resonant elements have been applied to oscillators, filters and antennas for decades [24–27]. Recently, DR with high efficiency, compact size and cost-effectiveness have attracted the researcher's consideration in sensing applications [26, 28–32]. As of now, this class of sensors work at very high frequencies (Terahertz) and mostly use whispering gallery modes (WGMs). Furthermore, a wide range of ethanol has not been studied yet.

This chapter is devoted to the dielectric resonator sensors in different configurations and structures working in microwave frequency range. In each sensor, the feeding mechanism is different according to the structure to get better efficiency. In this chapter, two different Dielectric Resonator (DR) sensors are studied. The proposed sensors consist of a DR in different configurations and feeding methods. The modal analysis and analytical circuit model are given. The first sensor, named Dielectric Resonator Antenna (DRA), is a novel DR sensor for liquid characterization. This is based on a cylindrical DR working in the 2.45-GHz band excited by slot feeding (DR feeding mechanisms will be explained in section 3.1). This feeding technique is based on a microstrip transmission line (TL) with a slot in its ground plane. The DR is placed over the ground plane and coupled to the TL through the slot. By creating a small pool on top of the DR surface, the liquid under test (LUT) can be placed and sensed as a slight change in the resonant frequency is induced. This frequency change depends on the dielectric characteristics of the LUT, allowing an accurate determination of solvent concentrations. The second sensor, named as DR shielded sensor (DRS), is excited by a parallel microstrip transmission lines. The main property of this structure is hosting the whole structure in a metallic box in order to avoid radiation loss. Unlike the DRA sensor, this uses a filtering approach instead of an antenna framework. This may make sensor more accurate and precise to any changes in the sample and it makes it suitable for measuring of small variations of liquids.

By considering a cylindrical DR, as commonly used due to its symmetrical structure and properties, different modes in different frequencies can be excited and confined inside the DR. The fundamental resonating modes supported by a cylindrical DR can be calculated with the following equations [105]:

$$(f_r)_{TE,nmp} = \frac{c}{2\pi\sqrt{\epsilon_r\mu_r}}\sqrt{\left(\frac{Bx_{np}}{a}\right)^2 + \left(\frac{(2m+1)\pi}{2h}\right)^2} \tag{3.1}$$

$$(f_r)_{TM,nmp} = \frac{c}{2\pi\sqrt{\epsilon_r\mu_r}}\sqrt{\left(\frac{Bx'_{np}}{a}\right)^2 + \left(\frac{(2m+1)\pi}{2h}\right)^2} \tag{3.2}$$

wherein Bx_{np} and Bx'_{np} correspond to the roots of the mathematical Bessel functions of the first kind and the relevant first-order derivatives, respectively. The

radius(a) and height (h) as well as relative permittivity of the constitutive materials for the DR have a strong impact on the resonant frequency of different modes. The resonant frequency will increase as either the radius or height decreases. Next section discusses different types of DR feedings.

3.1 DR feeding mechanism

In order to electromagnetically excite the DR, different feeding structures can be applied to the DR as illustrated in Fig. 3.1. All these configurations are able to feed energy to the DR while creating a significant impact on the resonant frequency of the prominent excited mode and its Q-factor. These methods can be generally classified into three different categories as: 1) direct transmission line (TL) connection to the DR, 2) coaxial cable implemented into the DR by drilling and 3) slot or aperture coupling by a microstrip TL or a coplanar waveguide (CPW) transmission line. There are some advantages and disadvantages in any feeding mechanism.

The coaxial feeding method is the most common one in DR feeding. However, in this case different modes can be excited leading to a deformed radiation pattern and co-existence of more than one pure DR mode and dissipating energy thereby. This deficiency can be controlled somehow by changing the position of the probe and increasing the coupling strength between DR and feeding line [106].

The microstrip fed line is mostly used in microwave circuits and is considered as the simplest way for DR excitation and it can be placed directly over the TL without the need for drilling or making an aperture into the ground plane. However, in this method, excitation of highly-undesired surface wave in the dielectric substrate is inevitable.

By considering a CPW feeding line, a high frequency response can be achieved as no parasitic discontinuities are in the ground plane in the form of all grounds in the same plane as the connection strip. However, heat dissipation is the main disadvantage of this technique.

The slot/aperture feeding scheme is used to tackle the mentioned problems. This aperture can be implemented into the ground plane of a microstrip transmission line and the DR can be excited using the coupling between the TL and aperture. The coupling strength can be controlled by either adjusting the size of the slot or moving the DR with respect to the slot. This method is attractive for the integration of DR into the printed fed structures, although there might be back radiation due to the aperture in the ground plane.

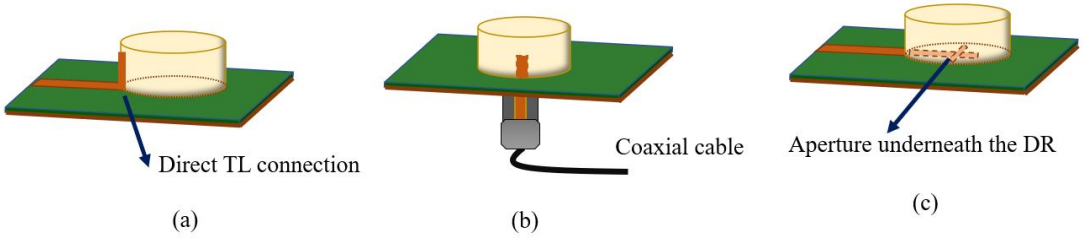

Figure 3.1: Different common feeding techniques applied to DR: (a) direct feeding using microstrip TL, (b) probe feeding, inserted inside the DR, (c) aperture feeding method.

3.2 3D Electromagnetic simulator

This thesis focuses on the design and analysis of DR sensors using a 3D electromagnetic simulator. The CST MWS (Computer Simulation Technology Microwave Studio) is a powerful tool for designing 3D structures, specially at high frequencies and mm-wave frequency range. This simulation software is based on the finite element method and as a feature, is very user-friendly. CST offers different modules in several problems and different solver techniques such as transient solver, frequency solver, and eigen-mode solver. The discretization of the structure, similarly to any numerical solver, plays a crucial role and it is really important for obtaining an accurate response, although at the cost of more time consumption for very fine meshing. The S-parameter extraction is commonly used for comparing the results and helpful in the optimisation approach. In this thesis, eigen-mode solver is used to find the prominent mode in the DR that it has maximum energy and then the frequency domain is applied to the solver for extraction of S parameters.

3.3 DR Antenna (DRA) design fed by an aperture

The topology of the proposed sensor is shown in Fig. 3.2. It consists of a microstrip TL and a slot-fed cylindrical DR. The axis of the DR is aligned with the z axis and the feeding microstrip TL (with width w and length l) is adjusted to 50Ω. The port of the sensor is located at the beginning of the microstrip TL. The slot is etched on the ground plane beneath the DR which is constituted by a dielectric cylinder with the radius r_d, height h and ϵ_r dielectric constant. The DR bottom is fixed on the slot and the metallic ground plane. The dimensions of the slot are w_S and l_S. A small cylindrical pool with radius r_h and height h_h is embedded on top of the DR. This tank is used to allocate the liquid samples under test.

The dielectric cylindrical cavity resonator is conceptually similar to a circular

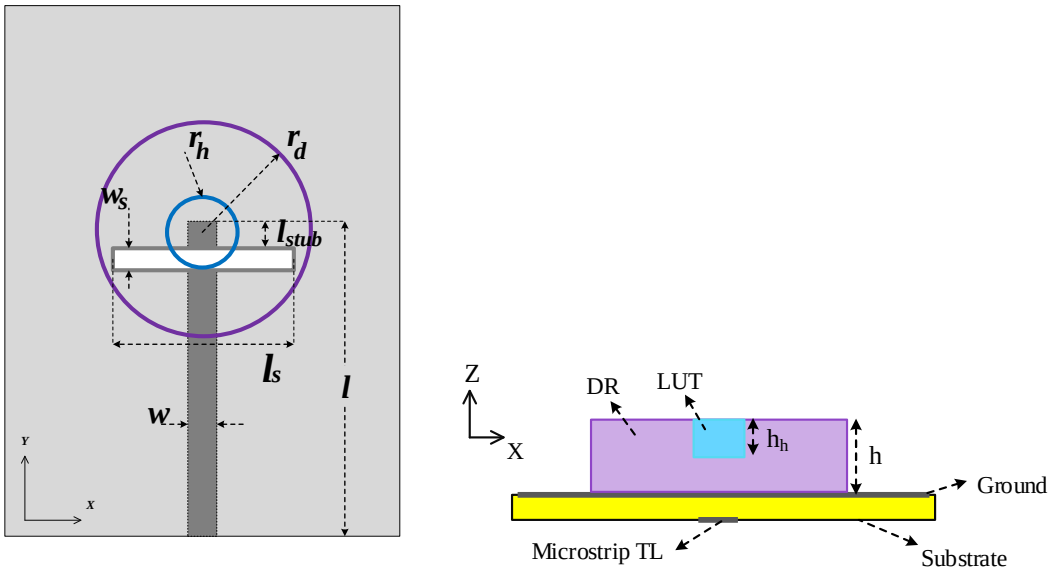

(a) (b)

Figure 3.2: DR Sensor (a) Front view, (b) Side view, with generic dimensions. The prototype's dimensions are reported in Table 4.2.

waveguide. The total energy corresponding to the electric and magnetic fields are stored inside the cavity, affected by the dielectric permittivity of the DR. According to Fig. 3.3, the cylindrical cavity resonator can be considered as a parallel RLC circuit where R, L, and C_1 are defined as the parallel resistance, inductance and capacitance of the DR. Accordingly, the reflection coefficient Γ_{in} can be obtained as

$$\Gamma_{in} = \frac{Z_{in} - Z_0}{Z_{in} + Z_0} \tag{3.3}$$

where Z_{in} is the input impedance of the circuit and Z_0 is the intrinsic impedance of the port.

The resonant frequency of the DR can be defined as $\omega_0 = \frac{1}{\sqrt{LC_1}}$ and the unloaded Q-factor of DR can be interpreted as $Q_0 = \frac{\omega_0 L}{R}$. In critical-coupled condition wherein Z_0 equals to Z_{in}, the reflection coefficient approaches to zero. Through the implemented slot, the DR is coupled to the excited electromagnetic waves inside the microstrip host line. This is shown by the mutual coupling capacitor defined as C_m. By loading the DR to the TL, the resonant frequency of the loaded DR and subsequent loaded Q-factor are changed to $\omega = \frac{1}{\sqrt{L(C_1+C_m)}}$ and $Q_L = \frac{\omega L}{(Z_{in}+R_{loss})}$ respectively. Here, R_{loss} is defined as lossy resistance corresponding to the TL and radiation dissipation.

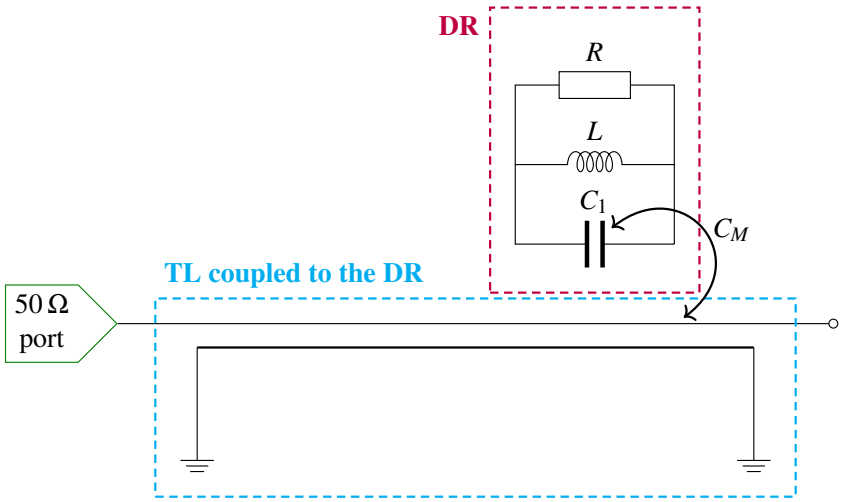

Figure 3.3: Circuit model of the DR coupled to the microstrip transmission line. The cylindrical cavity resonator is modeled as a parallel RLC circuit where R, L, and C_1 are defined as the parallel resistance, inductance and capacitance of the DR. The C_m capacitor is influenced by loading lossy liquids in the tank which is located on the sensitive area of the DR and accordingly the equivalent capacitance value $(C_1 + C_m)$ is changed.

The C_m capacitor is influenced by loading lossy liquids in the tank which is located on the sensitive area of the DR where the electric and magnetic fields confinement is strong. In particular, the total effective permittivity is perturbed when the hole is filled by the liquid sample (LUT). Therefore, every change in LUT leads to changes in ω and Q_L. Thus, this event makes changes in the Z_{in} and consequently the Γ_{in} changes. The changes observed in this parameter depends on the LUT. As a summary, the resonant frequency of sensor depends on the LUT and this is employed as the main sensing principle.

3.3.1 Modal analysis and perturbation method applied to the DRA sensor

Using electromagnetic theory, we can analyze the behavior of the DR sensor. A cavity electromagnetic model governs DR operation and the analysis of the confined fields inside the DR can be conducted using the cavity resonator model. In the simulations, first the Eigenmode solver in CST software is used to roughly find the fundamental resonant frequency of the DR and the fields at that resonant frequency. It is approximately considered that the outer surfaces of the cavity are

perfect magnetic conductors (PMC) because of the high permittivity of the DR and the high dielectricity of the structure. Therefore, all tangential magnetic fields and the surface current density are set to zero. This property can be interpreted as a high surface impedance. In other words, there is no way for electric currents (volume, surface, or edge currents) to flow into perfect magnetic conductor boundaries, as it would violate current conservation laws [105]. In this approach, the eigen equations can be applied for the prediction of the DR resonant frequencies [28]. For practical purpose, pure TM_{nmp} and TE_{nmp} modes exist when the fields do not depend on the angular coordinate. Otherwise, the propagating mode is a combination of a TM and a TE mode, defined as Hybrid modes represented as HEM_{nmp}. The subscripts n, m and p are nomenclatures identifying the mode classification. The lowest of them is HEM_{110} [107]. As the radius of DR increases, the number of TE and TM modes and subsequently the hybrid modes number increases. The $HEM_{11\delta}$ mode, so-called dipole mode, is widely used in the DR structures in which δ is a non-integer value less than unity.

For small values of r_d, the field propagating outside of the DR can extend for a long distance whereas the fields for a large-radius DR are stronger confined closer to the DR. In this case, the phase constant β approaches to $\sqrt{\epsilon_r}\beta_0$ when the radius approaches to infinity considering β_0 the phase constant in free space. Therefore, the phase velocity is less than that of free space [105]. Unlike the fields equations for TM and TE modes which include both $\cos(m\phi)$ and $\sin(m\phi)$, the HEM modes have only either $\sin(m\phi)$ or $\cos(m\phi)$ components.

According to the previous explanation, HEM modes are excited inside the DR used as the base of the proposed sensor (Fig. 3.2). More specifically, the fundamental excited inside the DR is $HEM_{11\delta}$ [108, 109]. The resonant equation corresponding to the understudy $HEM_{11\delta}$, for the least value of $\delta = 0$, simplifies to [105]:

$$(f_r)_{110} = \frac{c}{2r_d\pi\sqrt{\epsilon_r}} \times \left(1.71 + \frac{r_d}{h_d} + 1.578\left(\frac{r_d}{2h_d}\right)^2\right) \tag{3.4}$$

This resonant frequency corresponds to the unloaded equivalent cylindrical DR (i.e., the sensor without liquid loading). When a small amount of liquid is inserted in the cavity, the resonant frequency changes and an increment in the effective permittivity causes it to descend, as explained by eq. 3.4. On the other hand, the electromagnetic fields inside the DR remains almost unchanged. This can be also explained through the cavity perturbation technique. This technique is an accurate scheme which can be applied to analyse the change in the electromagnetic field distribution inside the cavity when the sample volume is very small to produce a negligible perturbation [110]. Here, the sample is considered as a thin-enough cylinder occupying the proposed hole which can satisfy the accuracy requirements for higher order modes. The fractional change in the resonant frequency due to

the LUT can be rewritten as follows (refer to the Appendix for more details):

$$\frac{\omega^{'}-\omega}{\omega}=\frac{-\iiint_v\left(\Delta\varepsilon\left|\vec{E}\right|^2+\Delta\mu\left|\vec{H}\right|^2\right)dv}{\iiint_v\left(\varepsilon\left|\vec{E}\right|^2+\mu\left|\vec{H}\right|^2\right)dv} \tag{3.5}$$

where E and H are the electric and magnetic fields of the equivalent cylindrical DR (without any tank), ω and $\omega^{'}$ are the resonant frequencies of the DR before and after placing LUT, respectively and Δ shows the variation in permittivity and permeability made by the LUT. According to Eq. 3.5, it can be clearly seen that by increasing the permeability and permittivity, there is a decrease in the resonant frequency, illustrating an increase in the stored energy in the resonant cavity. Furthermore, the resonant frequency variation depends on the location of the perturbation factor. In other words, this fractional change in the resonant frequency is the result of interaction between electromagnetic fields inside of the DR and the LUT.

3.4 DR shielded (DRS) sensor fed by a parallel microstrip transmission line

In this section, another sensor is studied with the DR. As the fields extend beyond the DR, these evanescent fields provide an external coupling to the vicinity of the dielectric resonators. Based on this concept, another structure used as a sensor is proposed in this section. This structure includes a DR coupled to parallel microstrip transmission lines. In order to eliminate the detrimental environmental effects, a metallic box surrounding the DR is employed to remove the radiation loss. This leads to a great accuracy and high resolution, suitable for precisely measuring small variations in concentration of material under test, especially in biological samples.

The DR sensor in the box structure is studied as second sensor in this chapter. This configuration is according to a a DR positioned in a shielded box and is fed using a parallel microstrip transmission lines. This structure is commonly used to work as an oscillator and this thesis is going through this DR- shielded structure as a sensor. In the following, the sensor is explained in detail.

Similar to the previous sensor structure, the discontinuity between relative permittivity of the DR and surrounding air leads to a large reflection coefficient at the interface between these materials resulting in a standing wave inside of the DR. This sensor is excited by a parallel microstrip transmission lines. The sensor structure is shown in Fig. 3.4. The goal is to have the whole structure in a

metallic box in order to avoid radiation loss. However, without the metallic box, it is practically working, as the measured values prove this concept in the following. In this approach, the liquid or the material under test (MUT) is placed on the hole

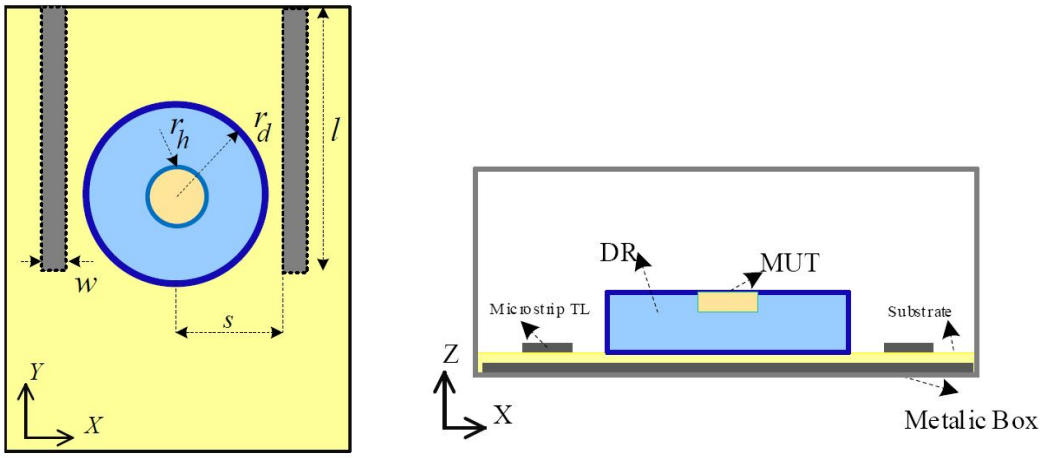

(a) (b)

Figure 3.4: Shielded DR sensor fed by a parallel microstrip transmission line (a) Front view and (b) Side view, the dimensions are $l = 30$ mm, $s = 17.4$ mm, $w = 2.95$ mm, $r_d = 17$ mm, $r_h = 4$ mm. The same DR in DRA sensor is used.

at the center of DR. The coupling coefficient depends on the distance between DR and TLs.

3.4.1 Modal analysis and perturbation method applied to the DRS sensor

In this configuration, the shielded DR is operating in fundamental $TE_{01\delta}$ mode in which δ is a non integer lower than the unity. The electric E-field is intensely confined at the center leading to an accurate response to any change in the field distribution. According to the perturbation theory, tuning the distance between the upper metal and the DR surface affects the stored electromagnetic energies of resonant element, and subsequently changes the propagating modes inside of DR. It should be considered that when the upper metallic plate comes closer to the DR surface, the resonant frequency increases. It is because the total tangential electric-field components are zero on the perfect electric conductor whereas the magnetic-field components are strongly perpendicular to the metal surface. The resonant frequency corresponding to the transverse electric (TE) can be written

as [105]:

$$(f_r)_{mnp}^{TE_z} = \frac{1}{2\pi\sqrt{\mu_d \epsilon_d}} \sqrt{\left(\frac{X_{nm}}{r}\right)^2 + \left(\frac{p\pi}{h}\right)^2} \tag{3.6}$$

wherein X_{np} are referred to as the eigenvalues for the dielectric rod resonator. The modal analysis is carried out using Eigen-mode solver in CST and the results are illustrated in the next chapter.

Chapter 4

Full-Wave Analysis, Simulation and measurement

This section is devoted to the analysis of the performance of the proposed sensor. The CST simulation and modal analysis as well as measurements are included in this chapter.

4.1 DRA Sensor

A full-wave simulation of the DRA proposed sensor was performed by using CST Studio Suite. Figure 4.1 shows the electric and magnetic field distributions of the fundamental mode. The expected $HEM_{11\delta}$ mode is excited inside of the DR in which δ is a non integer lower than the unity. These field distributions are similar to the ones of a conventional cylindrical DR [111]. The fields are confined in the pool when a sample is placed, as it can be seen in Fig. 4.1(e) compared to Fig. 4.1(d). This last interaction produces the desired frequency shift depending on the pool filling.

Parameter	TL Substrate (FR4)	DR (Zirconia)
ϵ_r	4.3	29.1
$\tan(\delta)$	0.025	0.0019

Table 4.1: Permittivity and $\tan(\delta)$ of the transmission line (TL) substrate and the DR used in the sensor.

Variable	Dimension [mm]
r_d	17
h	8
r_h	4
h_h	2.5
w	2.95
l	74
w_s	0.7
l_s	32
l_{stub}	6.65

Table 4.2: Dimensions for the fabricated sensor. Variables are referred to Figure 3.2.

Next, the sensor is tested with different ethanol-water solutions. Industrial and consumer products use ethanol in large quantities. A variety of products are made from ethanol, including drugs, plastics, lacquers, polishes, plasticizers, and cosmetics. In medicine, ethanol is used as an anti-infective and as an antidote for ethylene glycol or methanol overdoses. A variety of commercial products contain ethanol, including beverages, perfumes, aftershaves and colognes, medicinal liquids, mouthwashes, liniments, and some rubbing alcohol [112]. A description of the methodology for operating the sensor follows.

First of all, the structure depicted in Figure 3.2 was optimized to obtain a sensor working in the ISM 2.45-GHz band, chosen because this is a freely available band, widely used in wireless applications, and with a handy availability of off-the-shelf-components. CST Studio Suite was used to perform the electromagnetic analysis of the sensor and the optimization of the DR and the coupling TL. The dielectric characteristics of the sensor and the final dimensions used for the simulation and fabrication are shown in Table 4.1 and Table 4.2.

Then several mixture of ethanol and water are placed inside a small pool made in the DR ($\sim 130\ mm^3$). Due to its design, the electric-field distribution is strongly confined in the well region, interacting with the liquid under test (LUT) volume. The simulated results of the S_{11} parameter (reflection coefficient of the sensor, Γ_{in}) are shown in Figure 4.2.

It can be seen how the original sensor without LUT is resonating at 2.48 GHz (dashed line). To emulate the loading with different ethanol-water concentrations, results from the permittivity model described in Appendix B were used. Figure 4.2 also shows the behaviour of the sensor for the different solutions. As it could be expected, the resonance frequency increases as the ethanol concentration does, following the opposite trend of the disolution's permittivity. This is, higher permittivities are related to lower concentrations, of ethanol which, in turns, leads

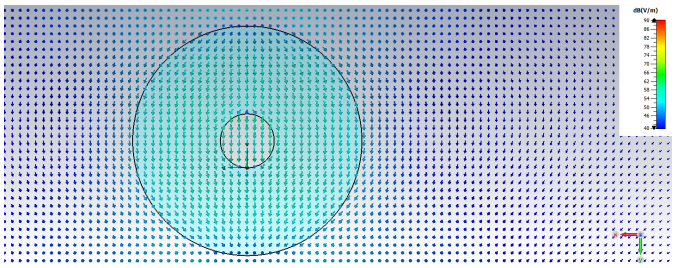

(a)

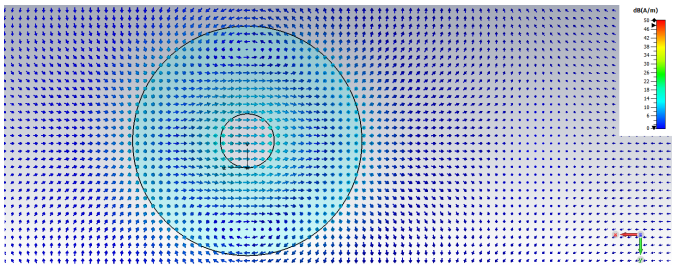

(b)

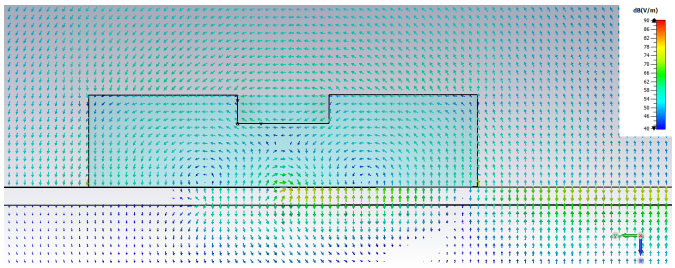

(c)

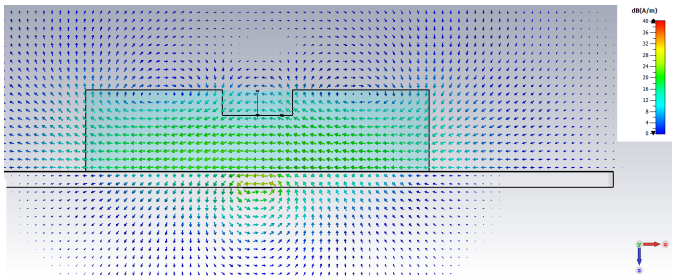

(d)

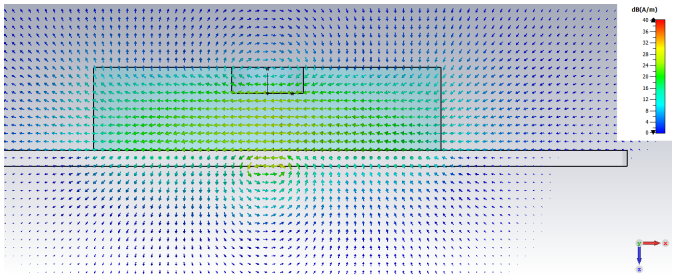

(e)

Figure 4.1: Electric and magnetic field distributions of the fundamental mode (a) E field top view (unfilled sensor), (b) H field top view (unfilled sensor), (c) E field side view (unfilled sensor), (d) H field side view (unfilled sensor), (e) H field side view (sensor with water).

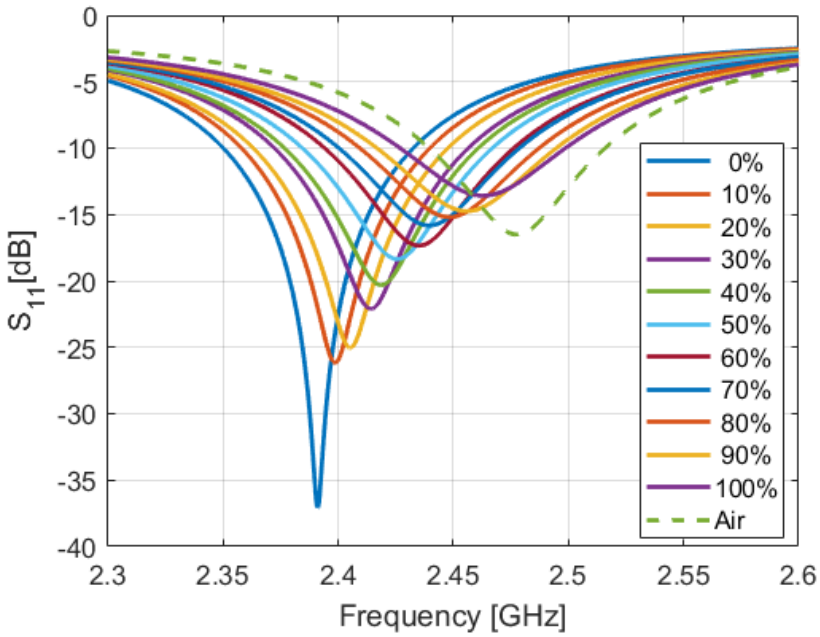

Figure 4.2: S_{11} simulated sensor response to different ethanol-water concentrations. Lines indicate the percentage of ethanol in water.

to higher resonance frequencies, as expected by eq. 3.4. In conclusion, simulation results are in agreement with the desired operation principle of the sensor.

4.1.1 Measurements and discussion for the DRA sensor

To evaluate the accuracy of the design outside of a simulation environment, the sensor depicted in Figure 3.2 has been fabricated and tested in a laboratory environment. A picture of the prototype can be seen in Fig. 4.3. The sensor has been fabricated by CarboSystem [113] and the base PCB by Eurocircuits [114] using standard processes, which helps in maintaining the cost of the sensor reasonably low.

Figure 4.3: Picture of the manufactured prototype.

Measurements referred in the following are done using an Anritsu MS46122B

Vector Network Analyzer (VNA) to extract the S_{11} parameter of the sensor in the working band when placing ethanol/water concentrations in the range of 0% to 100% (taking steps of 10%) and without any LUT (air). The final sensor will be fitted in an *ad-hoc* electronic transceiver similar to the one presented in [115].

To evaluate the design versus the simulation a series of 61 measurements per concentration, summing up to a total of 732 measurements (from 0% to 100% concentration and including the air), cleaning the sensor between tests with distilled water and drying it with a microfiber cloth. All the measurements were made at laboratory average temperature, that is, between 20 and 25 degree Celsius, to remove this variable from the study.

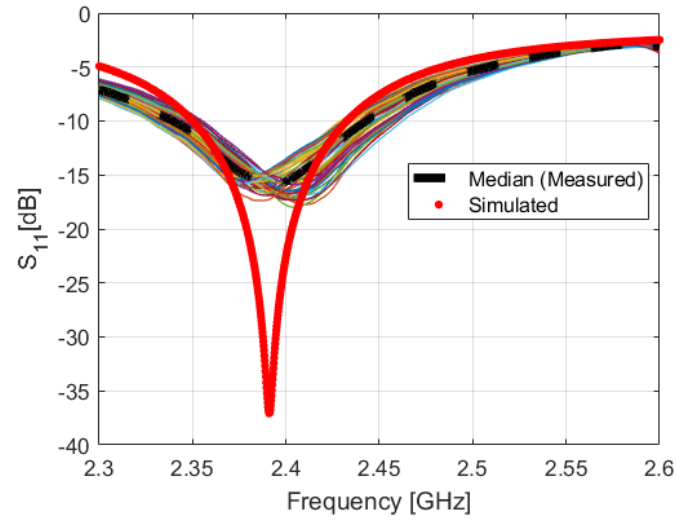

(a)

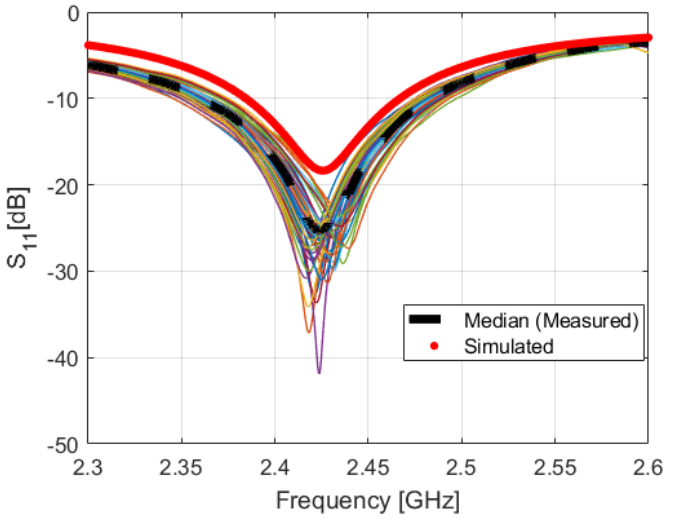

(b)

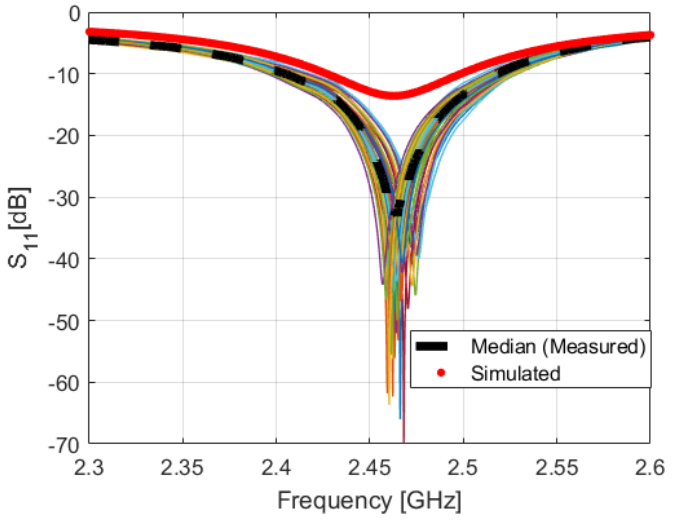

(c)

Figure 4.4: Sensor response for different ethanol concentration. Simulated (red) versus measured (the thick dashed line is the average of the 61 measurements done for each concentration, that are drawn in thin colored lines). (a) 0% ethanol, (b) 50% ethanol, (c) 100% ethanol.

Figure 4.4 shows a comparison of the S_{11} parameter for the simulated and fabricated sensor. Measurements on the fabricated sensor are done using different concentrations of ethanol and water. Figure 4.4(a), (b) and (c) shows the behaviour with distilled water (i.e., 0% ethanol), 50% of ethanol in water and 100% ethanol, respectively. Figures show colored lines with the different measurements taken, on top of them there is a black-dashed line indicating the median curve (here median represents the middle value of datasets) and a red-dotted line with the simulation result, for comparison.

It is worth to notice that, although the resonant frequency shifts and is different from the nominal frequency of 2.4 GHz, the changes are relatively tiny; using (eq. B.1 and eq. B.2) the maximum permittivity variation due to the frequency shift can be assessed as a mere 0.3 in absolute value. This implies that the change in resonance frequency is fundamentally due the percentage change in the LUT, as expected.

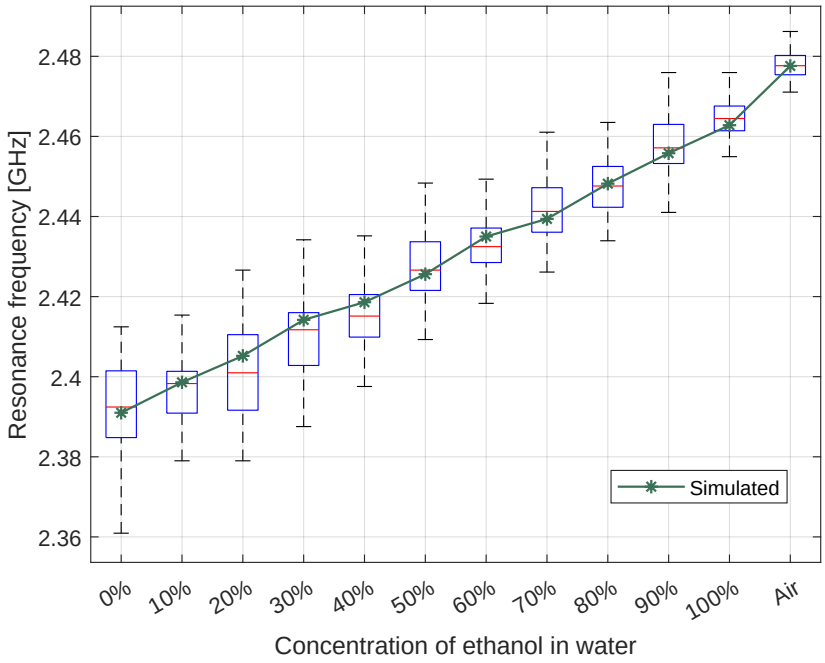

Figure 4.5: Statistics of the resonance frequency as a function of the ethanol concentration. Boxplots are for measured data (mean value and standard variation over 61 experiments per concentration) while the line is for the simulated sensor.

As it can be seen, although there are some variations in the measurement (due to the sensitivity of the DR and the possible differences in LUT quantities applied),

the overall trend is consistent. In addition to this, the position of the resonance in the simulated and average-value curve is in good agreement.

There exist a small discrepancy in the depth of the resonance, which can be attributed to a mismatch in the $\tan(\delta)$ value used in the simulation and the actual value for the DR.

To provide more detail about the repeatability of the measurements, Figure 4.5 shows a boxplot representation of the position resonance frequency for different concentrations. It can be seen how the statistics of the measurements are in good alignment with the simulated results, as the mean measured values (red line inside the box) are very similar to the simulated results (green line). This same figure shows a consistent trend in the resonance frequency change as a function of the concentration for both measurements and simulations. With respect to the sensitivity of the DR sensor, looking at the slope of the line in Figure 4.5, it can be approximated to 718 kHz per percentage of ethanol in water.

4.2 Full-wave analysis and CST results for DRS

This section is devoted to the analysis of the performance of the DRS proposed sensor. The DRS is simulated with different water-based ethanol solutions. The CST Studio Suite was used to perform the electromagnetic analysis of the sensor and the optimization of the DR and the coupling TL. The shielded metal on top of the sensor is considered as the boundary condition in the simulated analysis, modeled by a perfect electric conductor. DR sensor in coupled-line feeding configuration without metal shield is shown in Fig. 4.6.

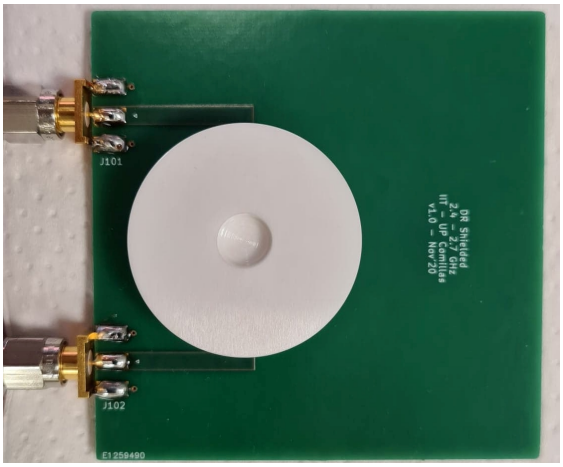

Figure 4.6: DR sensor in coupled-line feeding configuration without metal shield.

The TE mode has the most energy concentration and it is used as the main

prominent mode in this structure. The TE mode supported inside the DR is shown in Fig. 4.7.

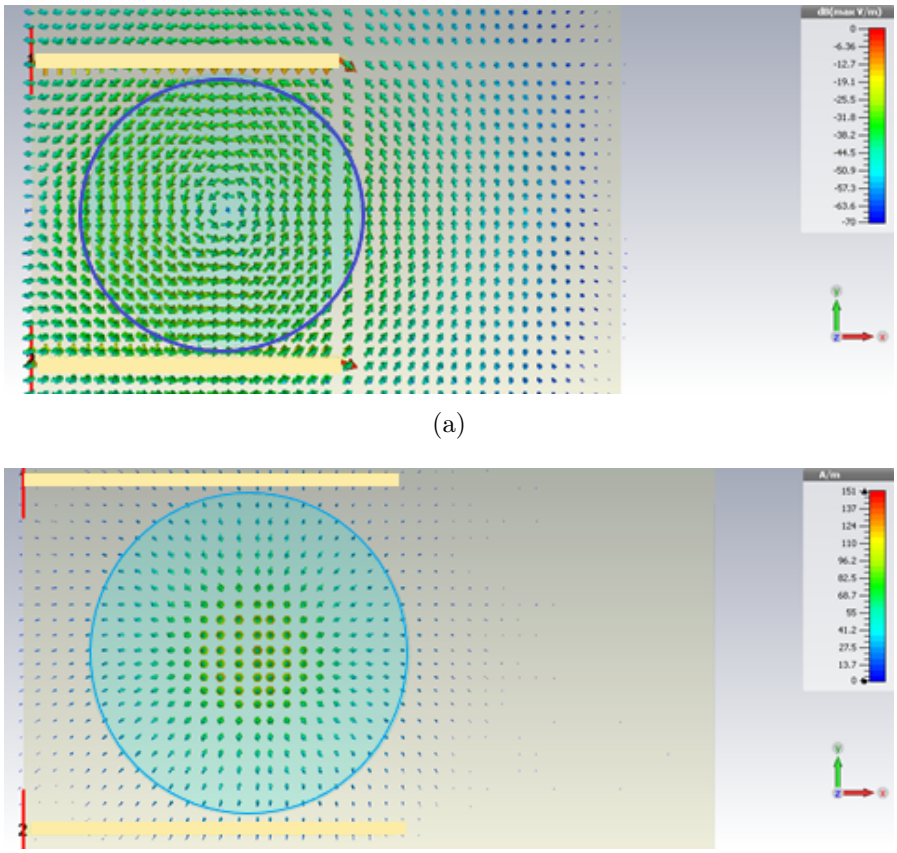

(a)

(b)

Figure 4.7: DRS TE mode supported by the shielded structure, (a) Electric field confinement and (b) H magnetic field inside the DR

The simulated results for different ethanol concentrations are shown in Figs. 4.8 and 4.9. Based on the achieved changes, the discrimination of ethanol should be feasible. The accuracy in this protected DR is promising in the simulated results and accuracy and high quality factor shows that this sensor can be a good candidate for biomedical application and sensor devices.

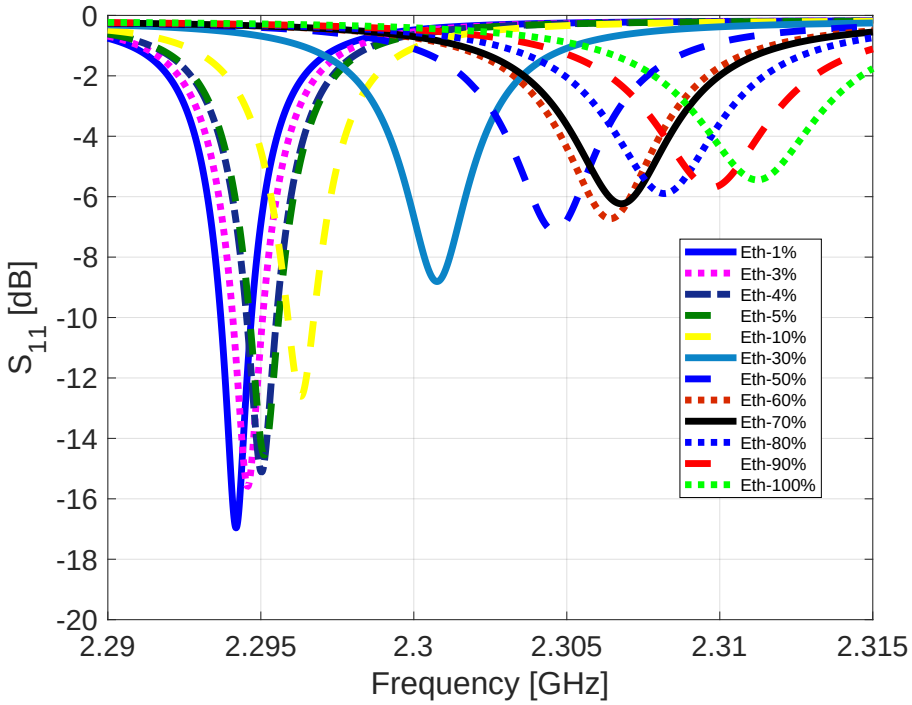

Figure 4.8: The frequency shift corresponding to the CST simulation of the DRS sensor for different ethanol concentrations

It can be clearly seen that by increasing the ethanol concentration, as higher permittivities are related to lower concentrations of ethanol, the resonant frequency follows an upward tendency and because of increasing loss factor, the minimum value of reflection coefficient has a downward trend, leading to subsequent less Q factor.

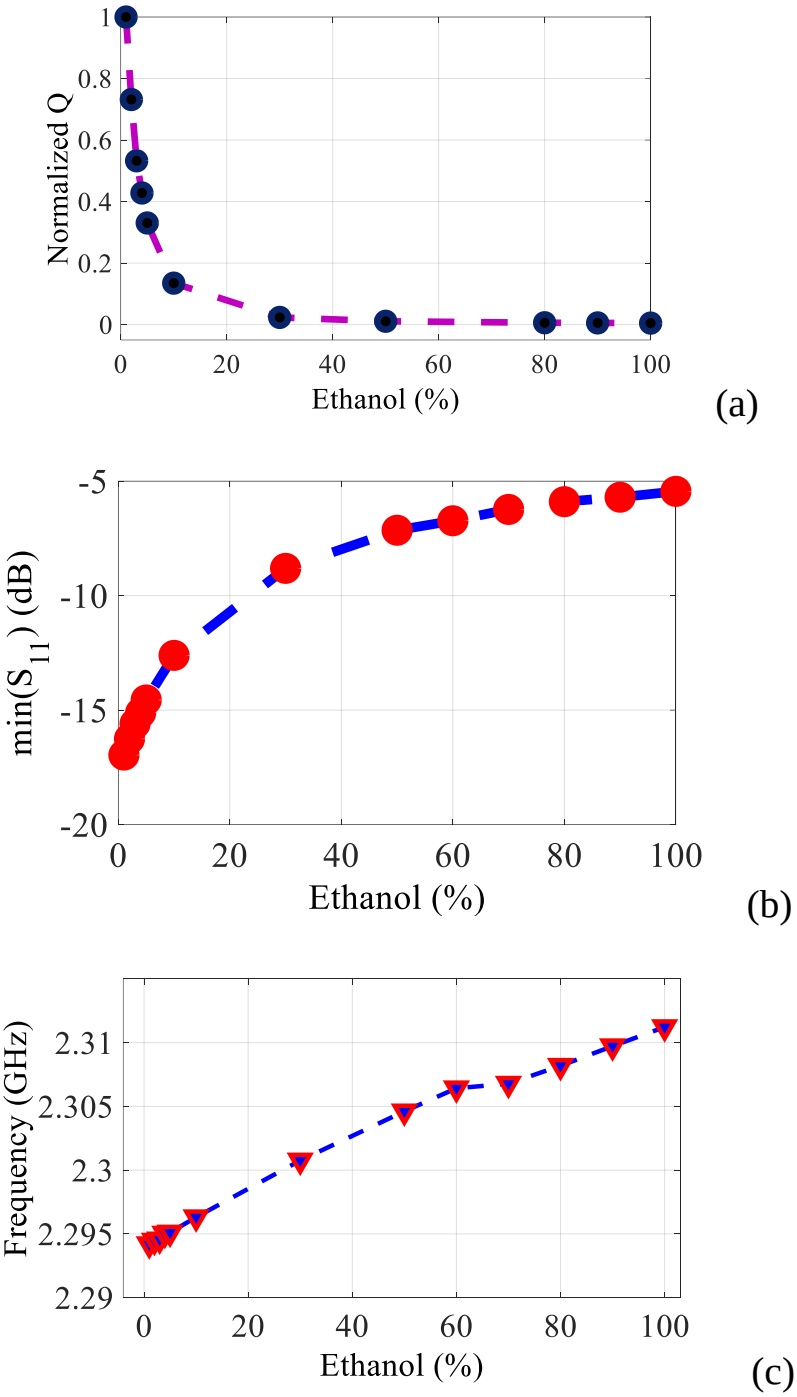

Figure 4.9: Full-wave simulation results for the DRS, (a) frequency shift versus different ethanol concentration, (b) minimum reflection parameters and (c) Q-factor of the sensor, normalized by the sensor response without LUT

4.2.1 Measurements for the DR sensor by removing the metal shield

Aside from covered DRS by a metal shield that has been simulated, the DR sensor without metal container has also been measured. Due to some complexities in the measurement process and to better understand the sensor functionality, the shield was removed. The sensor structure is shown in Fig. 4.6. As can be seen, two microstrip transmission lines couples to the DR, are connected to the vector network analyzer (VNA) and the scattering parameters are extracted and analysed in MATLAB. This sensor showing good sensitivity is able to sense the small values of ethanol. The measured results are demonstrated in Fig. 4.10 for different ethanol concentration as well as its small ethanol values in the solvent.

This experiment shows good results for ethanol concentrations from 0 to 96 % wherein very small concentrations of ethanol from 1 to 5 % show a clear shift in the resonant frequency. This sensor having a high sensitivity can be a promising device for detection of biological samples which need high accuracy. According to the Fig. 4.11, this sensor has a resolution of 8 MHz for 10% ethanol.

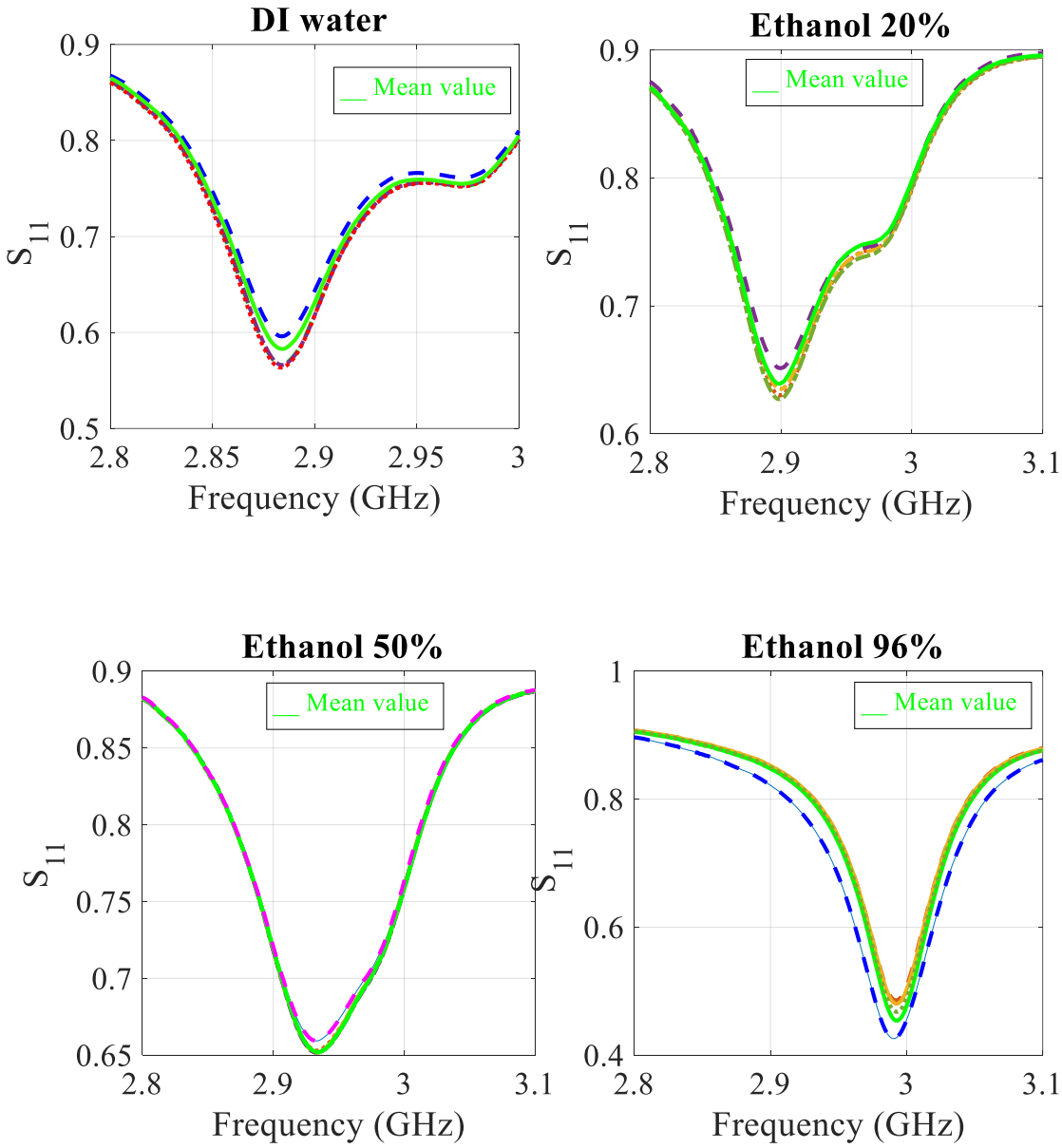

Figure 4.10: Measured scattering parameters of the un-shielded DR sensor for ethanol concentrations, each experiment has been repeated 5 times and the green line shows the mean value

and the frequency shift plot is shown in Fig.4.11

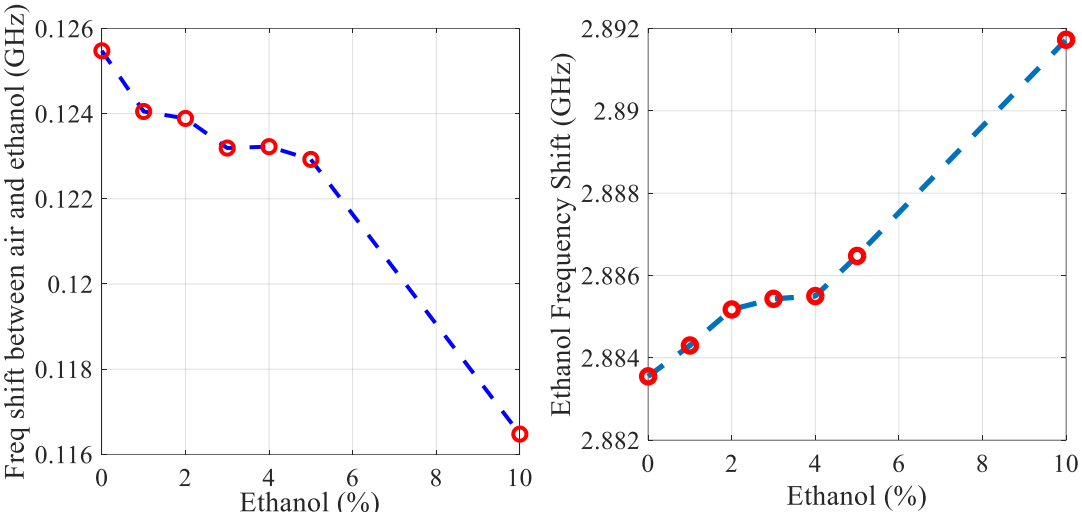

Figure 4.11: Sensor response for different ethanol concentrations.

Chapter 5

Metamaterial Sensors Applied to Electronic Part Design For Portable Applications

In several research papers that we have studied so far, the sensors have been used to characterize some different materials (constant permittivity and one specific concentration). In addition, discrimination of different chemical mixtures based on a fixed resonant frequency can be only conducted by the frequency shift approach whereas the dual-frequency measurement methods may be a promising and more reliable scheme enabling the chemical identification with different dielectric properties at different frequencies. Moreover, in medical and biological applications, there is an intensive need for a high-resolution sensor for different assays in laboratories.

On the other side, the common approaches for dielectric spectroscopy need various bulky and expensive complex measurement setup such as, for example, a vector network analyser (VNA) connected to the sensor part for the frequency response extraction. Due to the VNA complexity, it cannot be a suitable spectroscopy system for a handheld and on-board sensing device. In [94] the sensor is integrated with the electronic elements to be feasible as a portable device; the phase variations caused by the material/liquid under test (MUT/LUT) can be detected by different output power or output voltages in interferometry-based configurations. In a different approach, the electronic parts can also be integrated with a signal transmitter and a receiver consisting of a detector; for example, in [116], the sensor is stimulated in a wireless way and employs a Schottky diode detector (SDD) for dielectric characterization of oils' permittivities ranging from 2.45 to 5.77. The SDD produces a low-frequency periodic signal related to the sensor response and operates in a very narrow band (from 1.55 GHz up to 1.95 GHz) resulting in ambiguity in indicating the binary or multi-phase liquid mixtures; to resolve the

ambiguity, a detector working in different frequencies is needed.

In this section, a monopole antenna, loaded by a metamaterial (MTM) open complementary split ring resonator (OCSRR), is proposed as the sensor part to measure different concentrations of ethanol and the sensor is integrated to a voltage-controlled oscillator (VCO) and a SDD wherein both are operating in a dual-band approach. The wide-band operation of the whole system makes the sensor sensitive for dielectric spectroscopy in 2-2.5 GHz and 4-5 GHz frequency ranges. The second band (4-5 GHz) is used for discrimination of ethanol percentages that may show similar output voltages at the first frequency band. The structure of this chapter is descried as follows: First, the sensor operation principle is discussed and the sensor part is tested with ethanol solvents. The next part is devoted to the design of signal generator and detector employed by the sensor to be feasible as a handheld device.

5.1 Sensor Design and Operation Principle

The main part of the proposed sensor structure is a monopole antenna loaded by an OCSRR MTM resonator in the CPW configuration, as shown in Fig. 5.1. The OCSRR MTM resonator is etched on the low-impedance section of the sensor and the OCSRR is perpendicular to the direction of the wave propagation.

By inserting the sample on the OCSRR, the excited electromagnetic waves encounter a lossy material, leading to higher insertion loss. In addition, the total effective permittivity is perturbed by the sample. This event creates a shift in the resonant frequency of the OCSRR, which is employed as the sensing principle. This event can be interpreted by the perturbation theory. The perturbation technique is an accurate method that can be applied to analyze the change in the electromagnetic field distribution in a resonant structure when the sample volume is very small to produce a negligible perturbation [110]. The fractional change in the resonant frequency due to material placed on top of the resonator follows the perturbation method as written in eq. 3.5.

The sensor structure has been simulated using the CST commercial software. The low-cost substrate FR4 with the 1.5 mm height has been used for the sensor part and the feed line is matched to 50 ohms. As shown in Fig. 5.2, there are two different resonant frequencies in the frequency response of this dual-band sensor. The first one corresponds to the length of the monopole at 2.45 GHz and the second one is controlled by the OCSRR resonant frequency at 4.74 GHz; this sensor has a very good impedance matching from 2.3 GHz to 2.6 GHz and also from 4.2 GHz up to 6 GHz frequency ranges.

In order to achieve the best functionality, i.e., the maximum frequency shift, the most sensitive area of the resonator, in which the electric waves are intensively

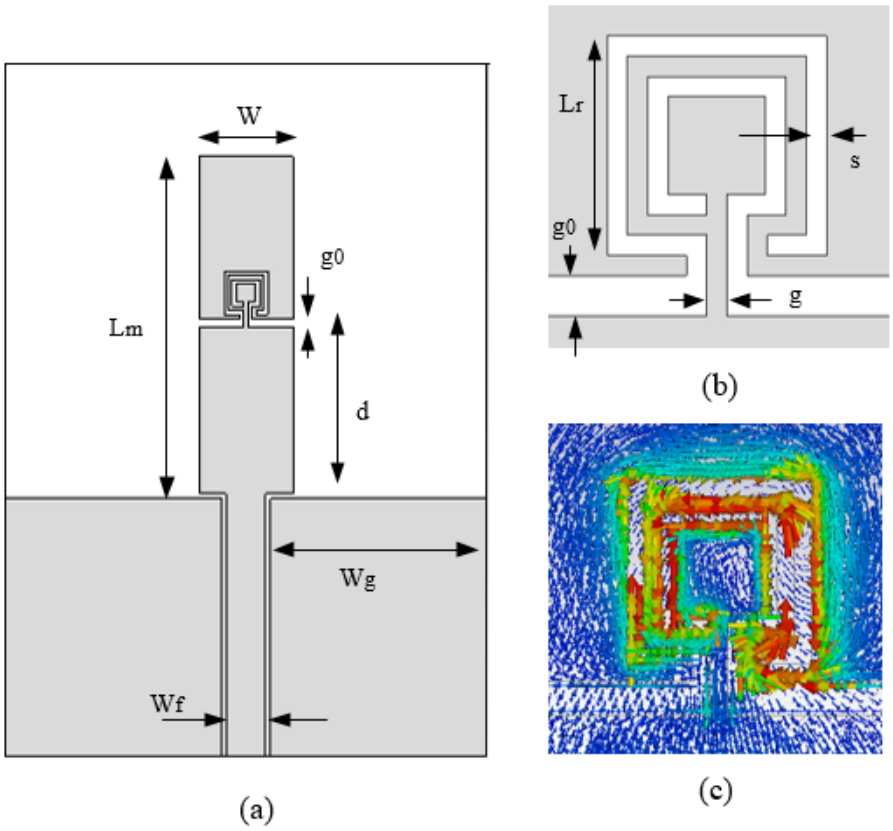

Figure 5.1: (a) Schematic layout of sensor, (b) OCSRR loaded as the sensitive area and (c) current distribution at the resonant frequency of OCSRR (i.e., at 4.74 GHz). The dimensions in mm are: $W = 5.85$, $L_m = 21$, $W_g = 13.5$, $g_0 = 0.5$, $d = 12.5$, $W_f = 2.44$, $g = 0.25$, $s = 0.25$, $L_r = 2.3$.

confined, should be used for the detection. The sensitive area of the OCSRR resonator is used as the sensor part. This fractional change in resonant frequency is the result of interaction between electromagnetic fields and the LUT. The electric field is stronger at the edges of the OCSRR resonator, making this regions suitable for high sensitivity to the dielectric changes.

5.2 Electronic parts integrated with the sensor

The electronic system to interrogate the sensor includes two different blocks: a signal generator and a signal detector. The sensor is connected to these components, all together as a portable and cost effective device. The signal generator uses a VCO, performing in two different frequency ranges between 2-2.5 GHz and 5-6

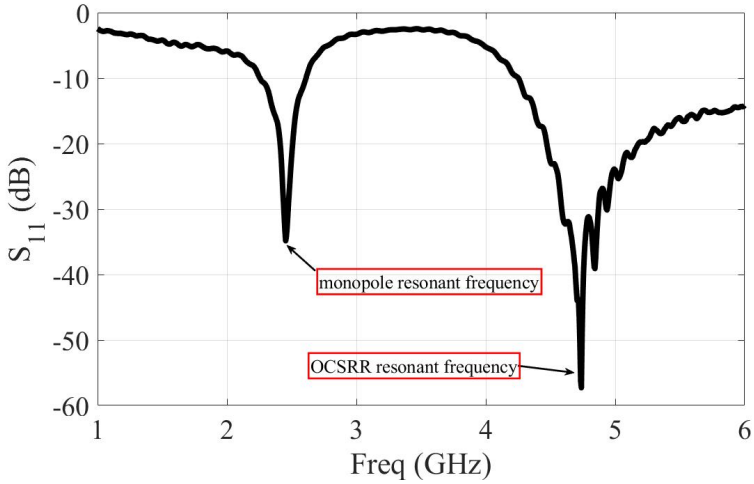

Figure 5.2: Measured reflection coefficient of the sensor part

GHz. On the other side, the signal detector as a Schottky diode detector produces a reasonable voltage which can be detected by a handheld voltmeter. They are explained in the following subsections.

5.2.1 Signal Generator

The signal generator, mainly based on a VCO can generate oscillating signals with variable frequencies. The produced signal is sent to the sensor and the wave electromagnetic properties are changed when encountered with the LUT. The VCO oscillation frequency is instantaneously controlled using a tunable input voltage which is generated by a simple DC-voltage supplier. The proposed VCO in this study, benefits from two working frequency bands which are controlled by switches. The first band ranging from 2-2.5 GHz and 5-6 GHz. The signal generator module is connected to the sensor by a circulator and is shown in Fig. 5.7. The circulator used in the system has insertion losses of 0.2 dB, an insulation ratio of 27.7dB and a VSWR of 1.1 dB. Its main objective is to separate the input and reflected signals of the sensor as the detector is connected to the circulator as well.

5.2.2 Signal Detector

The schematic layout of the dual-band signal detector comprising a zero-biased Schottky diode along with its equivalent circuit model are shown in Figs. 5.3*a* and *b*.

The SDD produces an output voltage proportional to the power of the signal received from the sensor part. The SDD is fabricated on a low-cost substrate with

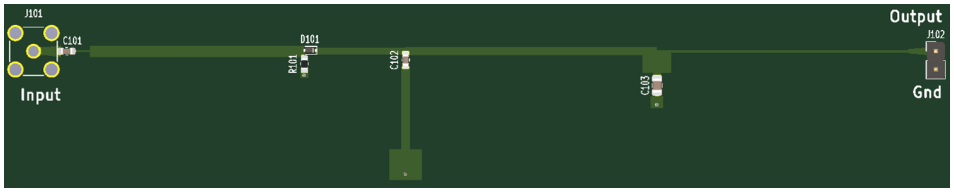

(a)

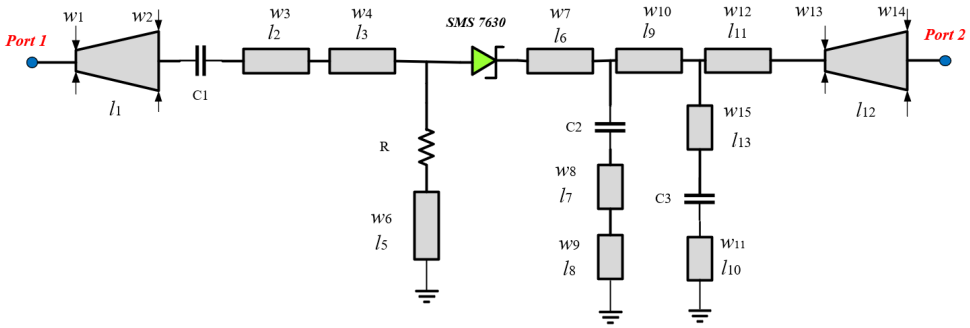

(b)

Figure 5.3: (a) Schematic layout of the SDD and (b) SDD circuit model. The optimised dimensions and circuit elements are: $w_1 = 1.14$, $w_2 = 1.6625$, $w_3 = 0.3$, $w_4 = 1.6$, $w_6 = 1.14$, $w_7 = 1$, $w_8 = 1.2$, $w_9 = 4.6$, $w_{10} = 1.14$, $w_{11} = 1.7$, $w_{12} = 0.32$, $w_{13} = 0.6$, $w_{14} = 1.14$, $w_{15} = 4.6$, $l_1 = 2$, $l_2 = 2.45$, $l_3 = 30.125$, $l_5 = 1.35$, $l_6 = 12.6$, $l_7 = 11.46$, $l_8 = 4.3$, $l_9 = 35.3$, $l_{10} = 1.7$, $l_{11} = 35.3$, $l_{12} = 3$, $l_{13} = 4.35$ $R = 50\,\Omega$, $C_1 = 3\,\text{pF}$, $C_2 = 0.3\,\text{pF}$, $C_3 = 1\,\text{nF}$ (all dimensions not explicitly set are in mm).

relative permittivity $\epsilon_r = 3.45$ with $\tan\delta = 0.0023$, thickness $h = 0.508\,\text{mm}$ and copper thickness of $18\,\mu\text{m}$. The zero-biased Schottky diode model is SMS-7630-079LF by Skyworks. The SDD is based on a series configuration, operating as a rectifier. The working principle is based on the envelope detection of the incoming signal depending on the input RF power or the power from the sensor, in the signal-rectification process. The simulated output voltage versus input voltage applied to the detector is shown in Fig 5.4

In a broad bandwidth, the system impedance matching is always as a challenging task. To tackle this problem, a $50\,\Omega$ resistor is added to the input circuit to give a good matching within the whole desired pass band. In addition, due to the trade-off between the impedance matching and sensitivity of the detector, the element values should be selected precisely. The design is carried out in Advanced Design System (ADS) software using large signal simulation and harmonic balance

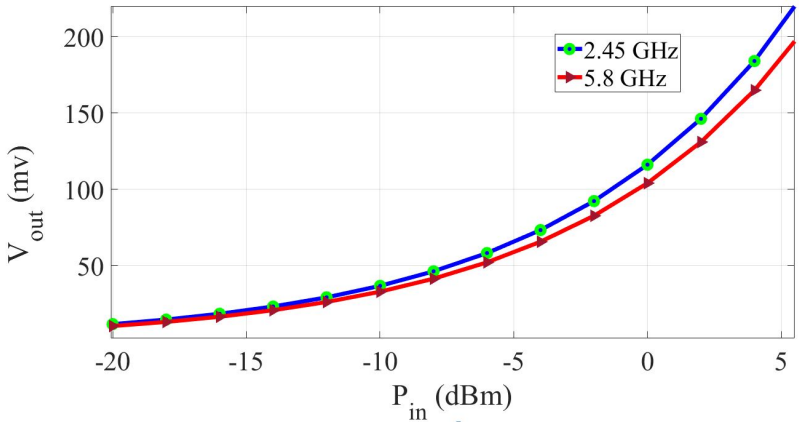

Figure 5.4: Simulated Output voltage of the SDD versus input power.

scheme [117]. The schematic of the circuit model of the designed SDD is shown in Fig. 5.5. The Schottky diode is simulated as a two-port network which is modeled

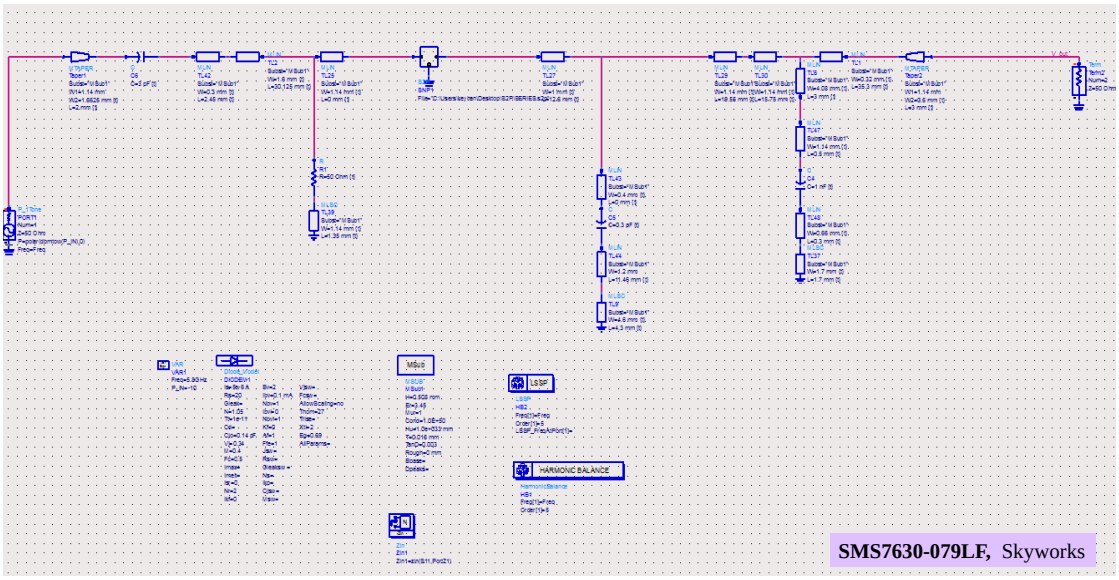

Figure 5.5: The schematic of the designed SDD using Advanced Design System (ADS). The harmonic balance and LSSP are used for harmonic analysis and scattering parameters extractions

according to the measured scattering parameters extracted by the manufacturer. The measured reflection coefficient of the SDD is shown in Fig. 5.6*a*. According to Fig. 5.6*b*, the detected voltage can sweep between 30 mv and 100 mv for an input

power between −10 dBm and 0 dBm respectively which proves a good sensitivity in addition to being suitable for detecting a wide dielectric range. As can be seen, there is a general good agreement between the ADS simulated results and measurements.

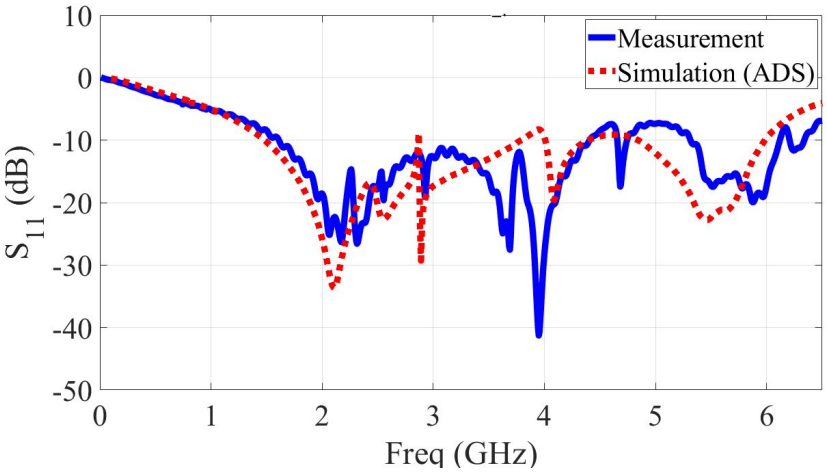

Figure 5.6: Frequency response (scattering parameters) of the SDD.

5.3 Sensor setup, Experimental Results and Discussion

Figure 5.7 shows the schematic of the whole sensing system as well as its block diagram. The proposed sensor is attached to the VCO signal generator and the SDD by a circulator. The input of the VCO is connected to the DC power supply and the output of the SDD is used as the output voltage and is read by a multimeter. Some containers are used for ethanol liquids with different concentrations.

In order to verify the sensor functionality, water-ethanol mixtures are tested by the proposed sensing system by placing a drop of the LUT over the sensor. The percentage of ethanol concentration changes from 10% up to 100% placed on the sensor part. As can be clearly seen in Fig. 5.8, at 2.45 GHz, the output voltage detected by the SDD ranges from 30 mV when the sensor is not loaded with any LUT and to 160 mV for the 50% ethanol. The output voltage decreases when the ethanol increases reaching to 40 mv for 100%. The second frequency band resonating at 5.8 GHz can be a beneficial and auxiliary band to discriminate the different concentrations of the LUT which shows similar output voltages at the end of SDD. For instance, the SDD shows 142 mv for both 10% and 60% at

2.4 GHz whereas it shows 100 mV and 138 mV at 5.8 GHz, corresponding to these percentages respectively.

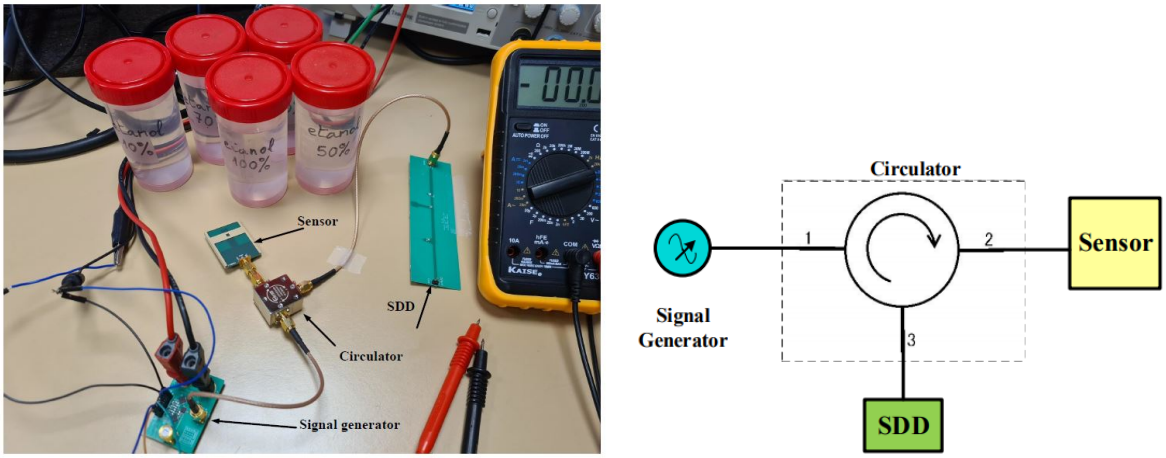

(a) (b)

Figure 5.7: (a) Complete experimental setup including the VCO, SDD and sensor part attached to a circulator and (b) its block diagram.

Separately, the sensor behaviour at 5.8 GHz can be interpreted as the output voltage and follows an upward trend from 100 mV for 10% ethanol to 140 mV for 40% ethanol and begins to descend to 110 mV for 100% ethanol. In this viability assessment phase, the experiment has been repeated several times with consistent results in each run; a more formal characterization is planned for the future.

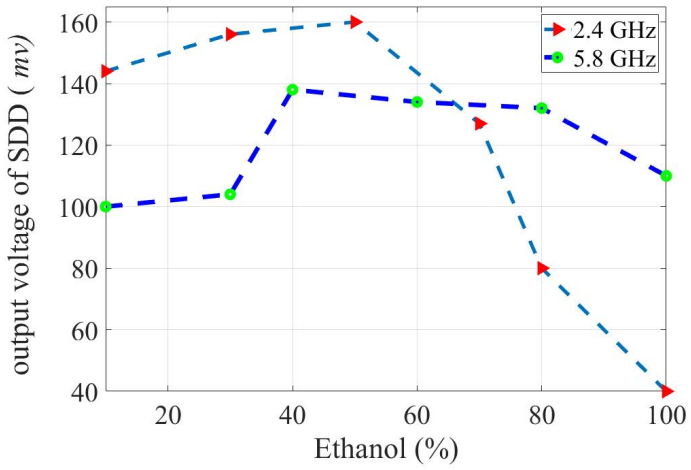

Figure 5.8: Measured SDD output voltage for different ethanol percentages at two different frequencies.

Chapter 6

Conclusion and Future Work

Nowadays, highly-sensitive sensors are necessarily needed in biomedical applications, food industries, environmental monitoring and etc. To characterize very small variations in the material properties, microwave sensors can be used. This thesis focuses on designing sensor structures, suitable for quantitatively measuring solvent concentration of chemical dilute in small quantities (drops) of water, such as ethanol, glucose, salt and more useful for blood examination in the laboratories. To this aim, different structures of sensors were studied and their advantages and disadvantages have been investigated. First, a review on the metamaterial-based sensors has been conducted. Due to higher quality and efficiency of the metamaterial (MTM) resonators compared to the conventional resonators, the MTM-based sensors can provide requisites for sensing applications. After a comprehensive study of more than 200 recently-published papers in the MTM-based sensor field, they have been classified into three main categories and they have been summarized into tables, presenting the sensors details for comparison. The MTM structures, explained in chapter 2, start with submersible sensors. The submersible sensors are promising in the applications with no concern about the amount of MUT and therefore, are useful in industries and soil engineering and so on. In the second class, the microfluidic sensors are compared; particularly in biomedical laboratories due to their accuracy and the small amount of needed sample. However, the submersible sensors acting as probes are considered to be more cost-effective and effortless instruments compared to the microfluidic-based sensors.
The array-configured sensors are large in size; however, the functionality of MTM-based sensors is improved by increasing the number of unit-cells. Although these sensors suffer from a large surface area, they are promising as a high-performance alternative when small size is not a concern.
The coupling-based sensors detect the MUT based on the perturbation of the symmetry plane by either asymmetric dielectric loading. This class of sensors could be beneficial to decrease the size of structure, however there is still room for improve-

ment as future work. According to the application, each category may be efficient and several MTM-inspired sensors in different types have been developed so far.

The main contribution of this thesis is presenting a new technology to develop highly-sensitive passive liquid sensors in the RF and microwave regime with a small size and high accuracy at the same time. Two sensors are proposed in this thesis and they are based on a cylindrical DR, one fed through a slot-coupled microstrip TL (DRA) and the other a parallel TL (DRS). In the DRS structure, in order to avoid the environment interference, we have proposed a metal house surrounding the DR and feeding lines. These sensors are explained in chapter 3 and 4, comprehensively. In the DR, a small pool is used for allocating the liquid under test (LUT), in which the sensor operates by shifting its frequency according to the electric permittivity of the liquid/material under test (LUT/MUT). This has been demonstrated by using an equivalent circuit approach and modal analysis. The cavity perturbation technique was used to study the impact of the LUT on the resonant frequency and modal distribution. Moreover, full-wave simulations were performed to check this theory. All the theory and simulations are consistent with the operation principle. The fundamental mode of a sensor involving the most energy portion of the wave, similar to the corresponding fundamental mode for a cylindrical DR, is dependent on the feeding structure and sensor. When the electromagnetic fields interact with the LUT in the pool, this produces a shift in the resonant frequency based on the permittivity of the LUT. The proposed technology was tested with a complete set of ethanol-water solutions for DRA and shielded-free DRS. A comprehensive method to characterize the mixture set was also presented in this thesis, included in the appendix part. In all cases, simulations have been carried out for assessing the performance of the sensor technology before manufacturing any prototype.

Both DRA and DRS prototypes, working in the low-GHz regime were designed, manufactured and measured. These sensors can be categorized as the first DR sensors working in the low-GHz band with higher sensitivity, and higher temperature stability. These DR sensors with less complexity compared to micro-fluidic sensors are smaller than the array MTM configurations. These sensors are useful to sense small volumes of samples like biological measurements and some industrial applications like food or chemical industry such as oil characterization. These are passive structure and no batteries are needed, thus all these characteristics make them good candidates for sensing small-volume liquid samples in mass applications.

Asides, trend toward 3-D printing techniques in electromagnetic applications is dramatically increasing as a low-cost alternative to expensive fabrication processes for small scale prototypes. The 3-D printing based on extrusion deposition technologies has been applied in designing the microwave components such as dielectric antenna. Different materials such as polymers can be printed. The DR with poly-

lactide acid (PLA) material can be employed in the form of sensor. Comparing the ceramic materials applied to realize the DR resonators, the PLA can be an efficient alternative. Although the lower permittivity of this kind of material makes the structure larger with less quality factor than that of the ceramic ones, they are simple-to-fabricate, and cost effective. The PLA-based resonators can be analyzed as similar manner as other DRs. This topic can be applied to a commercially-used sensing process in the future work.

In chapter 5, a new discussion was made related to the sensor portability. The common approaches for dielectric spectroscopy need various bulky and expensive complex measurement setups such as, for example, a vector network analyzer (VNA) connected to the sensor part for the frequency response extraction. Due to the VNA complexity, it cannot be a suitable spectroscopy system for a handheld and on-board sensing device. The proposed sensors in this thesis can be integrated with the electronic elements to be feasible as a portable device; the phase variations caused by the MUT/LUT can be detected by different output power or output voltages in an interferometry-based configurations. In a different approach, the electronic parts can also be integrated with a signal transmitter and a receiver consisting of a detector. Part of this thesis focuses on a dual-band metamaterial open complementary split ring resonator (OCSRR) loaded by a monopole antenna that has been used as a sensor. In order to make the sensor portable and cost-effective, the sensor has been integrated with a voltage-controlled oscillator (VCO) and a Schottky diode detector (SDD) electronic devices which are working in two bands. The proposed sensor has been experimented using the ethanol-water mixtures. The output voltages of the SDD, measured by a multimeter. This device as a handheld sensor can be useful for detecting binary mixtures and can be used in the biological applications and food industries.

As a result of this concept, DRA and DRS sensors can be integrated with the electronic parts used in the future road in order to be handheld and widely used by customers.

Appendix A

Extraction of frequency variation formula of the sensor

By considering E and H as the electric and magnetic fields of the original DR (without any hole) and $E^{'}$, $H^{'}$ as the perturbed electromagnetic fields, respectively, the Maxwell equations are satisfying

$$\vec{\bigtriangledown} \times \vec{E} = -j\omega\mu\vec{H} \tag{A.1}$$

and

$$\vec{\bigtriangledown} \times \vec{H} = j\omega\varepsilon\vec{E} \tag{A.2}$$

When the material filling a small part of the cavity resonator the Maxwell curl equations can be written as:

$$\vec{\bigtriangledown} \times \vec{E'} = -j\omega^{'}(\mu + \Delta\mu)\vec{H'} \tag{A.3}$$

and

$$\vec{\bigtriangledown} \times \vec{H'} = j\omega^{'}(\varepsilon + \Delta\varepsilon)\vec{E'} \tag{A.4}$$

Wherein the ω and $\omega^{'}$ are the resonant frequency of original and perturbed one respectively. The change in the permittivity and permeability are respectively noted as $\Delta\varepsilon$ and $\Delta\mu$. By conjugating the Equation A.1 and then multiplying by $\vec{H'}$ and similarly, by conjugating the Equation A.4 and then multiplying by $\vec{E}^{*}$, we have:

$$\vec{H'} \cdot \vec{\bigtriangledown} \times \vec{E}^{*} = -j\omega^{'}\mu\vec{H'} \cdot \vec{H}^{*} \tag{A.5}$$

and

$$\vec{E}^{*} \cdot \vec{\bigtriangledown} \times \vec{H'} = j\omega^{'}(\varepsilon + \Delta\varepsilon)\vec{E}^{*} \cdot \vec{E'} \tag{A.6}$$

By subtracting these two equations according to the vector identity equation of $(\bigtriangledown(\vec{A} \times \vec{B}) = \vec{B} \cdot \vec{\bigtriangledown}\vec{A} - \vec{A} \cdot \vec{\bigtriangledown}\vec{B})$, we have:

$$\vec{\bigtriangledown} \cdot (\vec{E}^{*} \times \vec{H}) = j\omega(\mu)\vec{H}^{*} \cdot \vec{H'} - j\omega^{'}(\varepsilon + \Delta\varepsilon)\vec{E}^{*} \cdot \vec{E'} \tag{A.7}$$

Similarly, this procedure should be applied to the eq. A.2 by multiplying $E^{'}$ and H^{*} which gives:

$$\vec{\bigtriangledown} \cdot (\vec{E^{'}} \times \vec{H^{*}}) = -j\omega^{'}(\mu + \Delta\mu)\vec{H^{*}} \cdot \vec{H^{'}} + j\omega\varepsilon\vec{E^{*}} \cdot \vec{E^{'}} \tag{A.8}$$

By adding the last two equations, and using the divergence theorem, and defining the integral over the resonator volume, the following equation is achieved as:

$$\begin{aligned} \iiint_V \vec{\bigtriangledown} \cdot (\vec{E^{'}} \times \vec{H^{*}} + \vec{E^{*}} \times \vec{H^{'}}) \cdot dv = \\ \iint_S (\vec{E^{'}} \times \vec{H^{*}} + \vec{E^{*}} \times \vec{H^{'}}) \cdot ds = 0 \end{aligned} \tag{A.9}$$

And after rearrangement it gives:

$$\begin{aligned} j \iiint_V [\omega\varepsilon - \omega^{'}(\varepsilon + \Delta\varepsilon)](\vec{E^{*}} \cdot \vec{E^{'}}) + \\ [\omega\mu - \omega^{'}(\mu + \Delta\mu)]\vec{H^{*}} \cdot \vec{H^{'}})dv = 0 \end{aligned} \tag{A.10}$$

Based on image theory, the sum of tangential electric fields on the ground plane are zero, i.e., $\hat{n} \times \vec{E^{'}} = 0$, According to the perturbation theory, it is expected that the electromagnetic fields are not greatly different from unperturbed ones when $\Delta\varepsilon$ and $\Delta\mu$ are small and the material under test is concentrated in a partially small volume. This approximation can be follows by assuming $E^{'}/H^{'}$ equals E/H respectively, as the $E^{'}$ and $H^{'}$ fields are practically unknown. Consequently, the fractional change in resonant frequency is obtained as follows:

$$\frac{\omega^{'} - \omega}{\omega} = \frac{-\iiint_v (\Delta\varepsilon \left|\vec{E}\right|^2 + \Delta\mu \left|\vec{H}\right|^2)dv}{\iiint_v (\varepsilon \left|\vec{E}\right|^2 + \mu \left|\vec{H}\right|^2)dv} \tag{A.11}$$

Appendix B

Mixture permittivity extraction and characterization

The proposed DR sensor is utilized for characterizing different solutions of liquids. In particular, an ethanol-water solution was used to test the proposed sensor. In order to model the effective permittivity of binary mixtures, several formulations are used [118]. Maxwell Garnett model [119] with a simple appearance is widely used in vast-variety applications [118] which is written as

$$\varepsilon_{\mathit{eff}} = \varepsilon_{r_1} + 3\,|m|\,\varepsilon_{r_1}\frac{\varepsilon_{r_2} - \varepsilon_{r_1}}{\varepsilon_{r_2} + 2\varepsilon_{r_1} - |m|\,(\varepsilon_{r_2} - \varepsilon_{r_1})} \tag{B.1}$$

wherein ϵ_{r_1} and ϵ_{r_2} are the dielectric constants of mixing two liquids with the mixing ratio of (1-$|m|$) and $|m|$, respectively, while $|m| \leq 1$. It should be considered that for large dielectric constants, there is a very nonlinear function for effective permittivity. Before using this model, the permittivity of each liquid should be extracted separately. As the dielectric permittivity depends on the operation frequency, Debye-Γ relaxation model is used as an efficient tool for the permittivity extraction of ethanol at the desired frequency and T = 25 $^{\circ}C$ (room temperature). The model equation is defined as

$$\varepsilon = \varepsilon_{\infty} + \frac{\varepsilon_{\infty} - \varepsilon_s}{1 + \dfrac{jf}{f_r}} - jf\Gamma \tag{B.2}$$

where ε_s and ε_{∞} are defined as static permittivity and infinite permittivity respectively. Furthermore, f and f_r are corresponding to the desired frequency and resonance frequency respectively.

The resulting dielectric properties of the binary ethanol-water mixture are shown in Figure B.1.There is a decrease of the relative permittivity and increase of the losses when the percentage of ethanol increases. These results make sense

because the relative permittivity and $\tan\delta$ of ethanol are much smaller and more higher than those of distilled water, respectively.

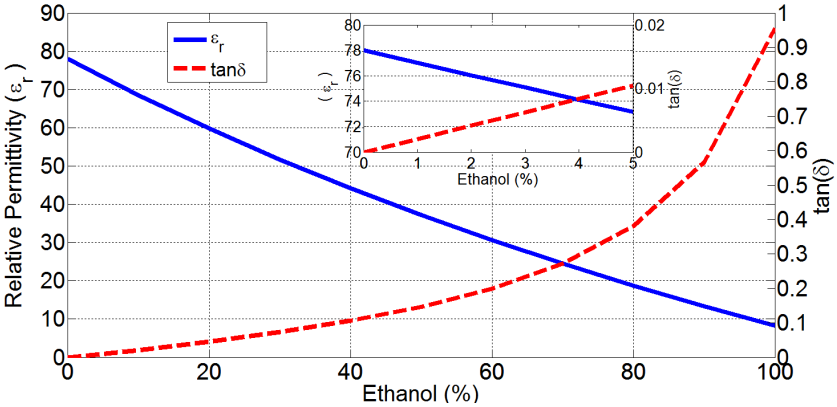

Figure B.1: Dielectric properties of the ethanol-water solution at 2.45 GHz.

This model is also applied to the permittivity and loss factor corresponding to the glucose and NaCl solutions as two commonly-used materials for sensing approach. The relative graphs have been shown below:

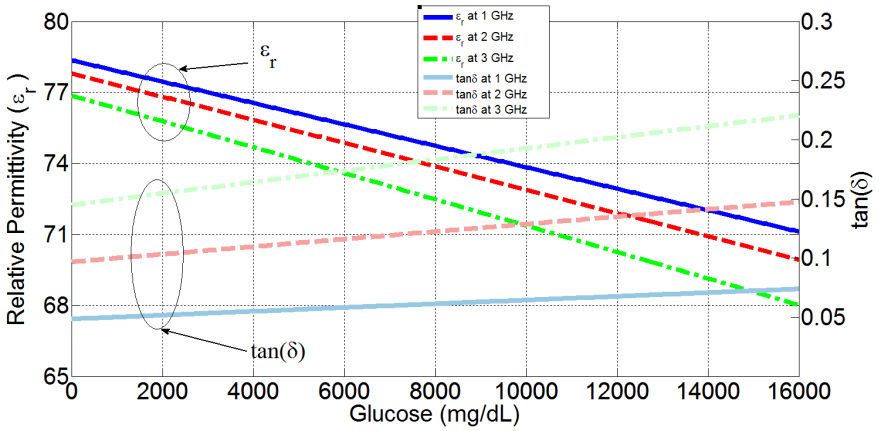

Figure B.2: Dielectric properties of the Glucose-water solution at 2.45 GHz.

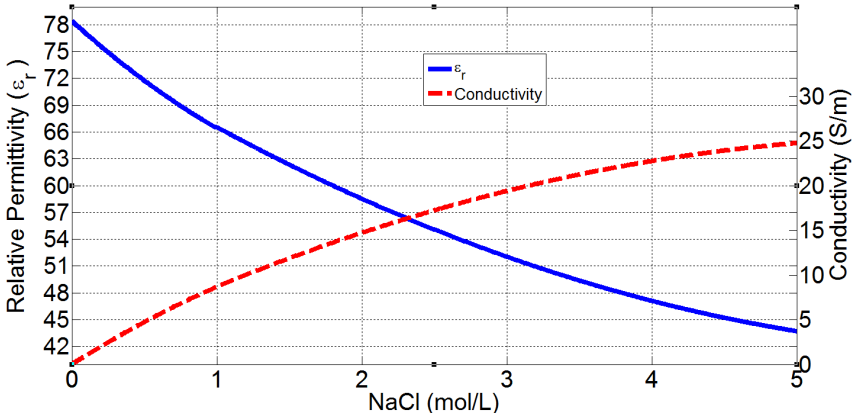

Figure B.3: Dielectric properties of the NaCl-water solution at 2.45 GHz.

Appendix C

Publications

1) M. G. Mayani, F. J. Herraiz-Martínez, J. Matanza. Domingo and R. Giannetti, **"Resonator-Based Microwave Metamaterial Sensors for Instrumentation: Survey, Classification, and Performance Comparison,"** in IEEE Transactions on Instrumentation and Measurement (Q1), vol. 70, pp. 1-14, 2021, Art no. 9503414,
doi: 10.1109/TIM.2020.3040484.

This review's purpose is to focus on recent metamaterial-based electromagnetic sensors, particularly on the structures that integrate the metamaterials in antenna or transmission lines for their further integration in measurement instruments. The approach followed in the review is to highlight sensitivity and quality factor (Q-factor) as they are crucial parameters in any sensor; the corpus of literature analyzed leads to the finding that the adoption of metamaterials is a key factor in successfully decreasing the size of the structures while maintaining a high Q-factor value and reducing losses. In addition, a new metamaterial-based sensors' taxonomy is proposed to classify them into three main categories: frequency-variation sensors, coupling-based sensors, and differential sensors. A tabular comparison of the specifications of different sensors provides further insights into their different capabilities and will allow future researchers to efficiently find and compare their prototypes with state-of-the-art devices.

2) M. G. Mayani, F. J. Herraiz-Martínez, J. Matanza. Domingo, R. Giannetti and C. Rodriguez-Morcillo. García, **"A Novel Dielectric Resonator-Based Passive Sensor for Drop-Volume Binary Mixtures Classification,"** in IEEE Sensors Journal (Q1), vol. 21, no. 18, pp. 20156-20164, 15 Sept.15, 2021,
doi: 10.1109/JSEN.2021.3094904.

In this study, a dielectric-resonator-based sensor is presented to characterize liq-

uids. The sensor is based on a dielectric resonator (DR) fed by a slot-coupling mechanism in the ground plane of a microstrip transmission line (TL). The obtained device is a fully passive sensor that a radiofrequency (RF) signal can interrogate. A small hole was drilled on the DR surface to allocate a drop of the liquid under test (LUT); as a consequence, the resonant frequency of the sensor will depend on the electromagnetic characteristics of the LUT. The device is modeled both with an equivalent circuit model and through an electromagnetic modal analysis. The cavity perturbation technique is used to study the impact of the LUT on the resonant frequency and modal distribution; full-wave simulations corroborate the theoretical results. Finally, a prototype of the proposed sensor tuned to work in the 2.45 GHz band has been designed, manufactured, and measured. The device is cost-effective given the small size and practical to use, thanks to the minimal volume of the pool, which calls for quantities of LUT in the order of 0.13 μl . The prototype has been tested with an ethanol-water solution set. The experimental results match well with simulations and show good repeatability. The sensitivity of the prototype resulted in being 718 kHz per percentage of ethanol in water.

3) M Gholami Mayani, FJ Herraiz Martínez, J Matanza Domingo, R Giannetti; **Highly sensitive dielectric resonator sensor for liquid characterization;** URSI conference, Malaga, Spain, 2021.

This article describes a novel 2 GHz dielectric resonator sensor (DRS). The dielectric resonator is made of ceramic material and is fed by a microstrip transmission line, using the aperture-feeding method. The sensor shows a high quality factor (Q-factor) with an associated high resolution. As a test, the sensor is used in an application for the characterization of liquid solvents such as Glucose and Ethanol at different concentrations.

4) M. G. Mayani, F. J. Herraiz-Martínez, J. Matanza. Domingo, R. Giannetti and C. Rodriguez-Morcillo. García, **"Dual-Band Metamaterial-inspired Microwave Sensor For Liquid Dielectric Spectroscopy,"** 2021 IEEE International Instrumentation and Measurement Technology Conference (I2MTC), 2021, pp. 1-5,
doi: 10.1109/I2MTC50364.2021.9460055.

In this paper, an open complementary split ring resonator (OCSRR)-loaded monopole antenna is used as a liquid sensor for discrimination of ethanol solvents with different concentrations. The resulting dual-band sensor is working at 2.45 GHz and 4.74 GHz and has been fabricated on the FR4 commercial substrate. The sensor

part is integrated with the electronic parts including a voltage-controlled oscillator (VCO) and a zero-biased Schottky diode detector (SDD) allowing the sensor to be low cost and portable. The proposed sensor has been find capable to discriminate a wide range of dielectric variations for ethanol concentration detection.

5) Lecture "Highly-sensitive dielectric resonator sensor for liquid characterization" 15th Workshop on Industrial Systems and Energy Technologies - JOSITE'2020. Technological Research Institute. Comillas Pontifical University . Madrid, Spain. Jul 2020.

Bibliography

[1] Viktor G. Veselago. Electrodynamics of materials with negative index of refraction. *Uspekhi Fizicheskih Nauk*, 173(7):790, 2003.

[2] D. R. Smith, Willie J. Padilla, D. C. Vier, S. C. Nemat-Nasser, and S. Schultz. Composite medium with simultaneously negative permeability and permittivity. *Phys. Rev. Lett.*, 84:4184–4187, May 2000.

[3] M Gil, J Bonache, J Garcia-Garcia, J Martel, and F Martin. Composite Right/Left-Handed Metamaterial Transmission Lines Based on Complementary Split-Rings Resonators and Their Applications to Very Wideband and Compact Filter Design. *IEEE Transactions on Microwave Theory and Techniques*, 55(6):1296–1304, 2007.

[4] M. Gil, J. Bonache, and F. Martín. Metamaterial filters: A review. *Metamaterials*, 2(4):186–197, 2008.

[5] M Duran-Sindreu, A Velez, G Siso, P Velez, J Selga, J Bonache, and F Martin. Recent Advances in Metamaterial Transmission Lines Based on Split Rings. *Proceedings of the IEEE*, 99(10):1701–1710, 2011.

[6] Francisco Javier Herraiz-Martínez, Ferran Paredes, Gerard Zamora, Ferran Martín, and Jordi Bonache. Dual-band printed dipole antenna loaded with open complementary split-ring resonators for wireless applications. *Microwave and Optical Technology Letters*, 54(4):1014–1017, apr 2012.

[7] Gerard Zamora, Simone Zuffanelli, Ferran Paredes, Francisco Javier Herraiz-Martinez, Ferran Martin, and Jordi Bonache. Fundamental-mode leaky-wave antenna (LWA) using slotline and split-ring-resonator (SRR)-based metamaterials. *IEEE Antennas and Wireless Propagation Letters*, 12:1424–1427, 2013.

[8] R. A. Romero, R. S. Feitoza, C. R. Rambo, and F. R. Sousa. A low-cost passive wireless capacitive sensing tag based on split-ring resonator. In *2015*

IEEE International Instrumentation and Measurement Technology Conference (I2MTC) Proceedings, pages 434–439, 2015.

[9] Mahdieh Gholami Mayani, Shahrooz Asadi, Abbas Pirhadi, and Sina Mortezazadeh Mahani. Design and analysis of a super compact wideband bandpass filter based on metamaterial resonators. *AEU - International Journal of Electronics and Communications*, 97:79–84, dec 2018.

[10] M. U. Memon, A. Salim, H. Jeong, and S. Lim. Metamaterial inspired radio frequency-based touchpad sensor system. *IEEE Transactions on Instrumentation and Measurement*, 69(4):1344–1352, 2020.

[11] W. Withayachumnankul and D. Abbott. Metamaterials in the terahertz regime. *IEEE Photonics Journal*, 1(2):99–118, 2009.

[12] S. Wikipedia and Books Llc. *Metamaterials: Dielectric, Superlens, Metamaterial Antennas, Terahertz Metamaterials, Metamaterial Cloaking, Photonic Metamaterials, Negative Index Metamaterials, Acoustic Metamaterials, History of Metamaterials, Tunable Metamaterials*. Books LLC, Reference Series, 2010.

[13] Didier Lippens. Overview of microwave and optical metamaterial technologies. In *Metamaterials and Wave Control*, pages 1–42. wiley, dec 2013.

[14] Tie Jun. Cui, David Richard Smith, and Ruopeng. Liu. *Metamaterials : theory, design, and applications*. Springer, 2010.

[15] M Bologna, A Petri, B Tellini, and C Zappacosta. Effective Magnetic Permeability Measurement in Composite Resonator Structures. *IEEE Transactions on Instrumentation and Measurement*, 59(5):1200–1206, may 2010.

[16] Juan Domingo Baena, Jordi Bonache, Ferran Martín, Ricardo Marqués Sillero, Francisco Falcone, Txema Lopetegi, Miguel A G Laso, Joan García-García, Ignacio Gil, Maria Flores Portillo, and Mario Sorolla. Equivalent-Circuit Models for Split-Ring Resonators and Complementary Split-Ring Resonators Coupled to Planar Transmission Lines. *IEEE Transactions on Microwave Theory and Techniques*, 53(4), 2005.

[17] J. B. Pendry, A. J. Holden, W. J. Stewart, and I. Youngs. Extremely low frequency plasmons in metallic mesostructures. *Phys. Rev. Lett.*, 76:4773–4776, Jun 1996.

[18] D R Smith, Willie J Padilla, D C Vier, S C Nemat-Nasser, and S Schultz. Composite medium with simultaneously negative permeability and permittivity. *Physical review Letters*, 2000.

[19] C Caloz and T Itoh. Transmission line approach of left-handed (LH) materials and microstrip implementation of an artificial LH transmission line. *Antennas and Propagation, IEEE Transactions on*, 52(5):1159–1166, 2004.

[20] Ricardo Marqués, Ferran Martín, and Mario Sorolla. *The Electrodynamics of Left-Handed Media*, chapter 1, pages 1–41. John Wiley & Sons, Ltd, 2007.

[21] Ali Maleki Gargari, Mohammad Hossein Zarifi, and Loïc Markley. Passive Matched Mushroom Structure for a High Sensitivity Low Profile Antenna-Based Material Detection System. *IEEE Sensors Journal*, 19(15):6154–6162, aug 2019.

[22] Nader Engheta and Richard W. Ziolkowski. *Metamaterials: Physics and Engineering Explorations*. John Wiley and Sons, sep 2006.

[23] H Ö Yılmaz and F Yaman. Metamaterial Antenna Designs for a 5.8-GHz Doppler Radar. *IEEE Transactions on Instrumentation and Measurement*, 69(4):1775–1782, apr 2020.

[24] Huang Wei and Ahmed A. Kishk. Compact dielectric resonator antenna array for microwave breast cancer detection. *2007 IEEE Region 5 Technical Conference, TPS*, pages 9–12, 2007.

[25] W. Huang and A. A. Kishk. Compact dielectric resonator antenna for microwave breast cancer detection. *IET Microwaves, Antennas and Propagation*, 3(4):638–644, 2009.

[26] M. Kamran Saleem, M. Abdel-Rahman, Majeed Alkanhal, and Abdelrazik Sebak. A cylindrical dielectric resonator antenna-coupled sensor configuration for 94 GHz detection. *International Journal of Antennas and Propagation*, 2014, 2014.

[27] Sounik Kiran Kumar Dash, Taimoor Khan, and Binod Kumar Kanaujia. Circularly Polarized Dual Facet Spiral Fed Compact Triangular Dielectric Resonator Antenna for Sensing Applications. *IEEE Sensors Letters*, 2(1):1–4, 2018.

[28] D. Kajfez and P. Guillon. *Dielectric Resonators*. Artech House microwave library. Noble Publishing Corporation, 1998.

[29] Sumyea Sabrin, Sergey Kharkovsky, and Robert Salama. Dielectric resonator antenna integrated sensors for characterization of concrete. *Proceedings of the International Conference on Sensing Technology, ICST*, 2017-Decem:1–6, 2018.

[30] Monika Chauhan, Ajay Kumar Pandey, and Biswajeet Mukherjee. A Novel Compact Cylindrical Dielectric Resonator Antenna for Wireless Sensor Network Application. *IEEE Sensors Letters*, 2(2):1–4, 2018.

[31] Amjad Iqbal, Amor Smida, Omar A. Saraereh, Qais H. Alsafasfeh, Nazih Khaddaj Mallat, and Byung Moo Lee. Cylindrical dielectric resonator antenna-based sensors for liquid chemical detection. *Sensors (Switzerland)*, 19(5):2–10, 2019.

[32] Irfan Ali, Mohd Haizal Jamaluddin, Abinash Gaya, and Hasliza A. Rahim. A dielectric resonator antenna with enhanced gain and bandwidth for 5G applications. *Sensors (Switzerland)*, 20(3):1–12, 2020.

[33] K W Leung. Development of Dielectric Resonator Antenna (DRA), 2012.

[34] Chin Lung Yang, Chieh Sen Lee, Kuan Wei Chen, and Kuan Zhou Chen. Noncontact measurement of complex permittivity and thickness by using planar resonators. *IEEE Transactions on Microwave Theory and Techniques*, 64(1):247–257, jan 2016.

[35] Tanveerul Haq, Cunjun Ruan, Xingyun Zhang, Ayesha Kosar, and Shahid Ullah. Low cost and compact wideband microwave notch filter based on miniaturized complementary metaresonator. *Applied Physics A: Materials Science and Processing*, 125:1–7, 9 2019.

[36] Margarita Puentes Vargas. Fundamentals of metamaterial structures. In *Planar Metamaterial Based Microwave Sensor Arrays for Biomedical Analysis and Treatment*, pages 7–31, Cham, 2014. Springer International Publishing.

[37] Athanasia Symeonidou and Katherine Siakavara. A novel microstrip antenna array with metamaterial-based electronic beam steering at 2.4GHz. *Progress In Electromagnetics Research C*, 38:27–42, 2013.

[38] Applications of Metamaterials - 1st Edition - Filippo Capolino - Rout.

[39] Gabriel Galindo-Romera, Francisco Javier Herraiz-Martínez, Marta Gil, José Juan Martínez-Martínez, and Daniel Segovia-Vargas. Submersible Printed Split-Ring Resonator-Based Sensor for Thin-Film Detection and Permittivity Characterization. *IEEE Sensors Journal*, 16(10):3587–3596, may 2016.

[40] Muhammed S. Boybay and Omar M. Ramahi. Non-destructive thickness measurement using quasi-static resonators. *IEEE Microwave and Wireless Components Letters*, 23(4):217–219, 2013.

[41] Chieh Sen Lee and Chin Lung Yang. Thickness and permittivity measurement in multi-layered dielectric structures using complementary split-ring resonators. *IEEE Sensors Journal*, 14(3):695–700, mar 2014.

[42] Aakriti Raj, Abhishek Kumar Jha, M. Arif Hussain Ansari, M. Jaleel Akhtar, and Sidhartha Panda. Metamaterial-inspired microwave sensor for measurement of complex permittivity of materials. *Microwave and Optical Technology Letters*, 58(11):2577–2581, nov 2016.

[43] T. Hao, C. J. Stevens, and D. J. Edwards. Optimisation of metamaterials by q factor. *Electronics Letters*, 41(11):653–654, 2005.

[44] Yuancheng Fan, Fuli Zhang, Nian-Hai Shen, Quanhong Fu, Zeyong Wei, Hongqiang Li, and Costas M. Soukoulis. Achieving a high-q response in metamaterials by manipulating the toroidal excitations. *Phys. Rev. A*, 97:033816, Mar 2018.

[45] A. E. Atia and A. E. Williams. Narrow-bandpass waveguide filters. *IEEE Transactions on Microwave Theory and Techniques*, 20(4):258–265, 1972.

[46] Jia-Sheng Hong and M J Lancaster. *Microstrip Filters for RF/Microwave Applications.* John Wiley & Sons, 2001.

[47] Cumali Sabah and Tayfun Nesimoglu. Design and characterization of a resonator-based metamaterial and its sensor application using microstrip technology. *Optical Engineering*, 55(2):027107, feb 2016.

[48] Rammah Ali Alahnomi, Zahriladha Zakaria, Eliyana Ruslan, Siti Rosmaniza Ab Rashid, and Amyrul Azuan Mohd Bahar. High-Q sensor based on symmetrical split ring resonator with spurlines for solids material detection. *IEEE Sensors Journal*, 17(9):2766–2775, may 2017.

[49] O. Altintaş, M. Aksoy, E. Ünal, and M. Karaaslan. Chemical liquid and transformer oil condition sensor based on metamaterial-inspired labyrinth resonator. *Journal of the Electrochemical Society*, 166(6):B482–B488, 2019.

[50] Lijuan Su, Xin Huang, Wei Guo, and Hao Wu. A Flexible Microwave Sensor Based on Complementary Spiral Resonator for Material Dielectric Characterization. *IEEE Sensors Journal*, pages 1–1, 2019.

[51] Niloofar Sharafadinzadeh, Mohammad Abdolrazzaghi, and Mojgan Daneshmand. Highly sensitive microwave split ring resonator sensor using gap extension for glucose sensing. In *2017 IEEE MTT-S International Microwave*

Workshop Series on Advanced Materials and Processes for RF and THz Applications, IMWS-AMP 2017, volume 2018-Janua, pages 1–3. Institute of Electrical and Electronics Engineers Inc., jan 2018.

[52] Larbi Benkhaoua, Mohamed Taoufik Benhabiles, Smail Mouissat, and Mohamed Lahdi Riabi. Miniaturized Quasi-Lumped Resonator for Dielectric Characterization of Liquid Mixtures. *IEEE Sensors Journal*, 16(6):1603–1610, mar 2016.

[53] Izyani Mat Rusni, Alyani Ismail, Adam Reda Hasan Alhawari, Mohd Nizar Hamidon, and Nor Azah Yusof. An aligned-gap and centered-gap rectangular multiple split ring resonator for dielectric sensing applications. *Sensors (Switzerland)*, 14(7):13134–13148, jul 2014.

[54] J. Naqui and F. Martı´n. Transmission lines loaded with bisymmetric resonators and their application to angular displacement and velocity sensors. *IEEE Transactions on Microwave Theory and Techniques*, 61(12):4700–4713, 2013.

[55] Tarakeswar Shaw and Debasis Mitra. Electromagnetic metamaterial based sensor design for chemical discrimination. In *IEEE MTT-S International Microwave and RF Conference, IMaRC 2017*, volume 2018-January, pages 271–274. Institute of Electrical and Electronics Engineers Inc., aug 2018.

[56] Pratik Porwal, Azeemuddin Syed, Prabhakar Bhimalapuram, and Tapan Kumar Sau. Design of RF sensor for simultaneous detection of complex permeability and permittivity of unknown sample. *Progress In Electromagnetics Research C*, 79:159–173, 2017.

[57] Chieh-Sen Lee, Bin Bai, Qin-Rui Song, Zhi-qiang Wang, and Guo-Fen Li. Open Complementary Split-Ring Resonator Sensor for Dropping-Based Liquid Dielectric Characterization. *IEEE Sensors Journal*, pages 1–1, aug 2019.

[58] Mohammad Tariqul Islam, Farhad Bin Ashraf, Touhidul Alam, Norbahiah Misran, and Kamarulzaman Bin Mat. A compact ultrawideband antenna based on hexagonal split-ring resonator for pH sensor application. *Sensors (Switzerland)*, 18(9), sep 2018.

[59] Ankita Verma, Sushmita Bhushan, Pramod Narayan Tripathi, Manish Goswami, and B. R. Singh. A defected ground split ring resonator for an ultra-fast, selective sensing of glucose content in blood plasma. *Journal of Electromagnetic Waves and Applications*, 31(10):1049–1061, jul 2017.

[60] Erick Reyes-Vera, G. Acevedo-Osorio, Mauricio Arias-Correa, and David E. Senior. A submersible printed sensor based on a monopole-coupled split ring resonator for permittivity characterization. *Sensors (Switzerland)*, 19(8), apr 2019.

[61] R. Sujith and Robin Augustine. CPW fed antenna for nearfield sensor applications. In *2018 IEEE Conference on Antenna Measurements and Applications, CAMA 2018*. Institute of Electrical and Electronics Engineers Inc., nov 2018.

[62] Taha A. Elwi. Metamaterial based a printed monopole antenna for sensing applications. *International Journal of RF and Microwave Computer-Aided Engineering*, 28(7):e21470, sep 2018.

[63] Wan Hafiy Wan Morshidi, Zarimin Zaharudin, Sheroz Khan, Anis Nurashikin Nordin, Faraz Ahmed Shaikh, Ismail Adam, and Kushsairy Abdul Kader. Inter-digital sensor for non-invasive blood glucose monitoring. In *2018 IEEE International Conference on Innovative Research and Development, ICIRD 2018*, pages 1–6. Institute of Electrical and Electronics Engineers Inc., jun 2018.

[64] Musab Asad, Sultan Al Neyadi, Othman Al Aidaros, Mahmoud Khalil, and Mousa Hussein. Single port bio-sensor design using metamaterial split ring resonator. In *International Conference on Electronic Devices, Systems, and Applications*. IEEE Computer Society, jan 2017.

[65] M. Arif Hussain Ansari, Abhishek Kumar Jha, Zubair Akhter, and M. Jaleel Akhtar. Multi-Band RF Planar Sensor Using Complementary Split Ring Resonator for Testing of Dielectric Materials. *IEEE Sensors Journal*, 18(16):6596–6606, aug 2018.

[66] Nilesh Kumar Tiwari, Surya Prakash Singh, and M. Jaleel Akhtar. Quad band metamaterial inspired planar sensor for dispersive material testing. In *IEEE MTT-S International Microwave and RF Conference, IMaRC 2017*, pages 120–123. Institute of Electrical and Electronics Engineers Inc., aug 2018.

[67] Maryam Saadat-Safa, Vahid Nayyeri, Mostafa Khanjarian, Mohammad Soleimani, and Omar M. Ramahi. A CSRR-Based Sensor for Full Characterization of Magneto-Dielectric Materials. *IEEE Transactions on Microwave Theory and Techniques*, 67(2):806–814, feb 2019.

[68] Vaishali Rawat, Rohini Kitture, Dimple Kumari, Harsh Rajesh, Shaibal Banerjee, and S. N. Kale. Hazardous materials sensing: An electrical metamaterial approach. *Journal of Magnetism and Magnetic Materials*, 415:77–81, oct 2016.

[69] Mohammad Abdolrazzaghi, Mojgan Daneshmand, and Ashwin K. Iyer. Strongly Enhanced Sensitivity in Planar Microwave Sensors Based on Metamaterial Coupling. *IEEE Transactions on Microwave Theory and Techniques*, 66(4):1843–1855, apr 2018.

[70] Zoran Jaksic, N. Dalarsson, and Milan Maksimovic. Negative refractive index metamaterials: Principles and applications. *Microwave Review*, 12, 04 2006.

[71] Greeshmaja Govind and M. Jaleel Akhtar. Metamaterial-Inspired Microwave Microfluidic Sensor for Glucose Monitoring in Aqueous Solutions. *IEEE Sensors Journal*, pages 1–1, sep 2019.

[72] Amir Ebrahimi, Withawat Withayachumnankul, Said Al-Sarawi, and Derek Abbott. High-sensitivity metamaterial-inspired sensor for microfluidic dielectric characterization. *IEEE Sensors Journal*, 14(5):1345–1351, 2014.

[73] Euclides Lourenco Chuma, Yuzo Iano, Glauco Fontgalland, and Leonardo Lorenzo Bravo Roger. Microwave sensor for liquid dielectric characterization based on metamaterial complementary split ring resonator. *IEEE Sensors Journal*, 18(24):9978–9983, dec 2018.

[74] Amyrul Azuan Mohd Bahar, Z. Zakaria, A. A.M. Isa, Rammah A. Alahnomi, and Norhanani Abd Rahman. Complex Permittivity Measurement Based on Planar Microfluidic Resonator Sensor. In *Proceedings - ANTEM 2018: 2018 18th International Symposium on Antenna Technology and Applied Electromagnetics*, volume 2018-August. Institute of Electrical and Electronics Engineers Inc., dec 2018.

[75] Thomas Chretiennot, David Dubuc, and Katia Grenier. A Microwave and microfluidic planar resonator for efficient and accurate complex permittivity characterization of aqueous solutions. *IEEE Transactions on Microwave Theory and Techniques*, 61(2):972–978, 2013.

[76] Hong Zhou, Donglin Hu, Cheng Yang, Cong Chen, Junwang Ji, Ming Chen, Yu Chen, Ya Yang, and Xiaojing Mu. Multi-Band Sensing for Dielectric Property of Chemicals Using Metamaterial Integrated Microfluidic Sensor. *Scientific Reports*, 8(1), dec 2018.

[77] Ahmed Salim and Sungjoon Lim. Complementary split-ring resonator-loaded microfluidic ethanol chemical sensor. *Sensors (Switzerland)*, 16(11), nov 2016.

[78] Javier Carnerero-Cano, Gabriel Galindo-Romera, Jose Juan Martinez-Martinez, and Francisco Javier Herraiz-Martinez. A Contactless Dielectric Constant Sensing System Based on a Split-Ring Resonator-Loaded Monopole. *IEEE Sensors Journal*, 18(11):4491–4502, jun 2018.

[79] G. Mois, S. Folea, and T. Sanislav. Analysis of three IoT-based wireless sensors for environmental monitoring. *IEEE Transactions on Instrumentation and Measurement*, 66(8):2056–2064, 2017.

[80] Hee Jo Lee and Jong Gwan Yook. Biosensing using split-ring resonators at microwave regime. *Applied Physics Letters*, 92(25), 2008.

[81] Christophe Calo and Tatsuo Itoh. Introduction. In *Electromagnetic Metamaterials: Transmission Line Theory and Microwave Applications*, chapter 1, pages 1–26. John Wiley & Sons, Inc., November 2005.

[82] Raimi Dewan, M.K.A. Rahim, M.R. Hamid, M.F.M. Yusoff, N.A. Samsuri, N.A. Murad, and K. Kamardin. Artificial magnetic conductor for various antenna applications: An overview. *International Journal of RF and Microwave Computer-Aided Engineering*, 27(6):e21105, aug 2017.

[83] Maidul Islam, S. Jagan Mohan Rao, Gagan Kumar, Bishnu P. Pal, and Dibakar Roy Chowdhury. Role of Resonance Modes on Terahertz Metamaterials based Thin Film Sensors. *Scientific Reports*, 7(1):7355, dec 2017.

[84] Yanbing Ma, Huaiwu Zhang, Yuanxun Li, Yicheng Wang, and Weien Lai. Terahertz sensing application by using fractal geometries of split-ring resonators. *Progress in Electromagnetics Research*, 138:407–419, 2013.

[85] Hyung Ki Kim, Dongju Lee, and Sungjoon Lim. A fluidically tunable metasurface absorber for flexible large-scale wireless ethanol sensor applications. *Sensors (Switzerland)*, 16(8), aug 2016.

[86] M. Bakır, M. Karaaslan, F. Dincer, K. Delihacioglu, and C. Sabah. Tunable perfect metamaterial absorber and sensor applications. *Journal of Materials Science: Materials in Electronics*, 27(11):12091–12099, nov 2016.

[87] S. Jun, B. Sanz-Izquierdo, and E. A Parker. A novel reconfigurable EBG structure and its potential use as liquid sensor. In *2019 13th European Conference on Antennas and Propagation (EuCAP)*, pages 1–5, 2019.

[88] Amir Ebrahimi, James Scott, and Kamran Ghorbani. Differential sensors using microstrip lines loaded with two split-ring resonators. *IEEE Sensors Journal*, 18(14):5786–5793, jul 2018.

[89] Paris Velez, Lijuan Su, Katia Grenier, Javier Mata-Contreras, David Dubuc, and Ferran Martin. Microwave Microfluidic Sensor Based on a Microstrip Splitter/Combiner Configuration and Split Ring Resonators (SRRs) for Dielectric Characterization of Liquids. *IEEE Sensors Journal*, 17(20):6589–6598, oct 2017.

[90] Paris Velez, Jonathan Munoz-Enano, Katia Grenier, Javier Mata-Contreras, David Dubuc, and Ferran Martin. Split Ring Resonator-Based Microwave Fluidic Sensors for Electrolyte Concentration Measurements. *IEEE Sensors Journal*, 19(7):2562–2569, apr 2019.

[91] Paris Velez, Katia Grenier, Javier Mata-Contreras, David Dubuc, and Ferran Martin. Highly-sensitive microwave sensors based on Open Complementary Split Ring Resonators (OCSRRs) for dielectric characterization and solute concentration measurement in liquids. *IEEE Access*, 6:48324–48338, aug 2018.

[92] Amir Ebrahimi, James Scott, and Kamran Ghorbani. Dual-Mode Resonator for Simultaneous Permittivity and Thickness Measurement of Dielectrics. *IEEE Sensors Journal*, pages 1–1, sep 2019.

[93] Lijuan Su, Javier Mata-Contreras, Paris Velez, and Ferran Martin. Splitter/combiner microstrip sections loaded with pairs of Complementary Split Ring Resonators (CSRRs): Modeling and optimization for differential sensing applications. *IEEE Transactions on Microwave Theory and Techniques*, 64(12):4362–4370, dec 2016.

[94] Ali Pourghorban Saghati, Jaskirat Singh Batra, Jun Kameoka, and Kamran Entesari. A Metamaterial-Inspired Wideband Microwave Interferometry Sensor for Dielectric Spectroscopy of Liquid Chemicals. *IEEE Transactions on Microwave Theory and Techniques*, 65(7):2558–2571, jul 2017.

[95] C. Damm, M. Schüßler, M. Puentes, H. Maune, M. Maasch, and R. Jakoby. Artificial transmission lines for high sensitive microwave sensors. In *Proceedings of IEEE Sensors*, pages 755–758, 2009.

[96] Tanveerul Haq, Cunjun Ruan, and Senior Member. Dual Notch Microwave Sensors Based on Complementary Metamaterial Resonators. *IEEE Access*, 7:153489–153498, 2019.

[97] Lyda Vanessa Herrera-Sepulveda, Jose Luis Olvera-Cervantes, Alonso Corona-Chavez, and Tejinder Kaur. Sensor and methodology for determining dielectric constant using electrically coupled resonators. *IEEE Microwave and Wireless Components Letters*, 29(9):626–628, sep 2019.

[98] Carlos G. Juan, Benjamin Potelon, Cedric Quendo, Enrique Bronchalo, and Jose M. Sabater-Navarro. *Highly-Sensitive Glucose Concentration Sensor Exploiting Inter-resonators Couplings*, pages 662–665. IEEE, oct 2019.

[99] Carlos G. Juan, Enrique Bronchalo, Benjamin Potelon, Cédric Quendo, Ernesto Ávila-Navarro, and José María Sabater-Navarro. Concentration Measurement of Microliter-Volume Water-Glucose Solutions Using Q Factor of Microwave Sensors. *IEEE Transactions on Instrumentation and Measurement*, 68(7):2621–2634, jul 2019.

[100] Paris Velez, Lijuan Su, J. Mata-Contreras, Ferran Martin, Katia Grenier, and David Dubuc. Modeling and analysis of pairs of open complementary split ring resonators (OCSRRs) for differential permittivity sensing. In *2017 IEEE MTT-S International Microwave Workshop Series on Advanced Materials and Processes for RF and THz Applications, IMWS-AMP 2017*, volume 2018-January, pages 1–3. Institute of Electrical and Electronics Engineers Inc., jan 2018.

[101] Erick Reyes-Vera, G. Acevedo-Osorio, Mauricio Arias-Correa, and David E. Senior. A submersible printed sensor based on a monopole-coupled split ring resonator for permittivity characterization. *Sensors (Switzerland)*, 19(8), apr 2019.

[102] Paris Velez, Lijuan Su, Katia Grenier, Javier Mata-Contreras, David Dubuc, and Ferran Martin. Microwave Microfluidic Sensor Based on a Microstrip Splitter/Combiner Configuration and Split Ring Resonators (SRRs) for Dielectric Characterization of Liquids. *IEEE Sensors Journal*, 17(20):6589–6598, oct 2017.

[103] Amyrul Azuan Mohd Bahar, Z. Zakaria, M. K. Md. Arshad, A. A.M. Isa, Y. Dasril, and Rammah A. Alahnomi. Real Time Microwave Biochemical Sensor Based on Circular SIW Approach for Aqueous Dielectric Detection. *Scientific Reports*, 9(1):1–12, 2019.

[104] Dan Sievenpiper, Lijun Zhang, Romulo F. Jimenez Broas, Nicholas G. Alexöpolous, and Eli Yablonovitch. High-impedance electromagnetic surfaces with a forbidden frequency band. *IEEE Transactions on Microwave Theory and Techniques*, 47(11):2059–2074, 1999.

[105] Balanis.C.A. *Antenna Theory Analysis and Design*. Wiley & Sons Inc, 1997.

[106] S. Keyrouz and D. Caratelli. Dielectric Resonator Antennas: Basic Concepts, Design Guidelines, and Recent Developments at Millimeter-Wave Frequencies. *International Journal of Antennas and Propagation*, 2016, 2016.

[107] Darko Kajfez and Ahmed A. Kishk. Dielectric Resonator Antenna - Possible Candidate for Adaptive Antenna Arrays, 2002.

[108] A. A. Kishk, A. Ittipiboon, Y. M. M. Antar, and M. Cuhaci. Slot excitation of the dielectric disk radiator. *IEEE Transactions on Antennas and Propagation*, 43(2):198–201, 1995.

[109] Anuj K. Ojha, Rutwik Jain, and Praveen Kumar AV. Magnetic quadrupole mode excitation of a cylindrical dielectric resonator antenna using planar feed. *Microwave and Optical Technology Letters*, 62(1):484–490, 2020.

[110] Halappa Gajera, Debatosh Guha, and Chandrakanta Kumar. New Technique of Dielectric Perturbation in Dielectric Resonator Antenna to Control the Higher Mode Leading to Reduced Cross-Polar Radiations. *IEEE Antennas and Wireless Propagation Letters*, 16:445–448, 2017.

[111] D. Kajfez, A. W. Glisson, and J. James. Computed modal field distributions for isolated dielectric resonators. *IEEE Transactions on Microwave Theory and Techniques*, 32(12):1609–1616, 1984.

[112] B. Strohm. Ethanol. In Philip Wexler, editor, *Encyclopedia of Toxicology (Third Edition)*, pages 488–491. Academic Press, Oxford, third edition edition, 2014.

[113] CarboSystems. https://carbosystem.com/en/.

[114] Eurocircuits. https://www.eurocircuits.com/.

[115] M. G. Mayani, F. J. Herraiz Martínez, Javier Matanza Domingo, R. Giannetti, and Carlos Rodríguez-Morcillo García. Dual-Band Metamaterial-inspired Microwave Sensor For Liquid Dielectric Spectroscopy. In *Proceedings of IEEE International Instrumentation & Measurement Technology Conference (I2MTC)*, Glasgow, Scotland, 2021. IEEE International Instrumentation & Measurement Technology Conference (I2MTC).

[116] Gabriel Galindo-Romera, Javier Carnerero-Cano, José Juan Martínez-Martínez, and Francisco Javier Herraiz-Martínez. An IoT reader for wireless passive electromagnetic sensors. *Sensors*, 17(4), 2017.

[117] PathWave Advanced Design System (ADS) Software | Keysight.

[118] Ari Sihvola. Mixing Rules with Complex Dielectric Coefficients. *Subsurface Sensing Technologies and Applications*, 1(4):393–415, 2000.

[119] A. A. Helmy, S. Kabiri, M. M. Bajestan, and K. Entesari. Complex permittivity detection of organic chemicals and mixtures using a 0.5–3-GHz miniaturized spectroscopy system. *IEEE Transactions on Microwave Theory and Techniques*, 61(12):4646–4659, 2013.